

Synthesis and characterization of Metal-Ceramic based Advanced Bio-Materials for Implant Applications

Doctoral Thesis

by

Rakesh Kumar

2017MEZ0023



Department of Mechanical Engineering
INDIAN INSTITUTE OF TECHNOLOGY ROPAR
March, 2024

Synthesis and characterization of Metal-Ceramic based Advanced Bio-Materials for Implant Applications

A Thesis Submitted
In Partial Fulfillment of the Requirements
for the Degree of

DOCTOR OF PHILOSOPHY

by

Rakesh Kumar

2017MEZ0023



Department of Mechanical Engineering
INDIAN INSTITUTE OF TECHNOLOGY ROPAR
March, 2024

Rakesh Kumar: *Synthesis and characterization of Metal-Ceramic based Advanced Bio-Materials for Implant Applications*

Copyright © 2024, Indian Institute of Technology Ropar
All Rights Reserved

Dedicated
to
My Parents, Family &
Late. Kumar Rajan (Sanjhle Papa)

Declaration of Originality

I hereby declare that the work which is being presented in the thesis entitled **Synthesis and characterization of Metal-Ceramic based Advanced Bio-Materials for Implant Applications** has been solely authored by me. It presents the result of my own independent investigation/research conducted during the time period from January, 2018 to November, 2023 under the supervision of Dr. Anupam Agrawal, Associate Professor in the Department of Mechanical Engineering. To the best of my knowledge, it is an original work, both in terms of research content and narrative, and has not been submitted or accepted elsewhere, in part or in full, for the award of any degree, diploma, fellowship, associateship, or similar title of any university or institution. Further, due credit has been attributed to the relevant state-of-the-art and collaborations (if any) with appropriate citations and acknowledgments, in line with established ethical norms and practices. I also declare that any idea/data/fact/source stated in my thesis has not been fabricated/ falsified/ misrepresented. All the principles of academic honesty and integrity have been followed. I fully understand that if the thesis is found to be unoriginal, fabricated, or plagiarized, the Institute reserves the right to withdraw the thesis from its archive and revoke the associated Degree conferred. Additionally, the Institute also reserves the right to appraise all concerned sections of society of the matter for their information and necessary action (if any). If accepted, I hereby consent for my thesis to be available online in the Institute's Open Access repository, inter-library loan, and the title & abstract to be made available to outside organizations.

Signature

Name: Rakesh Kumar

Entry Number: 2017MEZ0023

Program: PhD

Department: Mechanical Engineering

Indian Institute of Technology Ropar

Rupnagar, Punjab 140001

Date: 27th March 2024

Acknowledgements

I would like to express my sincere gratitude to the following organizations and personals for their support (technical or personal) for my research work and stay at IIT Ropar during my Ph.D. tenure.

- ❖ *Supervisor:* Dr. Anupam Agrawal (Associate Professor, Mechanical Engineering, IIT Ropar)
- ❖ *Director & Dean PG&R at IIT Ropar:* Prof. Rajeev Ahuja, and Prof. Rajendra Srivastava
- ❖ *Head of the Department:* Dr. Prabhat K. Agnihotri (HoD & Associate Professor, Mechanical Engineering, IIT Ropar)
- ❖ *Doctoral Committee Members:* Prof. Navin Kumar (DC-Chairperson), Dr. Chandrakant K. Nirala, Dr. Ravi Kant, Dr. Arvind Kumar Gupta
- ❖ *Faculties from Dept. of Mechanical Engineering at IIT Ropar:* Dr. Sachin Kumar, Dr. Srikant Sekhar Padhee, Dr. Ranjan Das, Dr. Ravi Mohan Prasad, Dr. Dhiraj K. Mahajan
- ❖ *Lab Staffs at IIT Ropar:* Mr. Varinder Kumar, Mr. Amit Kumar, Mr. Ram Kumar, Mr. Pankaj Thakur, Mr. Rajeev Kumar, Mr. Hemant Kumar, Mr. Amit Kaushal
- ❖ *Workshop Staffs at IIT Ropar:* Mr. Rambeer, Mr. Jaswinder, Mr. Girdhari, Mr. Jograj, Mr. Bhupinder, Mr. Randhir, and Mr. Jashkaran
- ❖ *AMT Lab Members at IIT Ropar:* Dr. Harish K. Nirala, Dr. Hreetabh Kishore, Mr. Prince Malik, Mr. Mainak Pal, Mr. Amit Kumar, Mr. Saurabh Rai, Mr. Yash Desai, Mr. Peeyush Mahajan, Mr. Aakash Agrawal, Mr. Shubhra Kamal Nandi, Mr. Anubhav, Mr. Dattatraya Bombe, Miss Shubhangee Singhal, Miss Sanyukta Marandi, Mr. Aviral, Mr. Suraj, Mr. Devraj, Mr. Neeraj, Miss. Tripty, Mr. Navneet and Dr. Ashutosh Rajput
- ❖ *Colleagues at IIT Ropar:* Dr. Ajay Singh, Dr. Somnath Gorai, Dr. Vishal Singh, Mr. Mukesh Kumar, Dr. Vellavalapalli Satish, Dr. Sohaib Raza, Dr. Avneesh Kumar, Dr. Vishal Agrawal, Mr. Shivanshu Dixit, Dr. Nishant Shakya, Dr. Binod Kumar, Dr. Rahul Nadda, Mr. Vikalp Shrama, Mr. Pulak Gupta, Mr. Gaurav Saraf, Mr. Rajat Dhiman, and Mr. Himanshu
- ❖ *Pehchaan Ek-Safar team at IIT Ropar:* Dr. Bellamkonda Dwiza, Mr. Chetan Kumar, Miss. Sanyukta Marandi, Mr. Yash Jain, Miss. Bhavna Kumari, Mr. Mukesh Kumar, Mr. Vedant, Mr. Ninad Hari Sutrave, Mr. Prem Dayal, Mr. Chena Ram, and Kids of PES.
- ❖ Thanks to my M. Tech and other friends for their motivation and time to time support.
- ❖ Special thanks should go to my parents and family members who gave me an enormous support at home. Thank you for your understanding and providing me freedom and time to carry out my Ph.D.

Thank you all...

Rakesh Kumar

March 2024

Certificate

This is to certify that the thesis entitled **Synthesis and characterization of Metal-Ceramic based Advanced Bio-Materials for Implant Applications**, submitted by **Rakesh Kumar (2017MEZ0023)** for the award of the degree of **Doctor of Philosophy** of Indian Institute of Technology Ropar, is a record of bonafide research work carried out under my (our) guidance and supervision. To the best of my knowledge and belief, the work presented in this thesis is original and has not been submitted, either in part or full, for the award of any other degree, diploma, fellowship, associateship or similar title of any university or institution.

In my (our) opinion, the thesis has reached the standard fulfilling the requirements of the regulations relating to the Degree.

Signature of the Supervisor

Name- Dr. Anupam Agrawal

Department- Mechanical Engineering

Indian Institute of Technology Ropar

Rupnagar, Punjab 140001

Date: 27th March 2024

Lay Summary

Have you ever considered why a human must undergo different implant surgery? What happens with the damaged bone due to an accident/injury? What does a doctor place inside the body to cure the damaged bones? How such devices (implants) are made? How do hard and complex metals function and behave inside the body? And how does a bone get repaired and start functioning properly after surgery?

Well, all these questions can be addressed with the help of knowledge of materials and manufacturing processes that are used to design and fabricate various implants and medical devices. Implants and medical devices are made of materials termed as “bio-materials,” their functioning inside a human body can be studied by analyzing their mechanical, tribological, and biological characteristics. Different metal, polymer, and ceramic materials are used to fabricate various implants and medical devices depending on their prerequisite properties. Various complications, limitations, and post-surgery impacts of different materials and designs used to fabricate implants exist. Stress-shielding and interfacial behaviour of implant and existing bone/tissue are significant issues an implant must encounter during its service inside a human body.

In this thesis work, a detailed study on fabrication and various characteristics of metal (pure-Ti) and ceramic (HAp) based bio-composites has been performed to develop a fundamental understanding and background of developing an advanced biomaterial for high-load bearing implant applications. The raw materials have been mixed and alloyed using a mechanical alloying process called as High Energy Ball Milling (HEBM) with varying compositions. Alloyed materials are tested to correlate their properties for suitability as possible biomaterials through the resulting powder material's structural, chemical/elemental, and biological characteristics. Then, the alloyed material has been compacted and sintered using the Microwave Hybrid Heating (MHH) process to achieve densification and strength in the green compact samples. The synthesized composites have been tested for mechanical, tribological, corrosion, and cytocompatibility properties to study their responses and relate their characteristics with its functioning and how the developed material will behave. The same HEBM alloyed materials have been stacked together in a gradient manner to develop a graded material called ‘Functionally Graded Material (FGM).’ The mechanical and tribological responses of developed FGM show a decreasing trend toward the gradation direction, which could possibly minimize the stress-shielding effect upto specific limits, and its enhanced bioactivity will improve the implant-tissue interfacial behaviour. Thus, it can be concluded that the developed metal-ceramic-based composite could be used to replace the existing mono-material implant with its improved characteristics.

Abstract

The demand for implants is increasing due to the aging population, trauma, injury, and daily lifestyle. An improved and advanced materials and processing technique is needed to reduce the complications caused by implants. Pure metallic biomaterials are widely used for orthopedic and high-load bearing implants as permanent replacements or to support damaged body parts as scaffolds and fixation devices. However, their high mechanical properties (modulus, hardness, etc.) and corrosive nature of metals negatively impact the surrounding bones and tissues, termed as “stress-shielding”. Stress-shielding is a phenomenon that causes damage to existing natural bones and surrounding tissues due to a mismatch in their mechanical characteristics (modulus, hardness, stiffness, etc.) with that of implants/scaffolds. This makes the implant-tissue interface critical, as it damages the existing natural tissue. In this work, metal-ceramic-based composites have been synthesized using mechanical alloying followed by sintering with microwave hybrid heating (MHH) to propose a possible advanced material for implant applications. Microstructural, Chemical, Material-phase, Mechanical, Tribological, Corrosion, and in-vitro cytocompatibility tests (MTT Assay) have been conducted to establish their effectiveness. The presence of functional groups of PO_4^{3-} and CO_3^{2-} as well as Ca:P ratio of 1.6 in the synthesized composites makes it suitable for implant applications chemically.

Further, the same homogeneously alloyed materials have been stacked to synthesize a functionally graded material (FGM) using the powder metallurgy route. The measured microhardness and frictional characteristics exhibit tailored properties along the gradation direction. These results inferred that the synthesized materials could minimize the stress-shielding effect and improve the implant-tissue interaction behaviour. The synthesis and a thorough characterization results strongly supports the fact that the FGM has the desired properties to mimic the architecture of natural bone (having varying density and mechanical strength in a gradient manner). Furthermore, using better biocompatible constituent materials, metals can appreciably enhance the bioactivity of the resulting material. Thus, the proposed advanced composite materials may be used to design and fabricate high-load-bearing implants with the required structural, mechanical, and biological properties.

Keywords: Biomaterials; Metal-Ceramic Composite; Functionally Graded Material; Mechanical Properties; Tribological Properties; Cytocompatibility.

List of Publications from Thesis

Publication in Peer-Reviewed Journals

1. **R. Kumar**, A. Agrawal, Micro-hydroxyapatite reinforced Ti-based composite with tailored characteristics to minimize stress-shielding impact in bio-implant applications, *J. Mech. Behav. Biomed. Mater.* 142 (2023) 105852. <https://doi.org/10.1016/j.jmbbm.2023.105852>.
2. **R. Kumar**, A. Agrawal, Bio-corrosion susceptibility of surface voids and pores in microwave sintered Ti-HAp based bio-composites, *Mater. Lett.* 361 (2024) 136168. <https://doi.org/10.1016/j.matlet.2024.136168>.
3. **R. Kumar**, A. Agrawal, Tribological and In-Vitro Biological Characteristics of Microwave Sintered Ti- μ -HAp-based Bio-composite for High-Load Bearing Implant Applications, (**Under review in Acta Biomaterialia, Elsevier**)
4. **R. Kumar**, A. Agrawal, Structural, Elemental, and In-vitro Bioactivity Characteristics of Ti-HAp-based Biomaterial, Synthesized by Mechanical Alloying for Load-bearing Implant Applications, (**Under review in Advanced Powder Technology, Elsevier**)
5. **R. Kumar**, A. Agrawal, Mechanical and Tribological Characteristics of Ti- μ -HAp Based Functionally Graded Biomaterials Fabricated Through Powder Metallurgy (Under Preparation to be submitted in **Journal of Alloys and Compounds**)

Publication as Book Chapters

1. **R. Kumar**, A. Agrawal, Emerging Functionally Graded Materials for Bio-implant Applications—Design and Manufacturing, in: *Addit. Manuf. Bio-Implants - Des. Synth.*, Springer, Singapore, 2024: pp. 137–146. https://doi.org/10.1007/978-981-99-6972-2_9.

Contents

Declaration of Originality	v
Acknowledgements	vii
Certificate	ix
Lay Summary	xi
Abstract	xiii
List of Publication From Thesis	xv
Contents	xvii
List of Figures	xxi
List of Tables	xxv
Abbreviations	xvii
Chapter 1	3
Introduction	3
1.1 Motivation	3
1.2 Issues with Materials used for bio-implants	6
1.2.1 Stress-shielding of Implants	6
1.2.2 Issues Due to Tissue-Implant Interface	8
1.3 Bio-Materials used for Implant Applications	10
1.4 Characteristics of Biomaterials	11
1.4.1 Biocompatibility	12
1.4.2 Surface Properties	13
1.4.3 Corrosion Properties	13
1.4.4 Mechanical Properties	13
1.5 Processing and Fabrication Methods	13
1.5.1 Powder Metallurgy	14
1.5.2 Casting	14
1.5.3 Additive Manufacturing	15
Chapter 2	19
Literature Review	19
2.1 Classification of Implants	20
2.2 Modern Bio-Materials	21
2.3 Metal-Ceramic Bio-Composites	23
2.4 Synthesis and Processing of Bio-composites	23
2.5 Bulk Mechanical and Tribological Behaviour of Bio-Composites	24
2.6 In-Vitro Mechanical and Biological characterization	25
2.7 Research Gaps	25

2.8 Objectives.....	26
Chapter 3.....	29
Processing and Characterization of Ti-HAp-based Bio-Material.....	29
3.1 Selection of Raw Materials and its Characteristics.....	29
3.2 High Energy Ball Milling (HEBM) of Raw Materials.....	30
3.3 Phase and Morphology of HEBM alloyed Powders	32
3.3.1 Phase and Crystalline Characteristics.....	32
3.3.2 Morphological Characteristics.....	35
3.4 Elemental and Functional Composition Characteristics of HEBM alloyed Powders.....	36
3.4.1 Elemental Characteristics.....	36
3.4.2 Functional Groups Characteristics.....	38
3.5 In-Vitro Cytocompatibility Test (MTT Assay) of HEBM Powders.....	39
3.6 Discussion.....	40
3.7 Summary.....	41
Chapter 4	45
Synthesis and Characterization of Ti-HAp-based Bio-Composites.....	45
4.1 Sintering of Metal-Ceramic based composite using Microwave Hybrid Heating	46
4.2 Morphological and Elemental Characterization of Sintered composite samples	49
4.3 Mechanical Characteristics of the Sintered composite samples.....	53
4.3.1 Nano-Mechanical Characteristics.....	53
4.4 Surface Tribological Characteristics of Sintered Composites.....	56
4.4.1 Surface Wettability.....	56
4.4.2 Surface wear.....	57
4.4.3 Corrosion Study.....	59
4.5 In-vitro Cytocompatibility of Sintered Composite Samples.....	64
4.6 Discussion.....	67
4.7 Summary.....	68
Chapter 5.....	71
Fabrication of Functionally Graded Bio-Material and its Characterization	71
5.1 Synthesis of Ti-HAp-based FGM.....	71
5.2 Morphological and Elemental Characterization using SEM-EDS....	72
5.3 Mechanical Characteristics of Sintered FGM.....	74
5.3.1 Density Measurement.....	74

5.3.2 Compression Behaviour	75
5.3.3 Microhardness	77
5.4 Surface and Wear Characteristics	78
5.5 Discussion	80
5.6 Summary	82
Chapter 6	86
Conclusions and Future Scope	86
6.1 Conclusions	86
6.2 Future Scope	87
Bibliography	89
Brief Bio-Data	102

List of Figures

Fig. 1.1- Projected aging population of India	4
Fig. 1.2- Global Bio-implant Market Size	5
Fig. 1.3- Examples of a few commercial Implants	6
Fig. 1.4- Phenomenon of Stress-shielding in femur bone-implant	7
Fig. 1.5- Anatomy of the natural femur bone	8
Fig. 1.6- Schematic of the bone-implant interface	9
Fig. 1.7- Classification of FGM	10
Fig. 1.8- Framework/Science of Bio-Materials evolution	11
Fig. 1.9- Essential characteristics of a bio-material	11
Fig. 1.10- Schematic representation of the process showing the centrifugal mixed-powder method	15
Fig. 1.11- Classification of AM Processes	16
Fig. 1.12- Schematic representation of different AM processes, (a) Fused Deposition Modeling process, (b) Selective Laser Melting Process, (c) Direct Energy Deposition Process, (d) Direct Write Technology	16
Fig. 2.1- Examples of a few Class-III load-bearing implants	21
Fig. 3.1- SEM Image of as-received irregularly shaped raw powders used in the study (a) Pure-Ti, and (b) μ -HAp	30
Fig. 3.2- EDX-based elemental composition results of raw materials (a) Pure-Ti, (b) μ -HAp	31
Fig. 3.3- Schematic representation of the HEBM process used to synthesis the bio-material	32
Fig. 3.4- XRD plots of Pure Ti and Ti+ HAp ball milled powders	33
Fig. 3.5- XRD characteristics (a) Average crystalline size obtained using Debye-Scherrer Equation, (b) Scherrer plot, (c) W-H Plot for the HEBM processed powders	34
Fig. 3.6- (a) HEBM processed Pure-Ti powder, (b-e) SEM images of Ti- μ -HAp mixed HEBM processed powders showing homogenized mixing and particle size reduction after milling	35
Fig. 3.7- XPS response of HEBM processed powder materials	37
Fig. 3.8- Transmittance results of the HEBM processed powders obtained using FTIR.	39
Fig. 3.9- MTT Assays result for cell absorbance with different duration of time	40
Fig. 4.1- Schematic representation of the synthesis of bio-composite using Powder metallurgy process	47

Fig. 4.2- Compaction and Sintering curve of alloyed Ti- μ -HAp powder for densification	47
Fig. 4.3- Failed samples during processing (a) 4 wt.% HAp sample, & (b) 5 wt.% HAp sample	48
Fig. 4.4- Measured density of the sintered composites samples using Archimedes' principle	48
Fig. 4.5- SEM images of untreated sintered samples representing the diffusion of μ -HAp with Ti (a) Pure Ti, (b) Ti+1 wt% μ -HAp, (c) Ti+2 wt% μ -HAp, and (d) Ti+3 wt% μ -HAp	49
Fig. 4.6- EDX-Mapping of untreated sintered samples representing the diffusion of μ -HAp with Ti (a) Pure Ti, (b) Ti+1 wt% μ -HAp, (c) Ti+2 wt% μ -HAp, and (d) Ti+3 wt% μ -HAp	51
Fig. 4.7- SEM Images of polished sintered samples representing the diffusion of μ -HAp with Ti (a) Pure Ti, (b) Ti+1 wt.% μ -HAp, (c) Ti+2 wt.% μ -HAp, and (d) Ti+3 wt.% μ -HAp	52
Fig. 4.8- Transmittance results of Ball-Milled powders using FTIR	52
Fig. 4.9- A schematic representation of nano-mechanical testing through the nanoindentation technique	54
Fig. 4.10- Nano-mechanical Load vs. Indentation depth responses of the sintered samples	55
Fig. 4.11- Nano-indentation responses of the sintered samples (a) Elastic Modulus, (b) Nano-Hardness.....	55
Fig. 4.12- Analysis of wettability of the sintered composites, (a) Schematic representation of wettability analysis, and (b) Comparative measured contact angle values of the sintered samples	57
Fig. 4.13- Frictional force and Coefficient of Friction data, (a)-(b) for a constant normal load of 20 N, (c)-(d) for continuously increasing normal load of 2-20 N	58
Fig. 4.14- Morphology of the scratch wear track for constant applied load (a) Pure-Ti, (b) Ti+ 1 wt.% HAp, (c) Ti+ 2 wt.% HAp, and (d) Ti+ 3 wt.% HAp	59
Fig. 4.15- (a) Relative density of sintered samples, (b) Three-electrode cell set-up for Electrochemical Corrosion test	60
Fig. 4.16- Schematic representation of the corrosion mechanism in Ti-HAp composite	61
Fig. 4.17- Polarization curves (Tafel plot) obtained from Electrochemical corrosion test	61
Fig. 4.18- Surface morphology of sintered samples, (A1-D1) polished as-sintered samples, (A2-D2) corroded surface after electrochemical corrosion	63
Fig. 4.19 - Adherence and growth of cells after first day of incubation	65
Fig. 4.20- Cytocompatibility analysis of the sintered composite samples using MTT Assays	66
Fig. 4.21- SEM images of adhered cell and apatite layer over the sintered composites	67

Fig. 5.1- Schematic of the steps followed to fabricate FGM using the PM route	72
Fig. 5.2- SEM image of sintered FGM through powder metallurgy route exhibiting variation in pores density too with varying composition	73
Fig. 5.3- Magnified image showing bonding of sintered particles	73
Fig. 5.4- EDS-Line mapping of sintered FGM	74
Fig. 5.5- Density of sintered samples measured using Archimedes' principle.....	75
Fig. 5.6- Compression behaviour of sintered FGM (a) compressive stress vs strain plot, (b) comparative modulus and compression before first fracture point	76
Fig. 5.7- Vickers micro-hardness values of sintered FGM	78
Fig. 5.8- Comparative frictional force and coefficient of friction	79
Fig. 5.9- Morphology of scratched wear tracks at different locations	79
Fig. 5.10- Mean values (with standard deviation) of the determined mechanical properties	81

List of Tables

Table 1.1- List of popular biomaterials and their extensive properties and appropriate applications that can be used to design and fabricate Implants	10
Table 3.1- Quantitative distribution of elements in HEBM processed powders detected using XPS	38
Table 4.1- Elemental composition (in %) of the sintered sample obtained through EDS	51
Table 4.2– Calculated plasticity index values of sintered Ti-HAp composites based upon Nano-Mechanical responses	56
Table 4.3– Electrochemical parameters acquired from Tafel analysis of sintered composite samples	62
Table 4.4– Elemental distribution (in %) over the sintered composite surface before and after the Electrochemical corrosion test	64
Table 5.1- Mechanical Properties calculated after compression test	77
Table 5.2- Mechanical properties for human cortical femur bone	80
Table 5.3- Ratio of modulus values to represent as a stress-shielding indicator	82

Abbreviations

AM	Additive Manufacturing
ASTM	American Society for Testing and Materials
CAGR	Cumulative Annual Growth Rate
CAD	Computer Aided Design
EDS	Energy Dispersive X-ray Spectroscopy
FDA	Food and Drug Association
FDM	Fused Deposition Modeling
FGM	Functionally Graded Material
FTIR	Fourier Transformed Infrared Spectroscopy
HAp	Hydroxyapatite
HBSS	Hank's Balanced Salt Solution
HCP	Hexagonal Closed Packed
HEBM	High Energy Ball Milling

MHH	Microwave Hybrid Heating
MMC	Metal Matrix Composite
MTT	(3-(4,5-dimethylthiazol-2-yl)-2,5-diphenyl tetrazolium bromide)
OCP	Open Circuit Potential
PCL	Poly Caprolactone
PLA	Poly(lactic) Acid
PM	Powder Metallurgy
SEM	Scanning Electron Microscopy
SLM	Selective Laser Melting
SLS	Selective Laser Sintering
XRD	X-ray Diffraction
XPS	X-ray Photoelectron Spectroscopy

Chapter-1

This chapter briefly discusses the motivation of the work carried out in the thesis with a basic introduction and definitions of the key terms.

Chapter 9

Emerging Functionally Graded Materials for Bio-implant Applications—Design and Manufacturing



Rakesh Kumar and Anupam Agrawal

1 Introduction

Human body architecture has several joints and connections contributing to its efficient functioning. Any damaged part must be replaced with an artificial or synthetic look-a-like part called a “Bio-Implant” [1]. As per the report published in 2018 [2] on bio-implant market analysis, its global market size was USD 65 Billion at a CAGR of 5.90%, which has tremendously increased in the latest report of 2022 [3] to USD 117.3 Billion and expected to raise upto USD 126.7 Billion by 2032 at a whopping CAGR of 10.00% during this time. This tremendous surge in implant market size exhibits the high demand for implant and implant surgeries caused due to accidents, sports injuries, severe health issues, etc. This demand for bio-implants has opened up a gateway for many research, start-up, and biomedical industries related to innovative designing, fabrication techniques, and development of advanced materials with enhanced mechanical, structural, and biological properties (Fig. 1).

With the increasing scientific and technological advancements, the quality and capability of these artificial implants are also increasing regularly. There are two crucial factors for the development of bio-implants, (a) the proper selection of biomaterial and (b) the proper selection of fabrication method [4, 5]. An ideal implant material should be durable, easily moldable, and, more importantly, biocompatible, allowing easy tissue growth. So, the process of tissue engineering starts with proper biomaterial selection, followed by the fabrication of implants. Recently, AM processes have somehow solved the fabrication issues with their unparalleled degrees of freedom (design, material, hierarchical structure, etc.) to fabricate any complex 3D

1.1 Motivation

Human body architecture has several joints and connections contributing to its efficient functioning. Any damaged part must be replaced with an artificial or synthetic

look-a-like part called a "Bio-Implant" [1]. As per the report [2], the older population accounted for 55.8 million people, 16.8 % of the total population of the United States. With an aging population (aging population distribution in India- **Fig. 1.1**) and an increase in affordable healthcare facilities, the need for bio-implants is growing in the present scenario. The implants must be made to near-net shape with high precision and enhanced biocompatibility. However, reliable, durable, and precise implant surgeries are expensive. *So, finding an appropriate solution to health-related issues through innovation in materials and manufacturing is the primary motivation of this thesis work.* As per the report published in 2018 [3] on bio-implant market analysis, its global market size was USD 65 Billion at a Cumulative Annual Growth Rate (CAGR) of 5.90%, which has tremendously increased in the latest report of 2022 [4] to USD 122.34 Billion and expected to raise at a whopping CAGR of 10.00% by 2032 (**Fig. 1.2**). This tremendous surge in implant market size exhibits the high demand for implant and implant surgeries caused due to age driven issues, accidents, sports injuries, severe health issues, etc. This demand for bio-implants has opened up a gateway for many researches, start-ups, and biomedical industries related to innovative designing, fabrication techniques, and development of advanced materials with enhanced mechanical, structural, and biological properties.

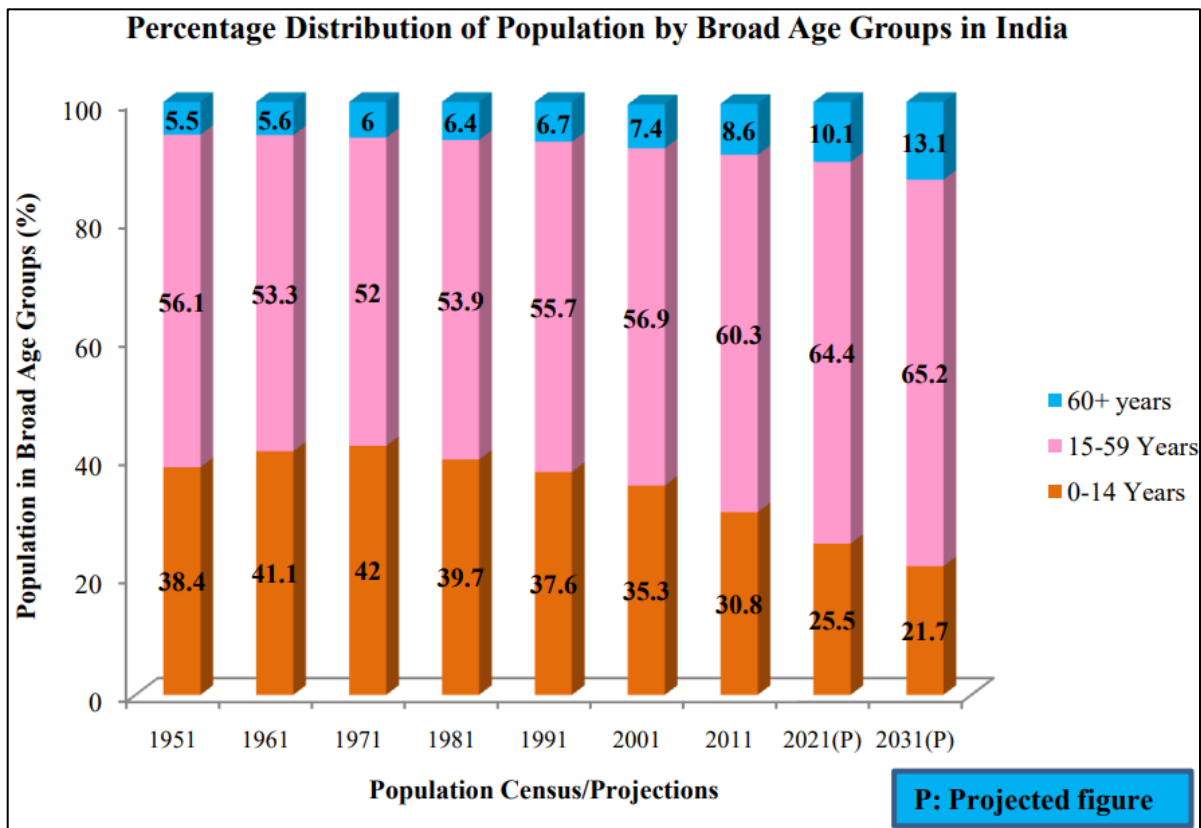


Fig. 1.1- Projected aging population of India (Courtesy- MSPI Report [5])

There are three important factors in the development of Bio-implants: (a) the selection of proper material [6,7], (b) the design of bio-implant, and (c) the appropriate selection of fabrication method. An ideal artificial implant should have proper roughness, interconnected pores, strength, and, more importantly, biocompatibility to allow easy tissue growth. It should be durable, easily moldable, and minimize the shielding effect

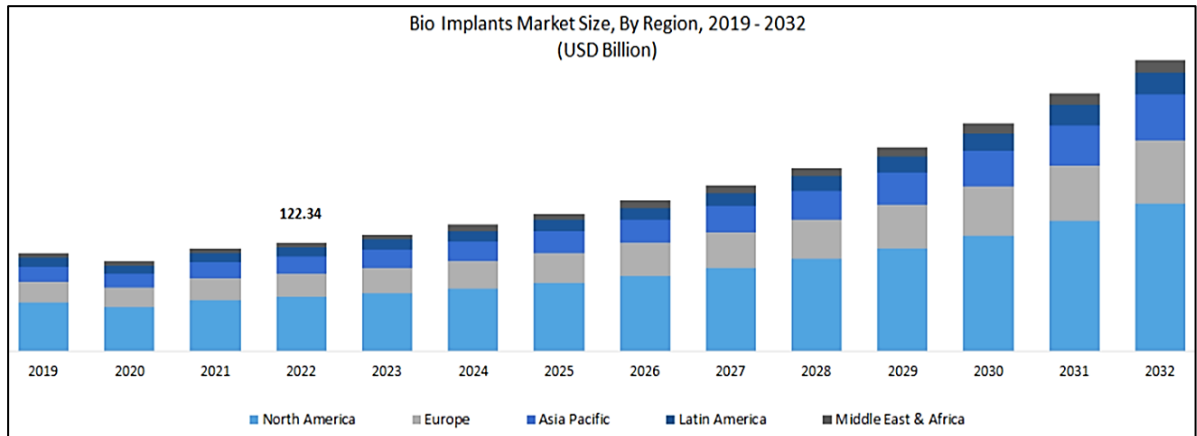


Fig. 1.2- Global Bio-implant Market Size [4]

between the implant and existing natural body parts. The tissue engineering process starts with proper biomaterial selection and design, followed by the fabrication. The functioning and lifespan of an implant mostly depend upon how it will behave in the presence of blood plasma, and its physical behaviour is totally material-driven. Hence, a material with good mechanical, chemical, and biological properties should be used to design and fabricate implants [8]. For many years, Stainless Steel or other Iron-based metallic materials have been primarily used as raw materials for various load-bearing implant manufacturing [9]. The density and high mechanical strength of Iron and Steel-based materials increase the overall mass of the implant, simultaneously causing damage to surrounding bone/tissues due to stress-shielding [10].

Titanium (Ti) and its alloys are extensively used biomaterials for numerous applications as implants (orthopedic and cardiovascular) and medical devices due to their superior biocompatibility compared to other pure metallic materials [11]. It has wide applications in various industries due to its high strength-to-weight ratio and non-corrosive behaviour. Hydroxyapatite (HAp) is a widely used bio-ceramic as it has the ability to regenerate bone after implanting with a healthy bone and provides enough strength to the surrounding bones [12]. The modulus for dense HAp varies from 5 to 18 GPa and exhibits brittle behaviour, with Vickers hardness in the range of 3–7 GPa [13]. These two materials can be potentially used to synthesize a composite material for possible usage for the fabrication of load-bearing implants.

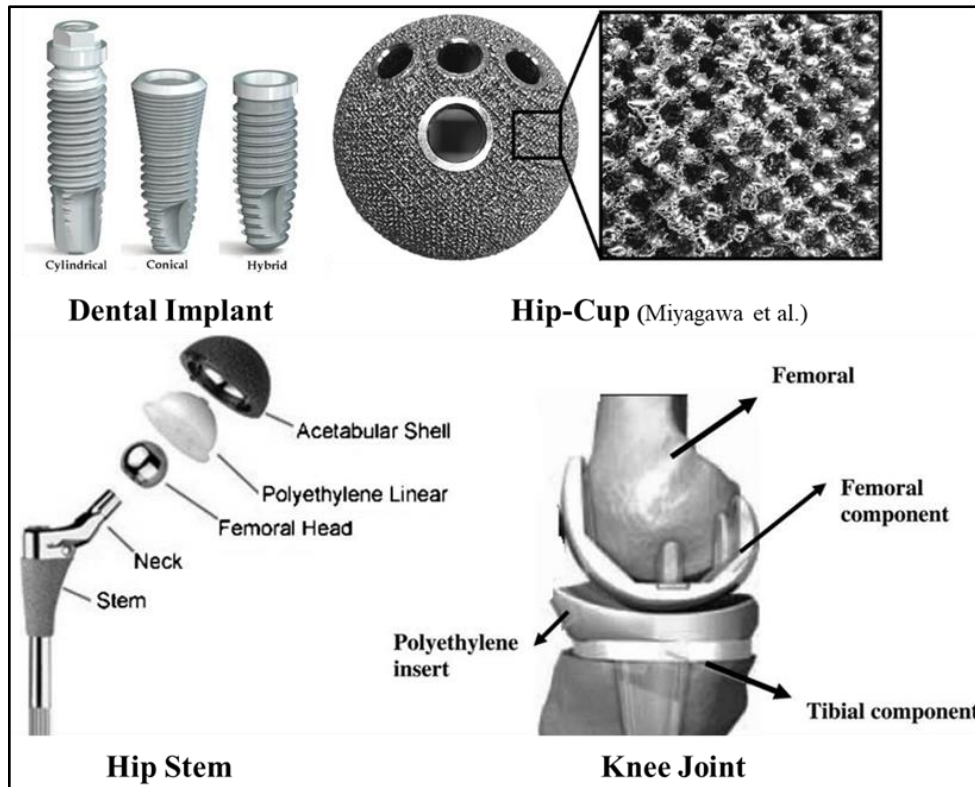


Fig. 1.3- Examples of a few commercial Implants [14]

1.2 Issues with Materials used for bio-implants

1.2.1 Stress-shielding of Implants

Stress-shielding is a phenomenon of bone implants that causes damage to existing natural bone and surrounding tissues due to a mismatch between the mechanical characteristics (modulus, hardness, stiffness, etc.) [15]. **Fig. 1.4** represents the schematic of how stress-shielding affects the existing bone/tissue. Hence, to have an implant with better load carrying, enhanced functioning, life span, and osseointegration, implants should have comparable mechanical properties to natural bone, i.e., by minimizing stress-shielding. Newly developed bio-materials need specific chemical, mechanical, and biocompatible properties to perform desired functions without affecting existing tissues, which can be derived from their constituent materials or attained through their processing/fabrication procedure.

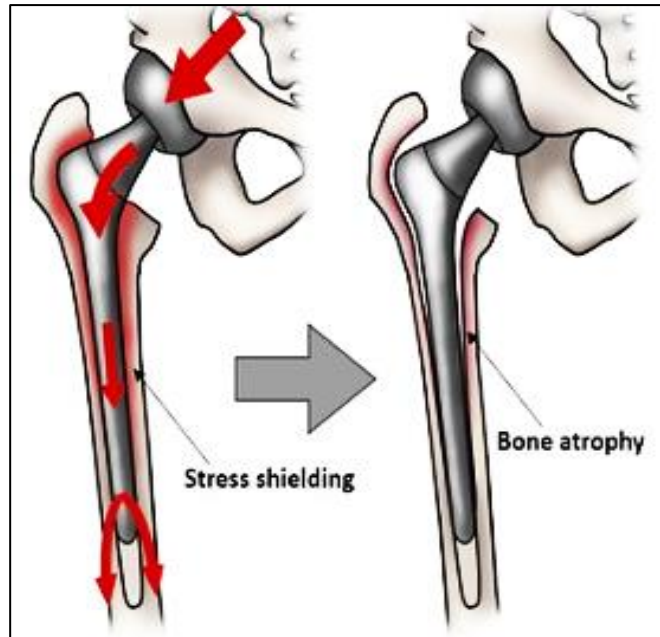


Fig. 1.4- Phenomenon of Stress-shielding in femur bone-implant (courtesy-Naim et al.[16])

The existing mono-material-based implants are inefficient because of their mechanical properties and bioactivity behaviour, and they sometimes cause toxicity due to the release of toxic particles/debris during use. Stress shielding occurs due to the more significant mismatch in mechanical properties in the case of metallic and high-load-bearing ceramic or polymeric material, which further causes the deterioration of existing bone and surrounding tissues. The main concern with an implant is its response to the tissue and its proper functioning. Recent advancements in biocompatible materials and design that mimic the bone architecture have shown minimization in these negative responses during its functionality [17]. Innovative/advanced materials must be designed to have functional properties according to the requirement to address the mechanical properties of artificial implants. Looking into the problems raised due to significant differences in mechanical behaviour and the need for functional properties, functionally graded materials (FGMs) emerge as the best viable solution to both issues [18].

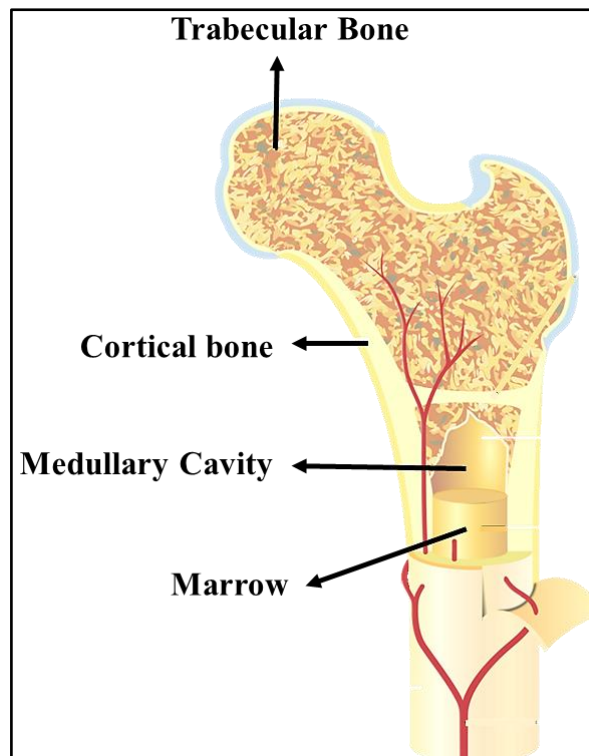


Fig. 1.5- Anatomy of the natural femur bone (courtesy- Qui et al.[19])

1.2.2 Issues Due to Tissue-Implant Interface

Implant retention is determined by interfacial phenomena such as friction or mechanical interlocking. Surface roughness influences its mechanical stability. Rough surface structures may stimulate the repair of bone tissue [20] and may also introduce mechanical effects in bone, such as interlocking due to bone growth into the surface. A better understanding of the bio-mechanical properties of newly formed bone around the implant interface may lead to a more accurate prediction of the surgical outcome of implant integration [21], preventing additional painful and expensive surgical interventions. Mechanical properties (shear properties, stiffness, etc.), surface properties (roughness, hardness, frictional properties, surface wear, etc.), and corrosion resistance properties of implant surfaces are essential to determine the interfacial behaviour of artificial implants for their suitable applications.

The phenomenon of osseointegration (healing of bone) is defined by Brånemark et al. [22]. The process of osseointegration at the implant-tissue interface is explained as follows: Just after surgery (**Fig. 1.6 a**), the implant surface is surrounded by blood (due to the reaming of the bone cavity) as well as dead and living bone tissues. Bone debris may also be present around the implant surface. During bone healing, several weeks/months after surgery, newly formed bone fills the gap between mature bone tissue and the implant surface (**Fig.**

1.6 b). Several weeks or months after the implant surgery, newly formed bone tissue is replaced progressively by mature bone tissue around the implant surface (**Fig. 1.6 c**).

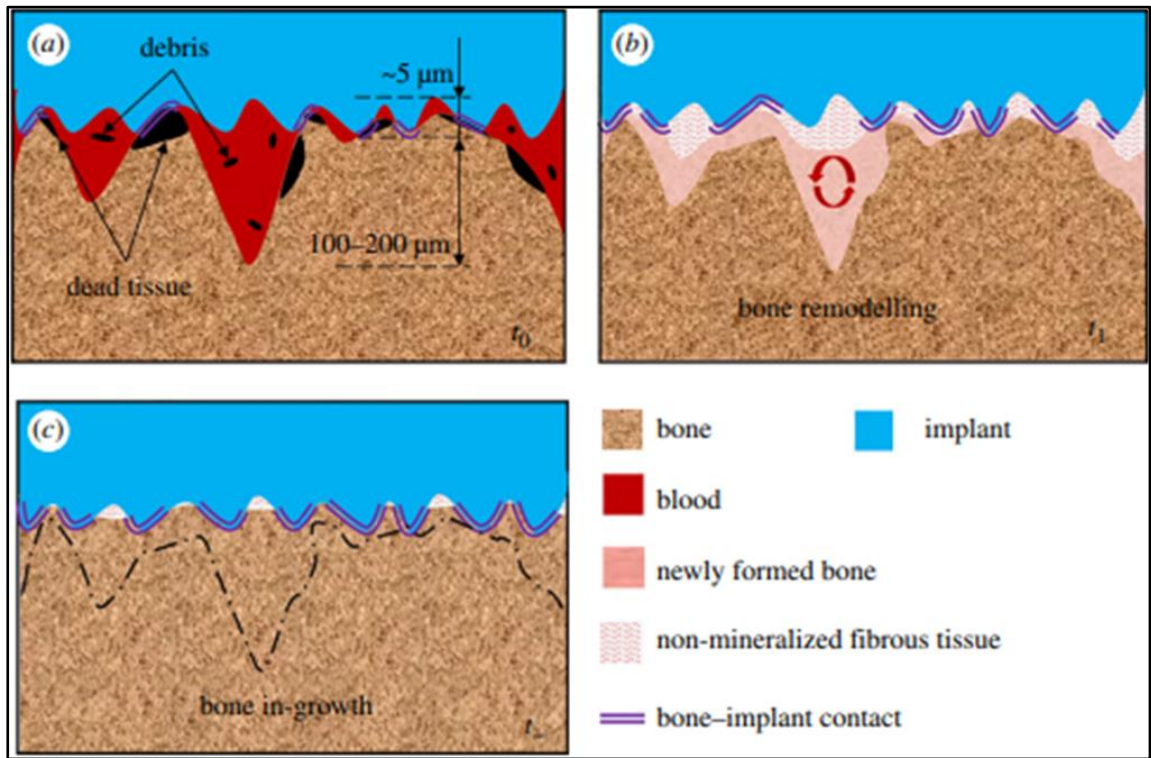


Fig. 1.6- Schematic of the bone-implant interface (courtesy-Gao et al. [23])

Mechanical rigidity, better mechanical and corrosive properties of different pure metallic materials used as implant material [24] since long back has limitations, i.e., stress-shielding effect, less bioactive, feeling of insensitivity, need of re-surgery, etc. Similarly, different bio-ceramics, having good biocompatibility properties, still have limited application in implant manufacturing because of their brittleness, low rigidity, and tough-to-process material [25,26]. Hence, there is a need to process metal and ceramic composites with their important contributing properties to develop an advanced and more reliable biomaterial for various implant applications. The concept of graded material could be another possible solution that may resolve the stress-shielding issue, and gradation with better biocompatible and soft materials can counter the implant-tissue interface issues [27]. The class of material that can be obtained by grading chemical/material/density/microstructure is termed Functionally Graded Material (FGM) (**Fig. 1.7**) [28]. Additionally, the developed synthetic biomaterials must have the desired biocompatibility and the properties to not harm the tissues for their usage as per the FDA guidelines.

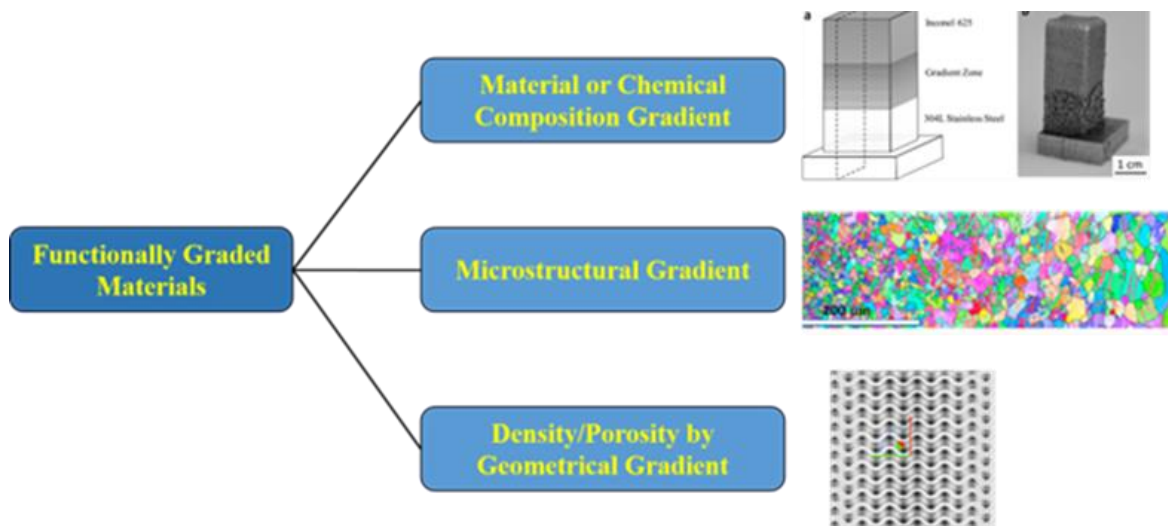


Fig. 1.7- Classification of FGM

1.3 Bio-Materials used for Implant Applications

Depending upon its end use, different materials, from polymers and ceramics to metals, have found their applications as bio-implant materials, depending upon their material characteristics and bioactivity [29–31]. Various lightweight polymers, such as poly-lactic acid (PLA) and polycaprolactone (PCL), are used as tissue replacements to treat wounds and as scaffolds to support other organs. Ceramics are primarily used for dental implants and as a scaffold to support high-load-bearing body parts. Similarly, metals are used primarily to replace high-load-bearing implants and manufacture biomedical surgery devices. State-of-the-art literature suggests that many metal-matrix composites emerge as a better alternative to metallic biomaterials with enhanced mechanical and bioactivity behaviour. Researchers tried to address stress-shielding and implant-tissue interface issues by combining different metallic, ceramic, and non-metallic materials with lower strength and enhanced biocompatibility compared to pure metallic material. Nonetheless, metallic or metal-based composite biomaterials [31–34] have been proven to be quite suitable for replacing hard bones, considering their mechanical and physical characteristics.

Table 1.1- List of popular biomaterials and their extensive properties and appropriate applications that can be used to design and fabricate Implants

Material and Alloy	Mechanical Property	Biological property	Applications
Titanium (Ti)	E- 100-110 GPa ρ - 4.5 g/cc	Biocompatible	Femur, Hip Cup, Dental Implants
Ti6Al4V alloy	E - 100-115 GPa ρ - 4.4 g/cc	Biocompatible	Femur, Hip Cup, Dental Implants
Iron (Fe)	E - 210 GPa ρ - 7.87 g/cc	Biodegradable	Implant Fixation and Medical Devices

SS 316L	E - 190 GPa ρ - 8.0 g/cc	Biocompatible	Implant Fixation and Medical Devices, Hip Cup, Maxillofacial Implant
CoCr	E - 240 GPa ρ - 8.5 g/cc	Biocompatible	Stent, Medical Devices
Magnesium (Mg)	E - 45 GPa ρ - 1.74 g/cc	Biodegradable	Scaffolds, bone-supporting implant
Tantalum (Ta)	E - 180-185 GPa ρ - 16.65 g/cc	Bioactive	High-load bearing Implants
Poly-lactic Acid (PLA)	E - 3-3.5 GPa ρ - 1.24 g/cc	Biodegradable	Cardiovascular Stents
Polycaprolactone (PCL)	E - 3.2 -3.7 GPa ρ - 1.14 g/cc	Biodegradable	Scaffolds
Hydroxyapatite (HAp)	E - 80-100 GPa ρ - 3.16 g/cc	Biocompatible	Dental, Scaffolds
Calcium Phosphate (CaP)	E - 80-100 GPa ρ - 3.14 g/cc	Biocompatible	Dental, Scaffolds

1.4 Characteristics of Biomaterials

Bio-materials can be defined as *"a material intended to interface with biological systems to evaluate, treat, augment, or replace any tissue, organ, or functions of the body"* [32,33]. Material properties can be characterized quantitatively using standardized tests under defined conditions. Once characterized, these properties can be used in conjunction with engineering design techniques to predict the behavior of the engineered product under the expected operating conditions. In biomedical applications, any material substituted into the human body should be highly acceptable to the biological system, with minimum adverse effects. Furthermore, the following factors that concern the healing process influence this process independently or as cofactors with other multiple factors. For example, mechanical properties would be very important for a hip-replacement implant because it would be expected to withstand heavy loads generated during walking, which can be as high as several times a person's body weight.

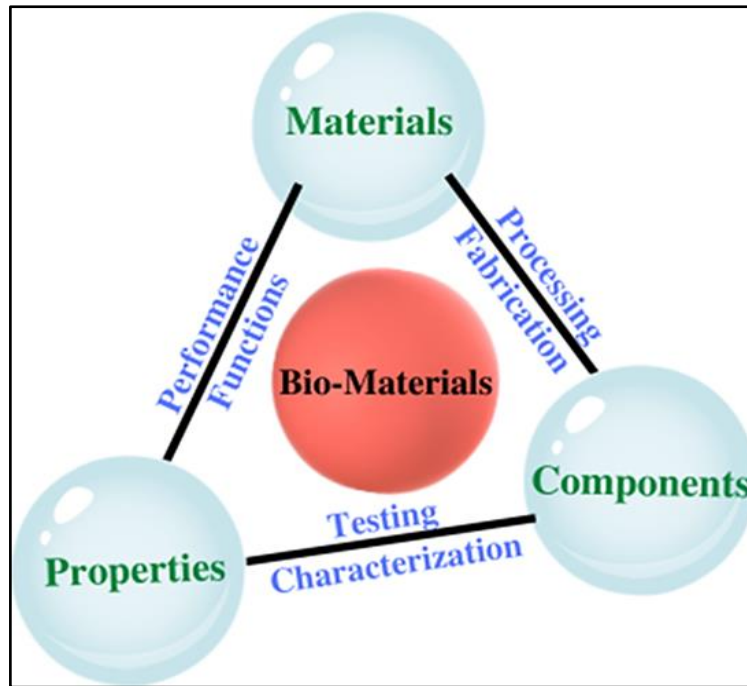


Fig. 1.8- Framework/Science of Bio-Materials evolution

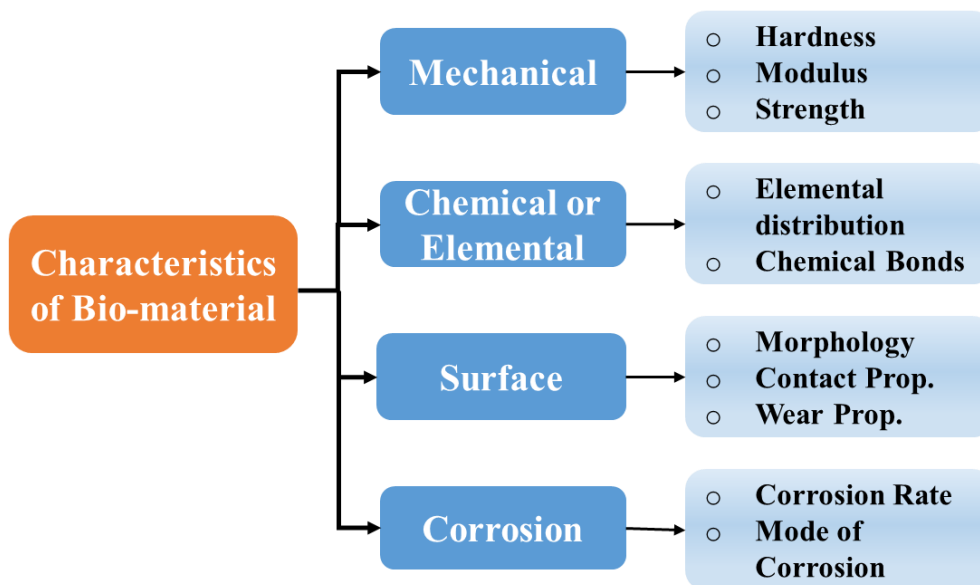


Fig. 1.9- Essential characteristics of a bio-material

1.4.1 Biocompatibility

A suitable biomaterial scaffold should not suppress the activity of normal cells and should be toxin-free during and after implantation [34]. Moreover, it should also create well-induced effects that may promote adhesion and healthy cell growth in the nanostructure microenvironment. This is mainly because of a larger specific surface area of nanostructures that can promote the adsorption of proteins, cell adhesion, and growth [35]. Hence, more attractive nanomaterials with good biocompatibility for biomedical

applications are being synthesized [8]. In the case of metallic implants, to have better cell adhesion, they should have a Ca: P ratio in the range of 1.6, and it may be detrimental to better apatite formation [36]. In academic research, in-vitro cytocompatibility tests are performed to study the biocompatibility of a material. Upon successful in-vitro studies, in-vivo tests can be performed on mice, rabbits, etc., with required ethical and clinical approvals.

1.4.2 Surface Properties

The surface of an Implant plays a vital role in its effective functioning. Surface roughness, hardness, coefficient of friction, wear-characteristics, wettability, etc., are the prime attributes that characterize an implant's surface properties. The biomaterial should demonstrate a high wear resistance and have a low friction coefficient when sliding over the body tissues. Any change of these parameters would structurally change the implanted biomaterial. The generated debris and metal ions can cause irritation and inflammation, leading to the destruction of bone structure, and in turn, the patient may need to undergo re-surgery.

1.4.3 Corrosion Properties

An implant made of a biomaterial with a low corrosion resistance can liberate metal ions in the body, resulting in toxic reactions. The implant functions in the presence of human body fluid and blood plasma, which may affect the implant surface by corroding and thus reducing the fatigue behaviour and effective life span.

1.4.4 Mechanical Properties

Good mechanical strength, load bearing, and load transfer are some basic properties an implant must possess. The mechanical strength of biomaterials has a broad range density. So, different geometries with different mechanical strengths have been designed to form ideal implants/scaffolds. Tensile/compressive strength, bulk modulus, shear modulus, stiffness, etc., are significant mechanical properties that must be tested for any load-bearing implant applications. Mechanical properties are prime characteristics that can control the stress-shielding effect of artificial implants.

1.5 Processing and Fabrication Methods

Bio-materials have been processed through various manufacturing processes to fabricate bio-implants and medical devices. These processes have evolved over time with scientific and technological development. Previously, the bio-implants were made via casting/forming followed by machining or finishing operations for metallic and ceramic

materials, whereas, for polymers, different molding processes were used. Bio-implant fabrication has become very convenient with the advent of additive manufacturing processes. There is a huge demand for the patient-specific implant, which has a long life, good mechanical, biological, and chemical properties, and is suitable for cytocompatibility.

1.5.1 Powder Metallurgy

Powder Metallurgy (PM) is a material processing technique that consolidates particulate material (i.e., powders of metals or non-metals). The PM process is a forming and fabrication technique consisting of three major processing stages. Firstly, homogenized powdered materials with small particles are prepared. Next, the powders are molded/compacted into the near-net shape of the required part through a die to produce a firm, cohesive bond between individual particles. Finally, the compacted parts were sintered at high temperatures and pressure for consolidation and densification.

1.5.2 Casting

Casting is the oldest manufacturing process used to fabricate bulk products using molten materials as raw materials. In this process, a liquid molten material is poured into the mold with the required shape/size as the final part, then allowed to solidify to get a final cast part. Different casting methods exist to synthesize composite materials, such as conventional casting, stir casting, centrifugal casting, etc. Stir casting is widely used to cast for synthesizing metal-matrix composites by stirring the melted metal and simultaneously adding reinforcements in the formed vortex. The stirring continues until the mixed melt converts to a molten/semi-solid state. Centrifugal casting is an advanced process used to fabricate hollow tubular kind of structures. This process is also widely used to synthesize compositionally gradient materials in bulk form [37,38], i.e., Functionally Graded Materials (FGM), by introducing different composition melt during the process at regular intervals.

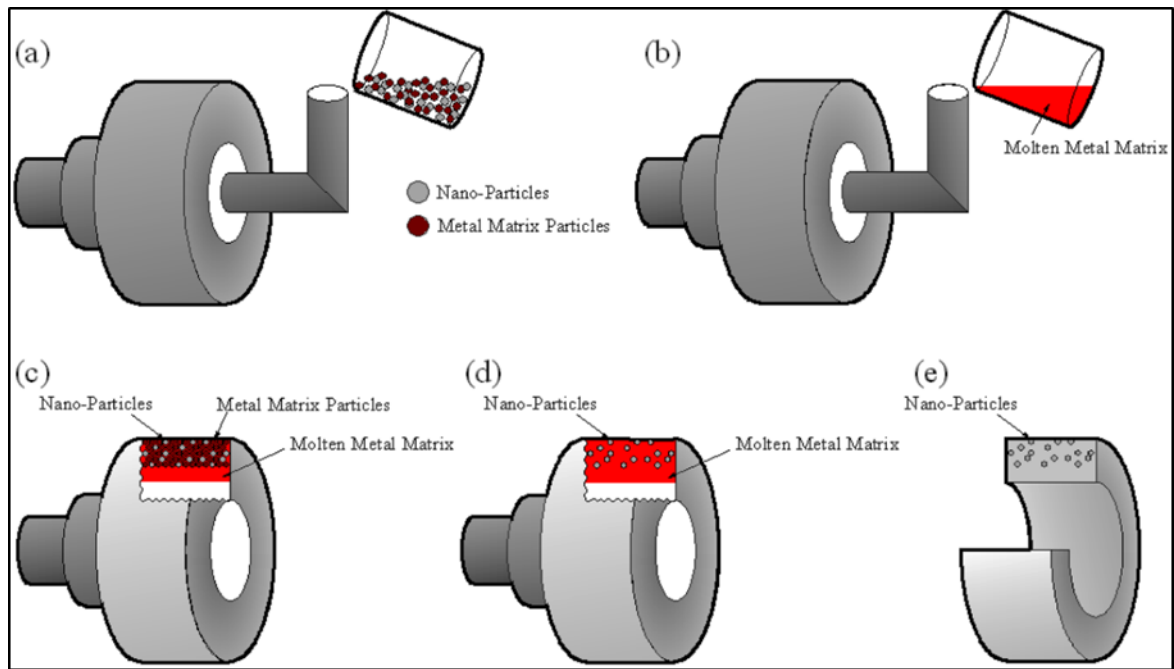


Fig. 1.10- Schematic representation of the process showing the centrifugal mixed-powder method (courtesy- Watanabe et al. [37])

1.5.3 Additive Manufacturing

Additive manufacturing (AM) is a layered material addition process to fabricate 3D components with the help of CAD geometry. AM has been classified into different categories depending on the type of material and physics used for material deposition/addition. Different AM processes have the capability of fabricating complex geometry as well as micron-sized features. Hence, AM processes are suitable for mimicking and fabricating the complex architecture of human bone. Stereo-lithography uses liquid resin of different photopolymers as raw material to make bulk parts, and this process is used to fabricate photopolymer-based implants. At the same time, polymer filaments are used for fabricating 3D bulk parts through the extrusion principle using the fused deposition modeling (FDM) process. Selective Laser Sintering (SLS) and Selective Laser Melting (SLM) processes are used to fabricate metal and ceramic-based implants using diffusion of fine powder particles with the help of a highly intense laser source. The SLM is widely used to fabricate near-net-shaped parts of metallic materials with greater accuracy.

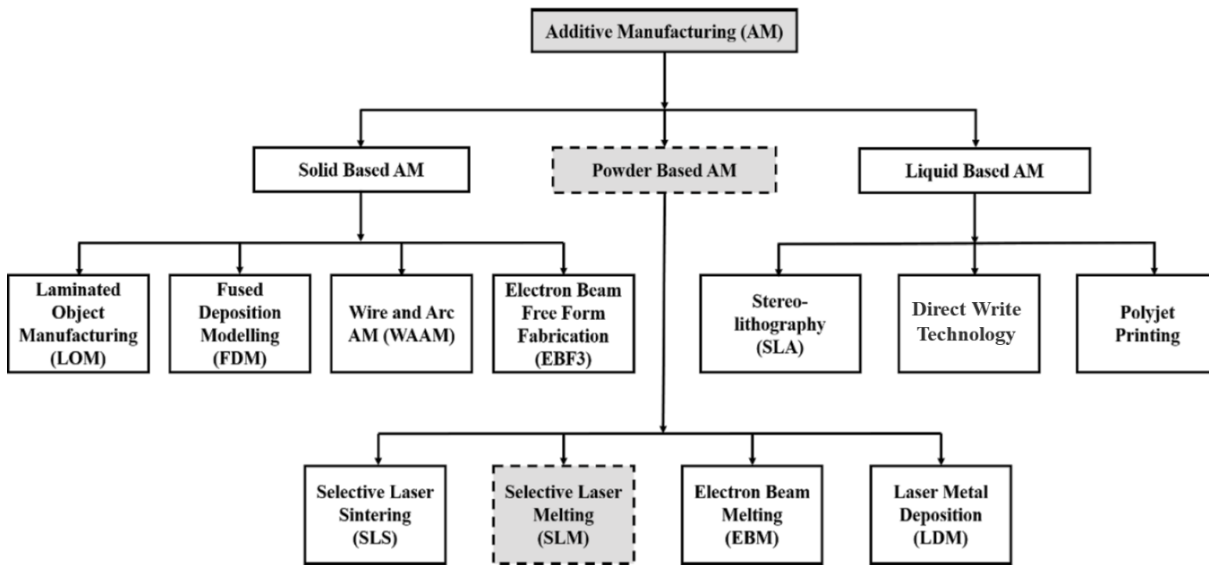


Fig. 1.11- Classification of AM Processes

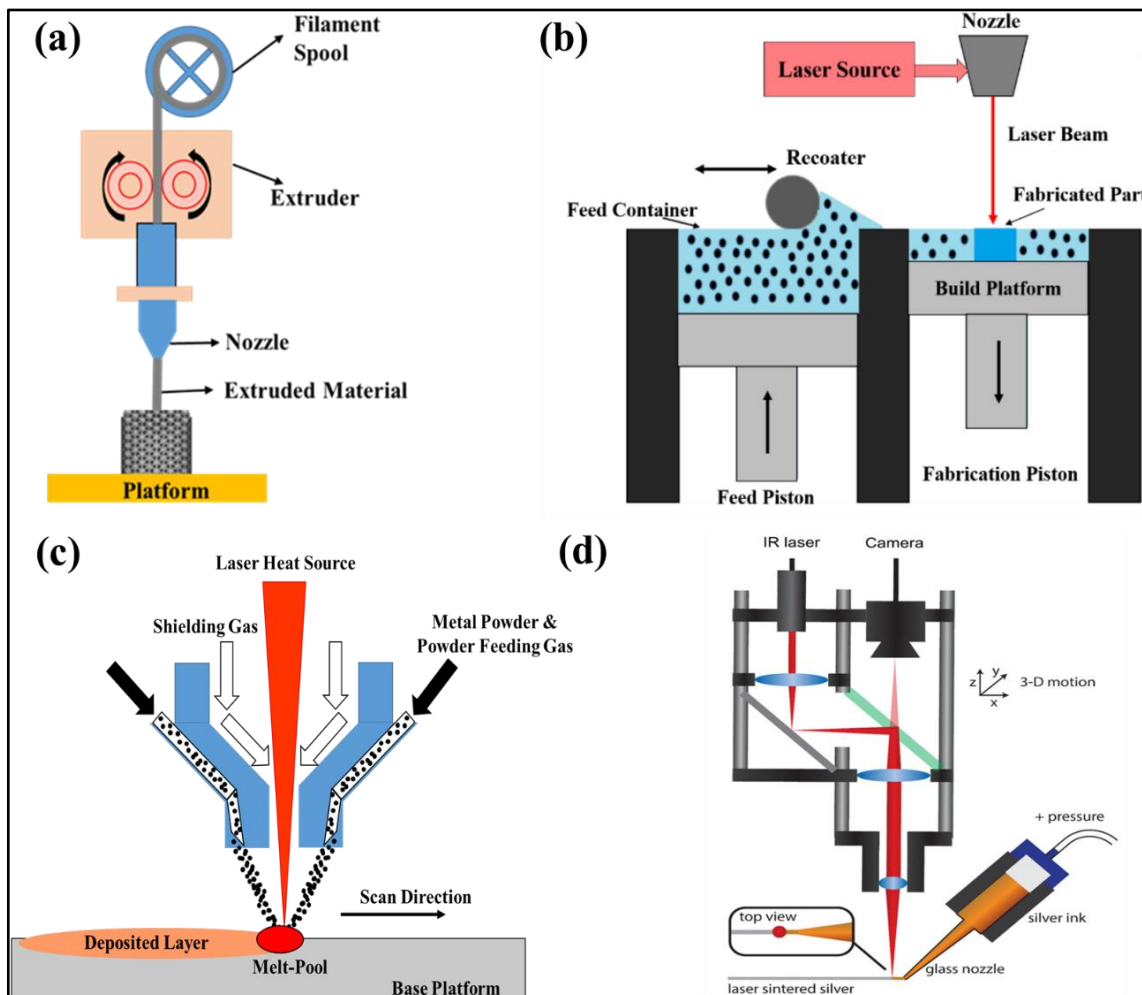


Fig. 1.12- Schematic representation of different AM processes, (a) Fused Deposition Modeling process, (b) Selective Laser Melting Process, (c) Direct Energy Deposition Process, (d) Direct Write Technology.

Chapter-2

Chapter 2

Literature Review

This chapter discusses the background of the development of biomaterials and their explanation for bio-implant applications. The chapter covers all aspects of developing advanced bio-materials, their fabrication processes, testing methods, and the relevant characteristics for different bio-implant applications.

There is a long history of biomedical implants and bio-materials. A brief timeline of the development of biomedical implants is presented below

- 3000 BC- Ancient Egyptians were the first to use a coconut shell as an injured skull and wood and ivory as false teeth.
- 1759 AD- Wooden pegs and twisted threads were used to bind the edges of torn brachial arteries.
- 1891- **Themistocles Gluck** [39] documented the first hip implant surgery as a ball-and-socket joint fashioned in Germany. This ivory was used because of its low cost, which further turned out to be a good material for human body tissue due to its good biomechanical bonding abilities.
- 1880-1900- with the invention of the first plastic as celluloid as a replacement for ivory, mostly used as billiards balls. With this revolutionary invention, plastic implants were introduced.
- 1940s - 1950s- During the Second World War, surgeons came across the potential benefit of man-made biocompatible plastic medical materials. In 1950, the knowledge about plastic and surgical techniques led to the development of the first pacemaker and modern ball-and-socket hip joint replacement.
- In the early 1960s- Canadian scientists McCulloch and Till recognized the presence of stem cells. Another invention introduced the first artificial disc known as the Fernström Ball and Polyethylene (PE) was used for the first time for hip replacement by Sir John Charnley.
- In the 1970s - 1980s, biomedical materials like Lycra, Teflon, Goretex etc., came into existence, and the first shoulder arthroscopy was performed.
- 1990s- Inspired by a wave of trials in the US against producers of silicone implants, the regulations surrounding biomedical materials were tightened up. This, in turn, led to further investment in specially formulated biomedical materials.
- In the mid-1990s, Research in tissue engineering started, and Carticel was the first product approved for marketing in the United States in 1996. In subsequent years, more development took place in skin substitution, knee cartilage repair, and bone repair.

- The 2000s: Further strides were made in the field of biomaterials, as a growing understanding of cellular and molecular ‘biocompatibility’ enabled advances in ‘biomimetic,’ the creation of man-made materials that mimic the materials in the natural world.
- Early 2000s: The invention of regenerative medicine received a further lift after research proved that so-called ‘adult’ stem cells are present in more tissues than was previously thought. The high levels of plasticity in these adult stem cells made them more adaptable to regenerative medicine.
- 2004- The introduction of innovatory Dyneema Purity Fibres (polymer fibers) strengthened the biomedical fibers developed thus far. These fibers enable faster healing and less expensive, smaller-scale surgery such as shoulder arthroscopy.
- 2008- The breakthrough development of Freedom Lumbar Disc (FLD), developed by Axiomed, a US medical devices company, improves the life of implants. This FLD is made up of metal endplates, which are porous and coated with titanium beads for osseointegration and a viscoelastic polymer (silicone polycarbonate urethane polymer) articulation.
- 2010s- The increased application of Additive Manufacturing in the medical field makes complex-shaped implants easy. It has also strengthened the research in the area of biomedicine in terms of rapid production.
- Post-2010- At this time, most of the growth has happened in the area of composition and alloying of materials to improve the strength and applicability of the newly developed materials.

2.1 Classification of Implants

Food and Drug Administration (FDA) of the United States regulates the use and application of medical implants [1]. The most important criteria are that the medical implant is intended to affect the structure or function of the body and not achieve its purpose primarily through chemical action, which is true for drugs. As per the regulatory control of medical devices by the FDA, medical devices are classified into three categories, i.e., Class-I devices with the lowest safety risk (elastic bandages, examination gloves, and most handheld surgical instruments, such as the arthroscope). This class of devices does not require much scientific evaluation. Second, comes the Class-II devices, which need to have more control, performance standards, and adequate surveillance to ensure safety. Under this category, devices used in orthopedic surgery include imaging devices, such as PACS, X-ray machines, fluoroscopes, surgical needles, suture material, infusion pumps, surgical drapes, etc. Then comes the Class-III category of devices, which must undergo scientific review detailing the safety and effectiveness of the device in order to obtain Premarket

Approval (PMA). This is the most scientifically rigorous classification of medical devices and encompasses most orthopedic devices, as these will be life-supporting and sustaining. In orthopedic trauma, Class-III devices include fixation devices such as intramedullary nails, cannulated screws, spine, hip, knee, plates, and external fixators etc. In this thesis work, the biomaterial that will be studied considers class III-related implants/devices. Class-III implants usually carry the maximum of the body loads and undergo wear and tear upon its substitution in the human body. The orthopedic implants are usually bone and joint replacement devices, and they must be made with a material with superior properties and good bioactivity and bioresorbable properties to allow the formation of an extra cellular matrix (ECM) upon implantation for tissue and cell growth [40].

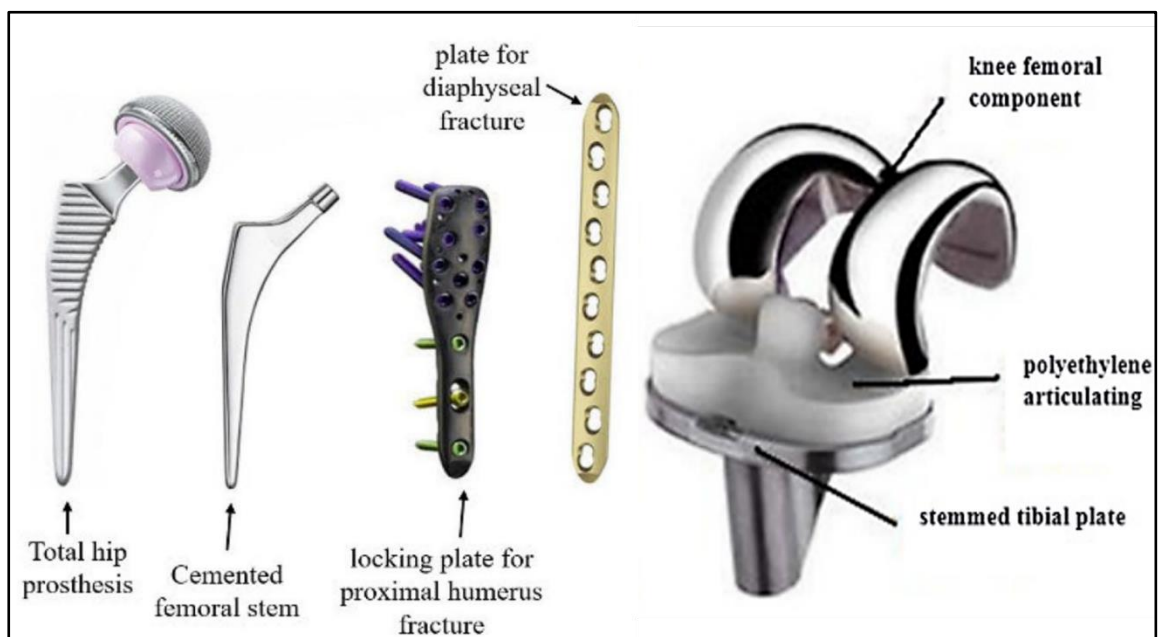


Fig. 2.1- Examples of a few Class-III load-bearing implants (courtesy- [41,42])

2.2 Modern Bio-Materials

Several engineering materials (metals, polymers, ceramics, synthetic materials, etc.) are emerging as innovative materials that are being used as implant materials [33,43]. These materials possess enhanced properties as compared to conventional materials used for decades.

Titanium and its alloys- Titanium (Ti) has been a widely researched material in recent years due to its superior properties and resource abundance. It has wide applications in different industries due to its high strength-to-weight ratio and non-corrosive behavior. The biocompatibility of Ti and its alloys has made it very popular in biomedical and health industries [11,44,45]. Ti-based alloys' mechanical strength and high wear and corrosion resistance make them the most suitable choice for orthopedic and high-load-bearing

implants [14]. The modulus of Pure Ti is about 110 GPa, which is much higher than the modulus of the cortical bone (i.e., 3.9-11.7 GPa [46] and the cancellous bone (i.e., 0.1-2 GPa [47]). Of the various studies on the tribological behaviour of Titanium and its alloys [14,48], most are related to coating the Ti surface with different metals and non-metals to improve its surface properties [25,49–52]. Ureña et al. [53] studied the influence of β -type Ti-Nb and Ti-Mo surfaces over powder metallurgy processed pure Ti using diffusion treatment and determined their tribo-corrosion and wear behaviour through electrochemical impedance spectroscopy (EIS) and tribo-electrochemical measurements, respectively. A similar kind of attempt has been made by Rahmati et al. [54] to study the corrosion behaviour of thin film coating of TaO₂ over Ti-6Al-4V alloy using physical vapor deposition magnetron sputtering, and it was tested in the presence of fetal bovine serum for corrosion and wear characteristics. The electrochemical corrosion properties of HEBM alloyed Ti6Al4V were also tested with simulated body fluid [55].

Magnesium and its alloys- Magnesium (Mg) and its alloys are light-weight material (density 1.76 gm/cc) and have lower mechanical strength (near about cortical bones) with a potential to serve as biocompatible, osteoconductive, degradable implants for load-bearing applications [56]. The rapid corrosion rate of magnesium in the electrolytic physiological environment is one of the most significant limitations of its use in orthopedic applications [57]. Researchers have observed that Mg-Zn, with heat treatment, shows better corrosion resistance and enhanced bioactivity due to grain refinement and can replace existing orthopedic fixation devices [58]. Tiyyagura et al. [59] coated the Mg surface with cellulose- and chitosan-based polymers; the study revealed a reduction in corrosion rate with improved mechanical properties and increased cell adhesion compared to pure Mg.

Tantalum-based Biomaterials- Tantalum (Ta) has emerged as a potential biomaterial for dental and bone implants because of its reported better anti-corrosive and osseointegration properties compared to Ti-alloys [60]; however, due to its tough processability, high cost, and limited availability, it is not widely used yet. Ta can be useful as a hip-implant, knee arthroplasty, and spinal surgery [61,62]. Porous Ta has a high volume-porosity with fully interconnected pores that show potential for secure and rapid bone ingrowth [63]; therefore, developing a porous structure using this material is gaining interest. Ta has been used as a coating as well as in bulk with Ti-alloys to enhance the corrosion properties [54,64].

Polymeric Biomaterials- In the past, a lot of researches has been carried out to fabricate various kinds of scaffolds using different polymers. When going over the

literature, it was found that polymers like poly(glycolic) acid (PGA), poly(lactic) acid (PLA), chitosan and its co-polymers, and poly-caprolactone (PCL) are often used as raw material for fabricating scaffolds [65]. Out of these, PLA is the most widely used bio-polymer material, which finds its use in pins and screws for orthopedics [66], bone scaffolds [67], and devices for the controlled delivery of drugs [68]. Gong et al. [69] have performed strain-controlled fatigue testing on porous PLA-based scaffolds obtained via 3D printing. Santoro et al. [70] have used poly(lactic) acid to make nano-fibrous scaffolds, which has increased the probable uses of PLA scaffolds in the field of drug delivery systems and regenerative medicines. Senatov et al. [71] worked with PLA and 15 wt.% hydroxyapatite to fabricate porous scaffolds and tested its mechanical properties and shape memory effect.

2.3 Metal-Ceramic Bio-Composites

Literature suggests that Metal-Ceramic-based composites can be used as implant materials with better feasible mechanical and biological properties. Thus, researchers have explored different metal-ceramic-based bio-composites for load-bearing implant applications. SS316L with 20-30% HAp has been synthesized using the powder metallurgy process [72]. Zr and ZrN-based ceramic coatings have been used with SS316L implants, and their mechanical, tribological, and electrochemical properties were studied [73]. CoCr-HAp-based composites have been synthesized and tested for electrochemical and tribo-corrosion behaviour [74,75]; the result reveals that the addition of HAp in CoCr reduces the corrosion rate, as well as lower Coefficient of Friction, was obtained during tribo-corrosion studies.

Titanium is a widely accepted biomaterial, and its composites with different ceramics and non-metals enhance its performance as a biomaterial. Ti-based composite (Ti-35Nb-2.5Sn-15-HAp) exhibits Young's modulus of about 20-22 GPa with 5.7% compressibility, which is close to the natural bone's modulus [76]. The material has shown good cell viability and proliferation. Nanocomposite using TiO and Zr powder has been synthesized, and its fracture toughness, wear characteristics, and corrosion properties have been studied for its applicability as hard bone tissues [77]. Morsi and Patel [78] studied the processing method and various Ti and TiB composite properties for possible orthopedic applications.

2.4 Synthesis and Processing of Bio-composites

Synthesis of bio-materials, particularly bio-composites, is challenging due to their peculiar properties. Powder metallurgy and casting processes are conventional ways of synthesizing metal matrix bio-composites. Conventional and microwave sintering processes are widely used to sinter MMC-based composites. The advantages of microwave sintering are its high and uniform heating rate, reduced contamination, etc. It has been

explicitly explored for different metal-based materials [79,80]. Researchers have explored multiple approaches to effectively sinter ceramics, e.g., multistage sintering, controlled/variable rate of heating [81], microwave sintering, and, more recently, using microwave hybrid heating (MHH) [82] etc. Spark plasma sintering [83,84] and laser sintering are advanced methods for composite processing and are widely accepted by researchers. The advantage of Spark plasma sintering is its compaction while sintering itself, which results in higher density and strength in the sintered parts. Novel porous Ti₃₅Zr₂₈Nb scaffolds have been fabricated using the PM process to study biocompatibility and bone-tissue engineering applications in orthopedics [85]. The mixing/alloying of HAp with different metallic biomaterials enhances bioactivity. Ti-10Nb-10Zr [86] based alloys have been sintered at varying temperatures to study their effect on porosity, microstructure, and mechanical properties. The samples fabricated at 1300°C and 1400°C exhibit suitable operating conditions for Ti-based alloys due to obtained porosity and compressive strength. Prakash et al. [87] fabricated low-modulus Ti-Nb-HA composites by microwave sintering with 50-60% porosity having 15-29 GPa modulus of elasticity and enhanced tissue growth and osseointegration. Later, Xu et al. [88] attempted to deposit a thin film of Ti-Nb-Si-N nanocomposite with varying compositions of Nb onto a Ti-alloy substrate exhibiting higher corrosion resistance and hardness compared to TiN and TiSiN coatings. Singh et al. [89] developed a Ti-matrix composite by spark plasma sintering and reinforcing TiB₂ particles with Ti₆Al₇Nb using low-energy ball milling. Researchers have fabricated different metal-metal FGMs effectively using powder metallurgy techniques (Al-Steel [90], SiC/Al-7Si-0.3Mg [91], etc.).

Selective laser sintering (SLS) and selective laser melting (SLM) are layered processes for fabricating bulk metal composites [92]. These processes are relatively newer and more flexible regarding complex part fabrication [93]. The additive manufacturing for composite processing is limited due to the non-availability of process parameters for such materials. The additive manufacturing process enables the use of multi-materials for the fabrication of implants with proper selection of material and process parameters [94]. The AM process's advantage is that it enables lattice-based porous structure design fabrication and implants with controlled porosity [95].

2.5 Bulk Mechanical and Tribological Behaviour of Bio-Composites

Bio-composites to be used as implant material should have enough strength and rigidity to withstand load and movement caused by the human body. However, metal-based materials possess much higher strength compared to natural human bone, which causes stress-shielding and affects the tissue and implant interface. A material with modulus

values in the range of 10-20 GPa (near the modulus of cortical bone) will be considered to be most suitable for implant applications. Combining different biocompatible elements (Ca, Zn, & Nb) with Mg significantly increases the bulk density and ultimate compressive strength compared to pure metallic Mg material [96]. The surface texture of implants improves surface wettability and tribological properties and allows better cell adhesion properties [49,97]. Tribology and wear resistance of a bio-material are crucial properties used for joint replacement implants, as replacement joints fail due to complications of the basic wear and debris generation process [98]. Thus, the longer life of replacement joints has consequently concentrated on developing materials and designs that minimize the generation of wear particles. The addition of ceramics improves wear properties and the life of an implant [99].

2.6 In-Vitro Mechanical and Biological characterization

Bio-implants are surrounded by biological fluids, blood plasma, and different naturally occurring body serums. The implants have to function in the presence of these liquids that contain salts of various minerals (i.e., Ca, Na, K, Mg, etc.) having a pH value of 7.4, which makes a reducing surrounding environment for metals and metal-alloys. This causes corrosion and degradation of implants rapidly during its service inside the human body. In-vitro testing studies the mechanical behaviour of implants/biomaterials in similar conditions [100]. An environment closed to the actual is created, and the samples are tested in it. This is an artificial physiological fluid called simulated body fluid (SBF). Researchers have evaluated different wear and tribological characteristics under in-vitro conditions to study the suitability of their proposed biomaterials [101,102]. Further, to study the bioactivity (cell culture and proliferation study), in-vitro cytocompatibility tests are performed using external seeding cells in the presence of suitable culture media [103,104].

2.7 Research Gaps

An implant should have good mechanical properties as per its applications under different loading conditions. Depending upon loading conditions, implants are classified into two categories, i.e., high load bearing (e.g., Hip-cup, femur replacement, knee implant, etc.) and low load-bearing implant (e.g., dental Implant, maxillofacial Implant, etc.). High load-bearing bones possess different structural and mechanical characteristics along their cross-section; this implies that an implant must have tailored material, porosity, and mechanical characteristics to replace such body parts. This tailoring may not only mimic the actual bone architecture and structural behaviour; instead, using suitable material can somehow resolve the stress-shielding issue between the implant and existing surrounding bone and tissues. The stress-shielding causes loss in bone density and aseptic loosening,

increasing the chances of periprosthetic fracture [105]. The tissue-implant interface characteristics of an implant have a vital role in an effective implant. Designing and fabricating an effective implant with optimum surface characteristics is still a big challenge, and a lot of research is going on to improve the interfacial properties.

2.8 Objectives

The main issue with an implant is its response to the tissue and its proper functioning. Recent advancement in the development of biocompatible material mimicking the body tissue has shown minimization in these negative responses while its functionality [106]. Plastics were widely used as bio-implant materials due to their easy processing, but recent research shows that biocompatible metals and ceramics are replacing plastic polymers in a majority of cases. These metals and ceramics have better mechanical and physical properties as compared to plastics. To address the mechanical properties issue of artificial implants, materials that will have functional properties according to the requirement have to be developed. Developing functionally graded materials (FGMs) can be the best possible solution. FGMs are specifically designed materials with gradient-tailored properties. In this, the property of material varies along different sections/orientations.

The following are the objectives of this thesis work,

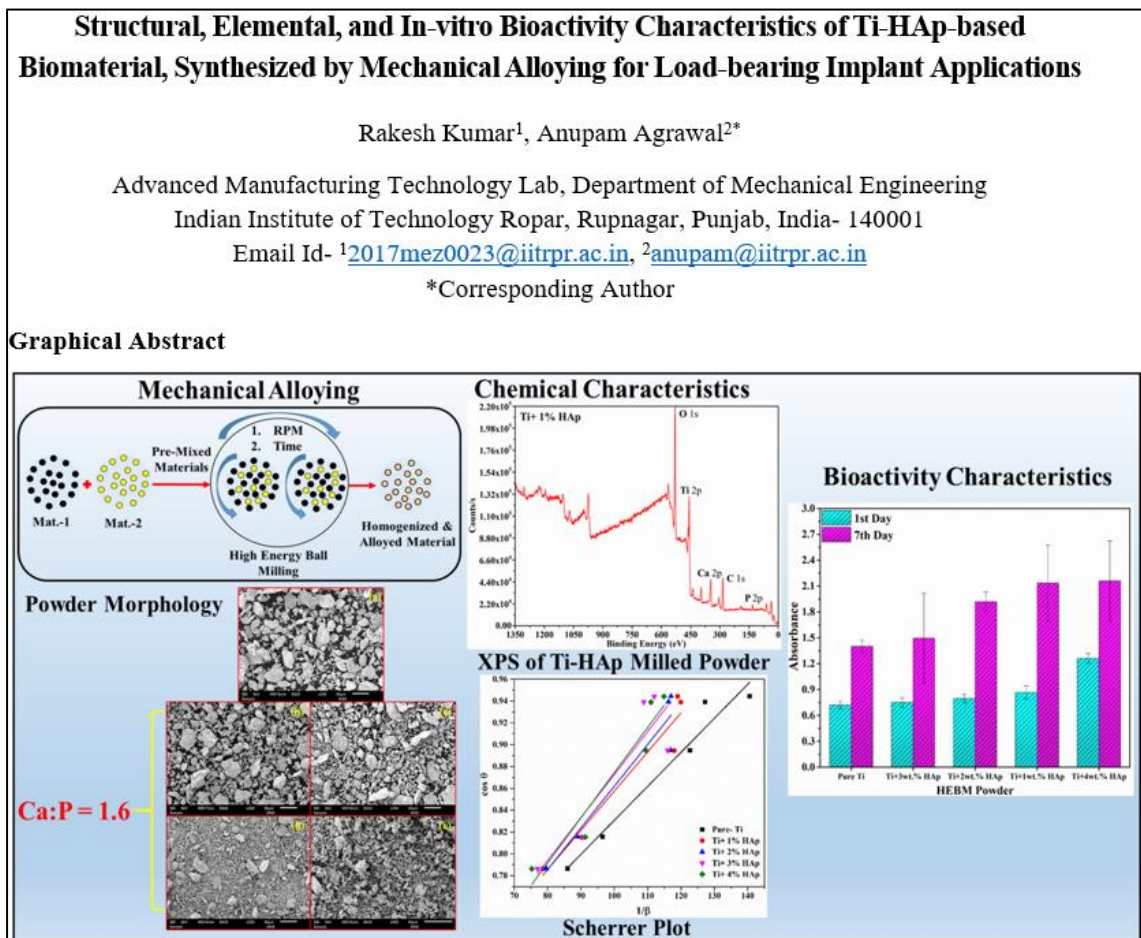
- ❖ Synthesis and characteristics of homogenously alloyed Ti-HAp powders using the HEBM process
- ❖ Fabrication of Ti-HAp-based bio-composite using PM technique and its mechanical, tribological, and in-vitro biological characteristics
- ❖ Fabrication and characterization of Ti and HAp-based Functionally Graded Bio-composite through PM technique to minimize stress-shielding effects

Chapter-3

Chapter 3

Processing and Characterization of Ti-HAp-based Bio-Material

This chapter discusses the first objective of the present work, i.e., the synthesis of Metal-Ceramic-based homogenously alloyed material for load-bearing implant applications. The synthesized materials were then comprehensively characterized for their morphological, chemical, structural, and biological properties.



3.1 Selection of Raw Materials and its Characteristics

In the present study, a biocompatible metallic material and a bio-ceramic, i.e., Ti and HAp, have been used as raw materials to develop bio-composites. Commercially Pure Ti (CP-Ti with ~ 97% purity) of average mesh size 120 and micro-sized HAp (μ -HAp) bio-ceramic having a mesh size of 270-300 has been used as raw materials (**Fig. 3.1**). It was processed through High Energy Ball Milling (HEBM) to prepare the desired biomaterial. Ti is a metallic element with a hexagonal closed-packed (HCP) crystal structure. It has a low density and thermal conductivity and is pronounced as ‘tough to machine’ with a ‘high

strength-to-weight ratio' material. It exhibits superior biocompatibility compared to Iron-based metals and alloys. Hydroxyapatite (HAp) is a naturally occurring mineral in the form of calcium apatite and is classified as bio-ceramic, having the chemical formula $\text{Ca}_{10}(\text{PO}_4)_6(\text{OH})_2$. It can be synthesized using several methods, such as wet chemical deposition, biomimetic deposition, sol-gel route (wet-chemical precipitation), or electrodeposition [107,108]. The raw materials were inspected for their purity by calculating the elemental distribution through Energy Dispersive X-Ray Spectroscopy (EDS) equipped SEM (**Fig. 3.2**).

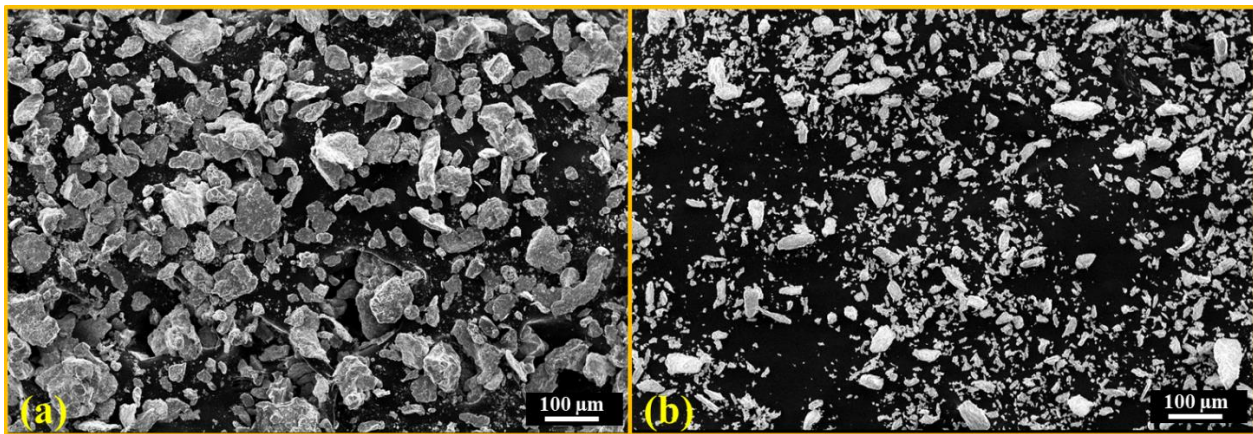


Fig. 3.1– SEM Image of as-received irregularly shaped raw powders used in the study (a) Pure-Ti, and (b) μ -HAp

3.2 High Energy Ball Milling (HEBM) of Raw Materials

A process called “mechanical alloying” (MA) had been developed, which produces homogeneous composite particles with an intimately dispersed, uniform internal structure. Mechanical alloying (involving two or more materials) are generally referred to as high-energy ball-milling (HEBM) techniques employed to process materials in the solid state. HEBM is one of the effective processes for fabricating metal-ceramic composite powders as it allows incorporation of the ceramic phases into the metal particles. HEBM is a solid-state alloying and homogenization process. This powder material is alloyed using high-speed rotation of milling jars containing hard ceramic balls with raw powder particles to impart high binding energy. The high binding energy allows diffusion of two distinct powder particles and results in a homogenous mixture of particles with unique properties (**Fig. 3.3**). The premixed pure-Ti and 1- 4 wt. % μ -HAp powders are milled using Fritsch Pulverisette-5 planetary ball mill at 400 RPM for an effective 4hrs. The ball-to-powder ratio is maintained at 10:1 to homogenize powder particles properly. The high milling speed, collision frequency, and impact energy cause aggregation of milled powder particles. Thus, an intermittent rotation with to and fro movement (clockwise and anti-clockwise in consecutive cycles) with a dwell time of 10 mins after each rotation of 15 mins is used. This

allows the milling jars to cool down and eliminate the possible weldment of powder particles with the jar and balls. Hence, uniformly dispersed and homogeneously alloyed powders have been obtained after the HEBM process.

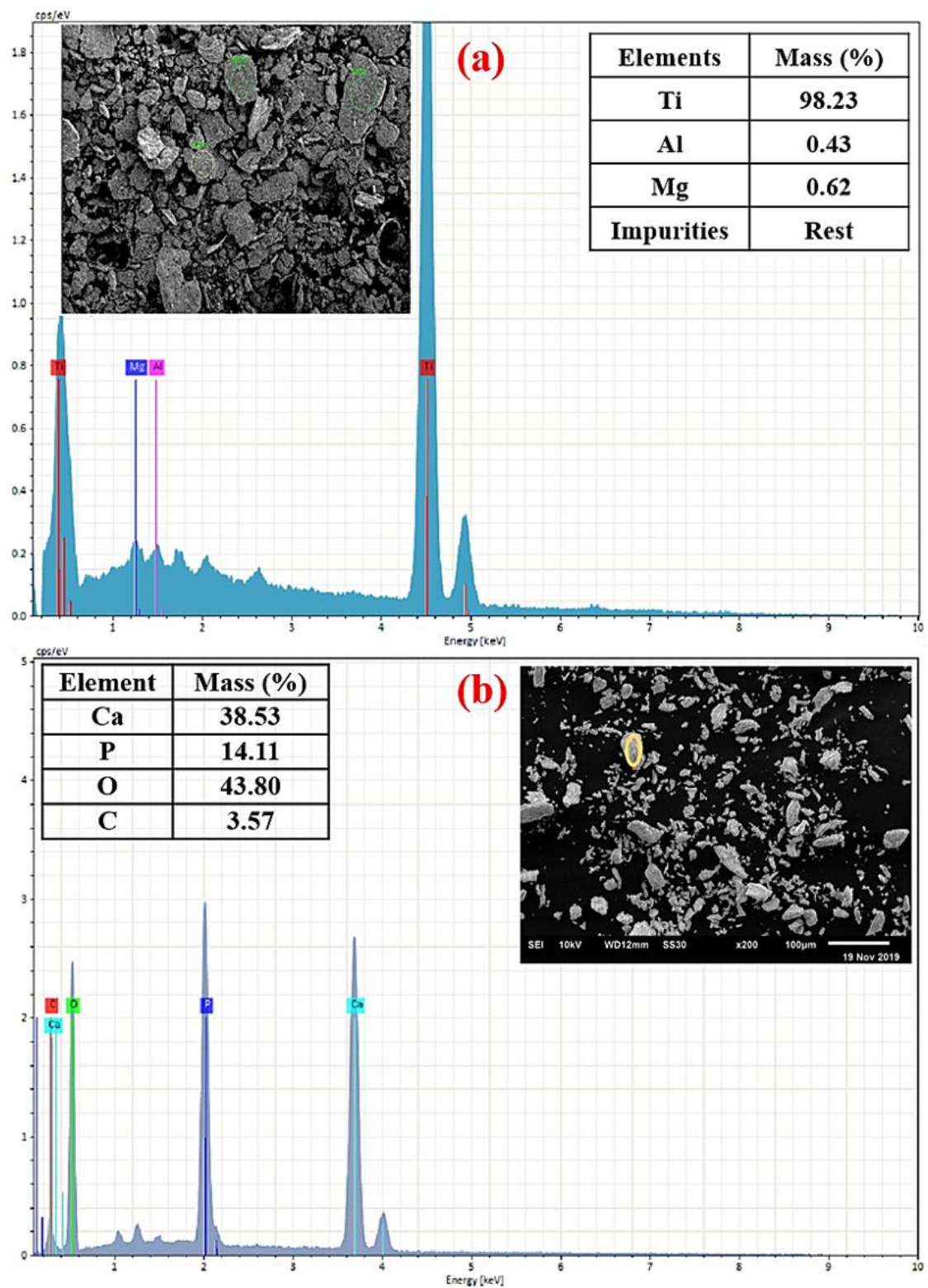


Fig. 3.2- EDX-based elemental composition results of raw materials (a) Pure-Ti, (b) μ -HAp

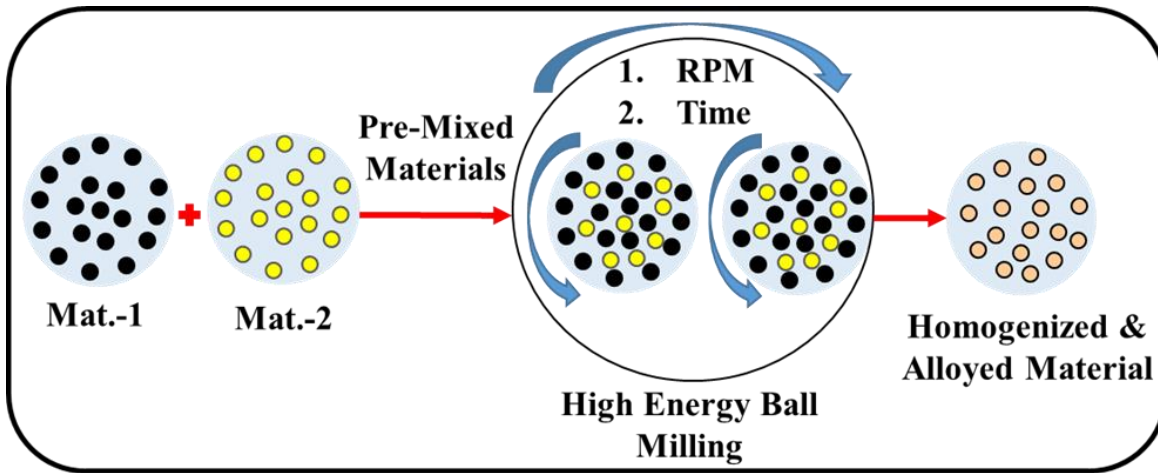


Fig. 3.3- Schematic representation of the HEBM process used to synthesis the bio-material

3.3 Phase and Morphology of HEBM alloyed Powders

3.3.1 Phase and Crystalline Characteristics

The HEBM alloyed powder has been inspected using XRD to study the phases, crystalline size, and related crystalline information. The XRD plot of HEBM Ti- μ -HAp based alloyed powders with varying compositions is presented in **Fig. 3.4**. The obtained XRD patterns have been matched with JCPDS file no. 21-1272 (for Ti) and JCPDS file no. 09-0432 (for HAp) to detect the exact peak location and its identification. The obtained diffractogram of processed Ti- μ -HAp-based alloy in this study is very similar to the work of [Niespodziana \(2019\) \[109\]](#). The sharp and distinct peak for all samples signifies that it retain the crystallinity even after the high energy interaction due to milling. However, the crystallinity of the inspected milled powders decreases with increasing HAp constituent, and it may be due to the occlusion (entrapment/absorption of one material inside the other) and strain effect of the resultant powders. The minor peaks at 40-50° for pure-Ti powders get diminished with the addition of HAp, exhibiting a reduction in crystallinity with increasing HAp and proper alloying of the samples. Various characteristics that can be drawn using XRD data, i.e., crystalline size, peak broadening characteristics, and strain characteristics, have been studied in the powders using various characterization approaches. Bragg's law (**Eq. 3.1**) determines the inter-planar spacing and phases of peaks to characterize the milled powders. The calculated average inter-planar spacing for the significantly distinct peaks of the milled powders has been 1.76 Å.

$$\text{Bragg's equation- } d\text{-spacing or Inter-planar Spacing, } d = \frac{n\lambda}{2 \sin \theta} \quad (3.1)$$

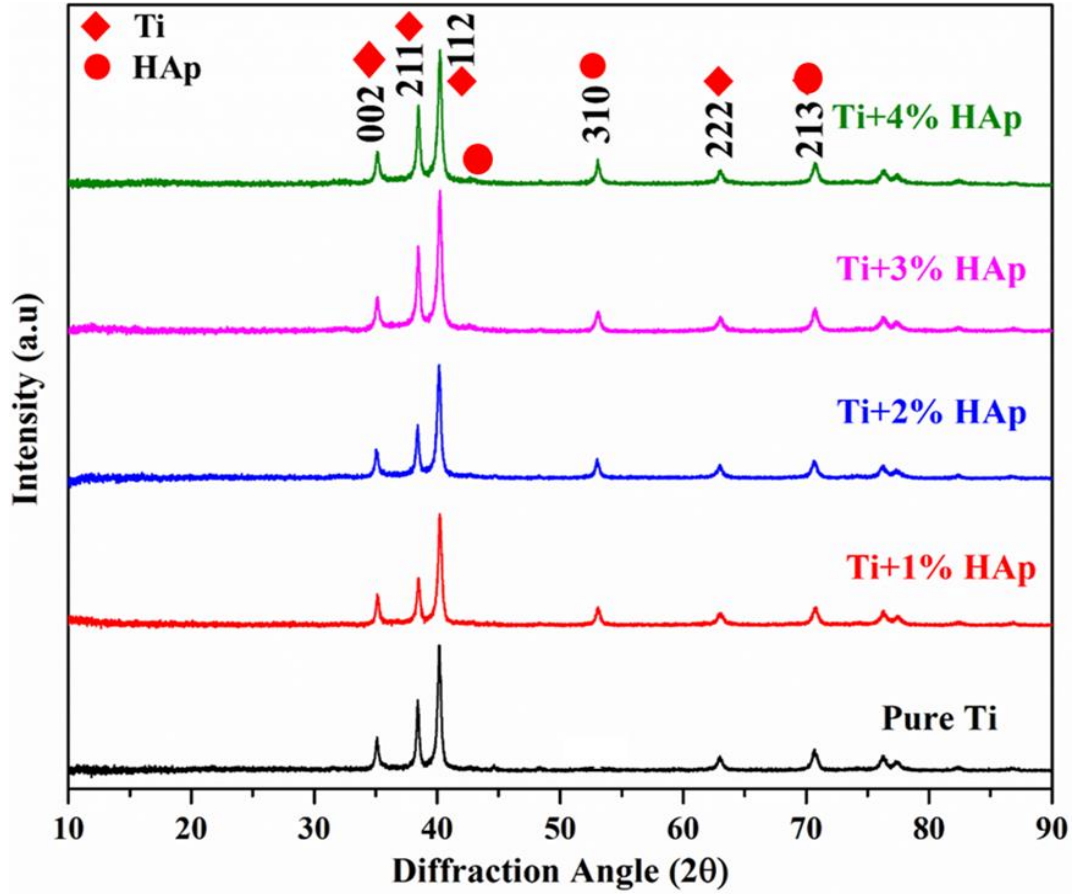


Fig. 3.4- XRD plots of Pure Ti and Ti+ HAp ball milled powders

The Debye-Scherrer method (Eq. 3.2) has been used to estimate each milled powder sample's crystalline size (D). This method gives a relation between the crystalline size and the full-width half maximum (FWHM, i.e., β) or peak broadening phenomenon of the inspected powder using the following equation:

$$\text{Debye-Scherrer Equation-} \quad D = \frac{k\lambda}{\beta \cos \theta} \quad (3.2)$$

here, k is the Scherrer constant (in this study, $k= 0.94$), which depends upon the instrument alignment. **Fig. 3.5(a)** represents the calculated average crystalline size considering significant peaks from the XRD plot. The average crystalline size has been calculated by determining the y-intercept of the Scherrer plot (**Fig. 3.5(b)**). The crystalline size decreases with increasing HAp composition in the milled powder material, which signifies that the sample has been homogenized properly and significant peak broadening also occurs. Scherrer plot (shown in **Fig. 3.5(b)**) with the linear fit (correlation coefficient (i.e., R) lies in the range of 0.906 to 0.980 for all the linear fits) represents a broadening of distinct peaks with relatively high intensity, and it has been observed that a significant change in peak broadening from pure-Ti to 1 wt. % HAp sample, and further, it gradually

decreases with increasing HAp concentration. The broadening of peaks signifies smaller crystalline size and inhomogeneous composition (i.e., crystallinity decreases). Further, the effect of crystalline size, strain, and other elastic properties on peak broadening has been calculated using the Williamson-Hall method (W-H equations) [110].

$$\text{Strain } (\epsilon) = \frac{\beta}{\tan \theta} \quad (3.3)$$

$$\beta = \frac{k\lambda}{D_{W-H} \cos \theta} + 4\epsilon \tan \theta \quad (3.4)$$

After rearranging the **Eq. 3.4** can be rewritten as,

$$\beta \cos \theta = \frac{k\lambda}{D_{W-H}} + 4\epsilon \sin \theta \quad (3.5)$$

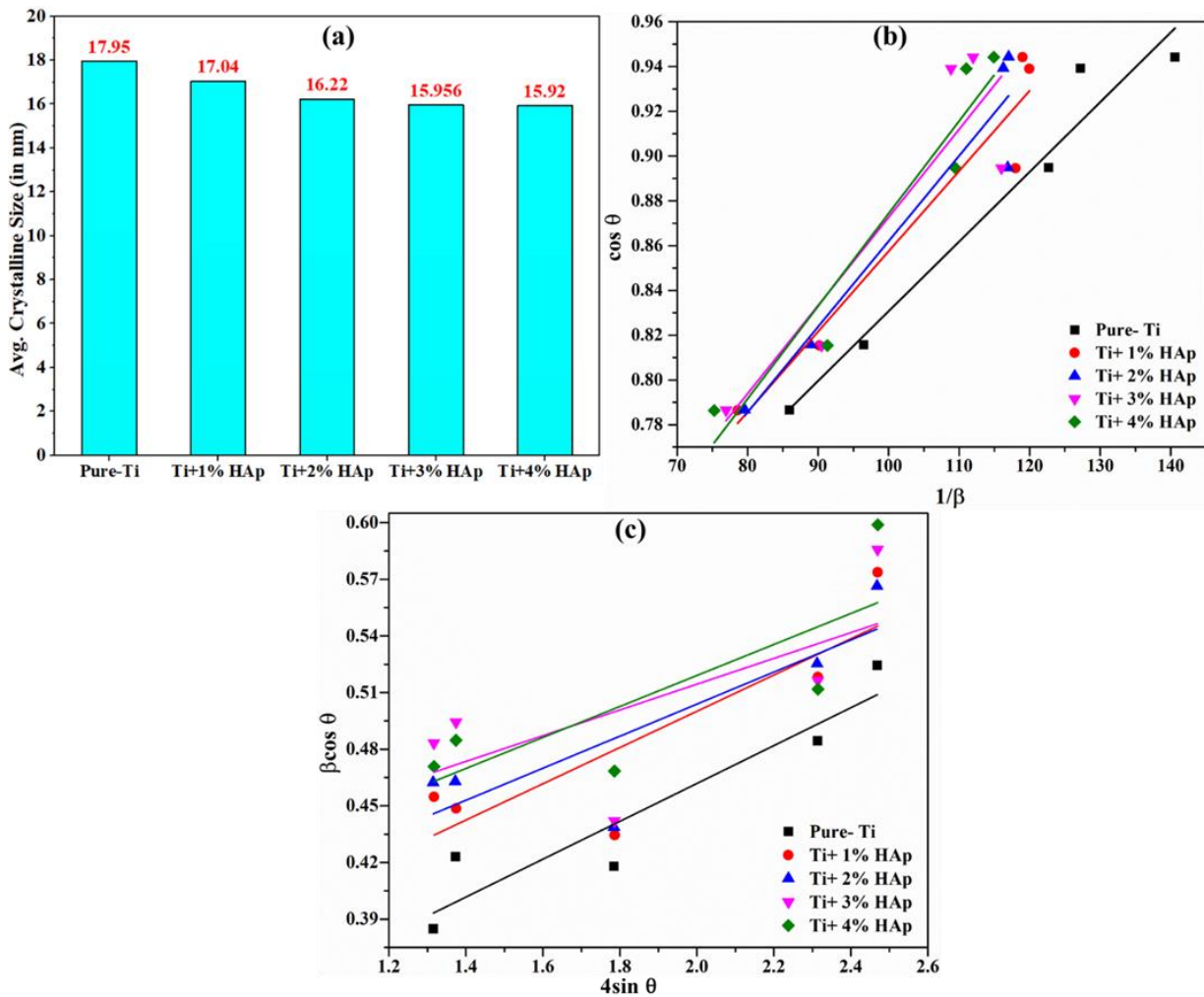


Fig. 3.5- XRD characteristics (a) Average crystalline size obtained using Debye-Scherrer Equation, (b) Scherrer plot, (c) W-H Plot for the HEBM processed powders

The lattice strain has been determined using W-H equations. **Fig. 3.5(c)** shows $\beta \cos \theta$ vs. $4 \sin \theta$ plot for each milled sample for significant peaks with high intensity from the XRD data. The data points have been linearly fitted (correlation coefficient (i.e., R) lies in the

range of 0.804 to 0.940 for all the linear fits), and the strain data can be calculated from the slope of the fitted curves. The W-H equation represents that the strain in HEBM powders decreases with increasing HAp content due to the reduced crystallinity of the resulting powders. Since all the $4\sin\theta$ points exhibit similar values in the W-H plots, it indicates the anisotropy of the milled powders.

3.3.2 Morphological Characteristics

The HEBM is a conventional process of alloying and homogenizing raw material in powder form. **Fig. 3.6** represents the SEM micrographs of HEBM processed irregularly

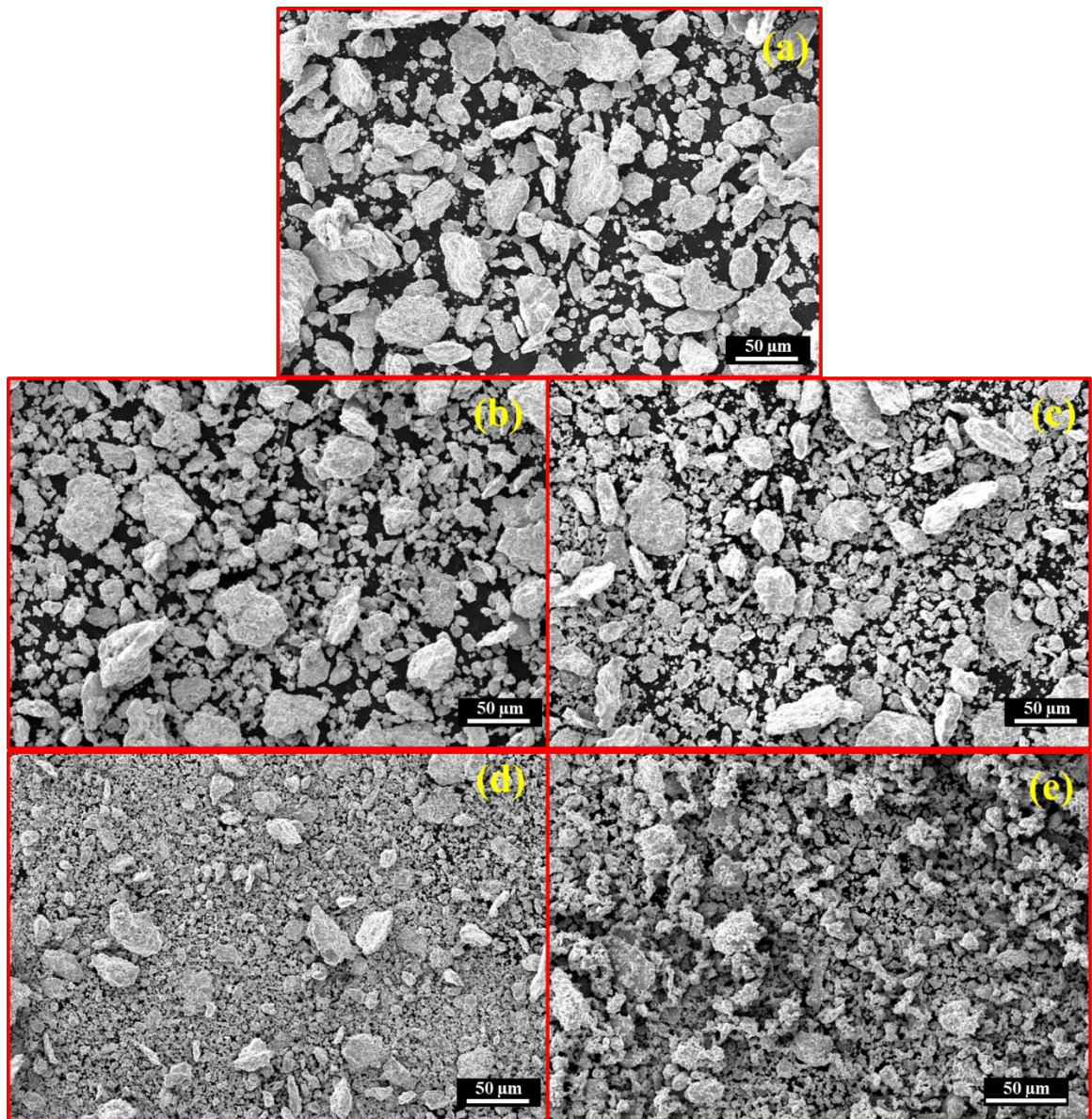


Fig. 3.6- (a) HEBM processed Pure-Ti powder, (b-e) SEM images of Ti- μ -HAp mixed HEBM processed powders showing homogenized mixing and particle size reduction after milling.

shaped powder particles. The milling parameters, i.e., milling speed, time, etc., are the deterministic factors of the quality and size of the milled powder. The high milling speed imparts high-impact energy to the raw powder material, leading to severe plastic deformation and fracture of particles and, hence, reduction in size and homogenous diffusion of individual particles. As a result of high-energy milling, a reduction in particulate size and increased agglomeration of powder particles have been observed with increasing HAp content. It happens because of the occlusion of resultant particles, as brittle ceramic HAp particles may adhere over the Ti particles [111]. The milling has been performed with tungsten carbide (WC) vials and balls having relatively higher hardness than the milled raw powders. Hence, no such contamination was observed, as evident from the morphological and elemental analysis of milled powder samples.

3.4 Elemental and Functional Composition Characteristics of HEBM alloyed Powders

3.4.1 Elemental Characteristics

The X-ray photoelectron spectroscopy (XPS) analysis is carried out to identify the elements within a material (elemental compositions) and their chemical state through a spectroscopic technique based on the photoelectric effect. The XPS provides a plot of the number of electrons detected at a specific binding energy, corresponding to the electrons' electron configuration within the atoms. The homogenization and alloying of raw materials are also evident from the XPS results plot for the HEBM powder samples (**Fig. 3.7**). The sharp peaks of Ti-2p, O-1s, and C-1s are observed in all the milled powder, the presence of O-1s in the pure-Ti sample is due to the formation of oxides with high energy milling. The continuous collision with hard balls generates intense heat, which causes the formation of oxides with the milled powders. At the same time, the sharp C-1s peak is observed due to the carbon tape used for holding the powder sample and residues of burnt powder particles due to intense heat generated during the HEBM process. Ti-element shows two peaks between the 455-465 eV binding energy ranges, exhibiting their enrichment in the tested powder samples. The HAp mixed samples show distinct peaks of Ca-2p and P-2p for all the compositions. The subsequent amount of individual elemental composition is presented in **Table 3.1** for its quantification. The Ca:P ratio is well maintained above the value of 1.6 [112], suitable for its application as an implanted biomaterial.

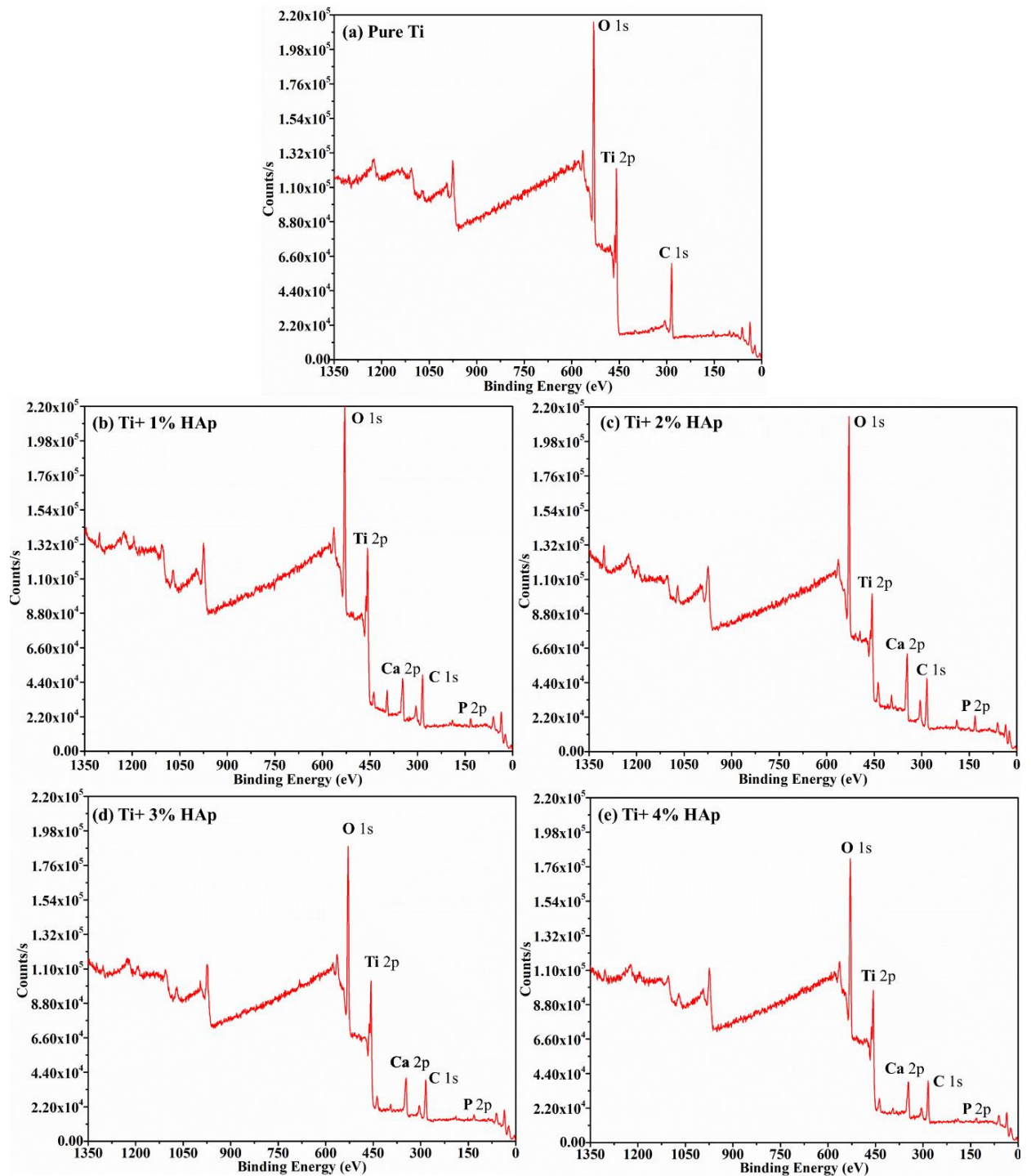


Fig. 3.7- XPS response of HEBM processed powder materials

3.4.2 Functional Groups Characteristics

The energy absorption or emission by the solid, liquid, and gas samples can be analyzed with the help of Fourier-transform infrared spectroscopy (FTIR spectroscopy). An FTIR spectrometer simultaneously collects high-resolution spectral data over a wide spectral range. It works on the principle of measuring the amount of light a sample absorbs at each wavelength. The FTIR spectroscopy results in terms of % transmittance for each

Table 3.1- Quantitative distribution of elements in HEBM processed powders detected using XPS processed powder

Samples	Relative atomic percentage				
	Ti-2p	O-1s	C-1s	Ca-2p	P-2p
Pure Ti	14.98	44.83	40.18	-	-
Ti+ 1wt.% HAp	16.08	45.15	30.97	4.82	2.99
Ti+ 2wt.% HAp	15.26	48.22	28.99	5.29	2.23
Ti+ 3wt.% HAp	15.18	47.59	29.03	5.95	2.25
Ti+ 4wt.% HAp	11.24	46.75	28.81	7.53	5.67

HEBM have been shown in **Fig. 3.8**. Here, the FTIR plot exhibits the chemical bonds and available functional groups with their respective frequency, which can contribute to its bioactivity properties [113]. The Ca-O exists at a lower wave-number range, i.e., 400-500 cm^{-1} . A covalent bond with a Ca-molecule stabilizes the compound in this frequency range [114,115]. Due to the higher sintering temperature dihydroxylation of HAp, hydroxyl band intensity decreased at $\sim 435 \text{ cm}^{-1}$ [116]. The PO_4^{3-} functional group shows intense peaks in the frequency range of 900-1600 cm^{-1} , exhibiting the co-existence of apatite and carbonate groups in the presence of HAp [115]. At frequency level 2300 cm^{-1} , the transmittance intensity relatively decreased with increasing HAp composition due to the presence of the P-O group in the compound. Corresponding to the $\sim 3570 \text{ cm}^{-1}$ frequency band, the stretching in the O-H bond increases with increasing HAp content [117], exhibiting strong hydroxyl groups and effective alloying of the constituent material [118]. It is because of the absorption of water molecules in the inspected HAp-rich powder samples, and its absorption intensity increases beyond 3746 cm^{-1} .

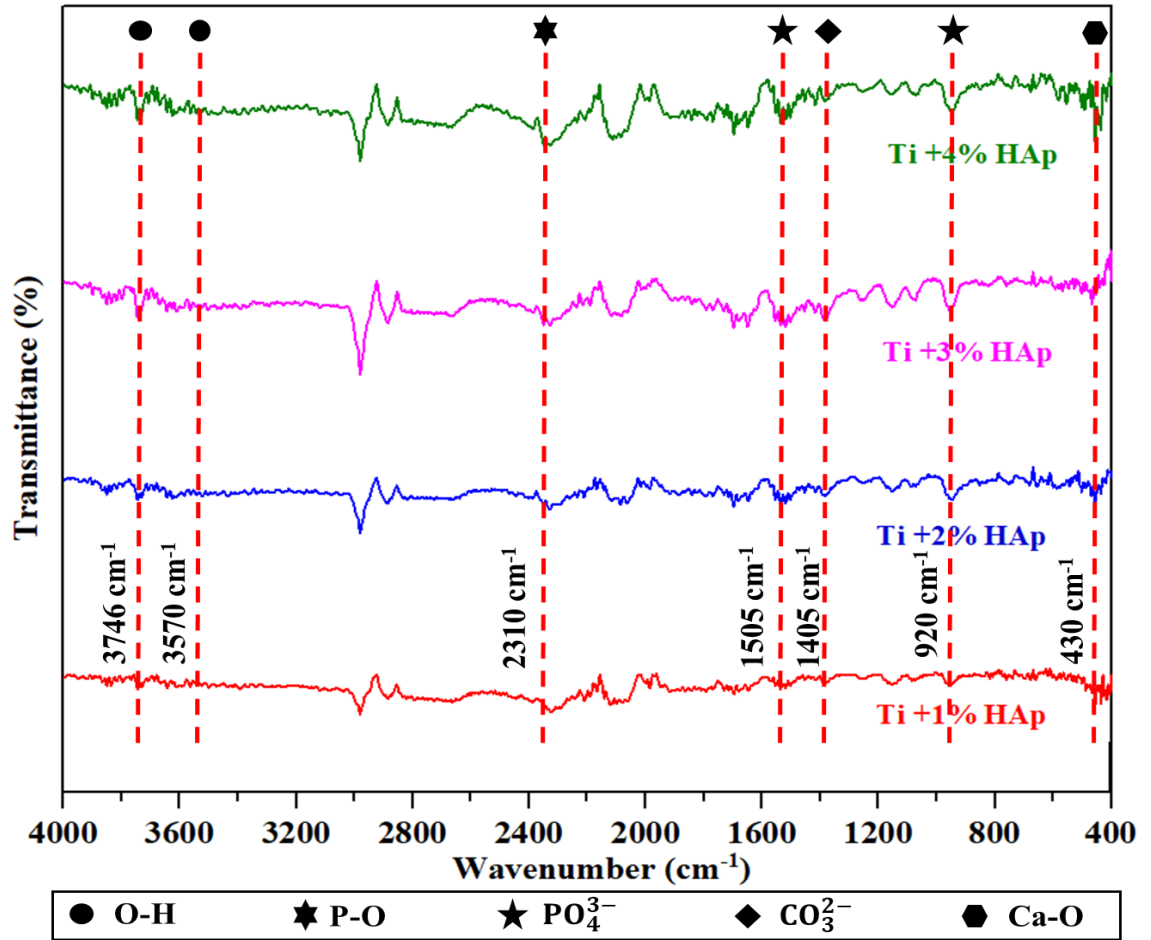


Fig. 3.8- Transmittance results of the HEBM processed powders obtained using FTIR

3.5 In-Vitro Cytocompatibility Test (MTT Assay) of HEBM Powders

The HEBM Ti- μ HAp powders have been tested for an In-vitro biocompatibility test using an MTT assay. It is a colorimetric assay method to determine metabolically active cells on the surfaces of materials quantitatively. Mitochondrial enzymes of metabolically active cells react with Tetrazolium salt (3(4, 5-dimethylthiazol-2-yl)-2, 5-diphenyl tetrazolium bromide (MTT) and form purple color formazan crystals. The HEBM-processed samples have been washed with media solution and incubated in a separate well for four hours. Initially, fresh cells were cultured in the RPMI media for four hours and then centrifuged before seeding to the powder samples. After that, UV-treated 10 mg of powders of each composition are seeded with mouse fibroblast cells in simulated body fluid media (i.e., RPMI). Further, the cell-seeded samples were kept in a CO₂ incubator (with 5% CO₂ and 95% relative humidity) at 37.4°C for 1 Day and 7 Days, respectively. After incubating for the designated period, the MTT solution was taken out and treated with DMSO solution. Then, the treated samples were inspected for cell absorbance and viability results by comparing them with the cells cultured in controlled media. A Thermo Scientific™ Multiskan-GO Microplate Spectrophotometer has been used to analyze cells'

quantitative absorbance at 570 nm wavelength for the mechanically alloyed powders. Three similar distinct wells with the same MTT solution were prepared for each sample category to calculate the average cell absorbance. It is observed that the metabolically active cells have increased in the HEBM seeded well compared to controlled ones. **Fig. 3.9** shows the measured cell absorbance results for each HEBM powder sample with different culture durations. The cell absorbance results show that the Ti- μ -HAp homogenized powder samples have more absorbance with increasing HAp composition [119,120].

Moreover, the cell growth rate is also improved with higher-composition samples. Thus, the samples with high HAp provide a more viable cell culture and growth environment. The recorded absorbance using a microplate spectrometer is directly proportional to the quantity of cells absorbed within the samples and thus indicates the viability of mechanically alloyed powder samples.

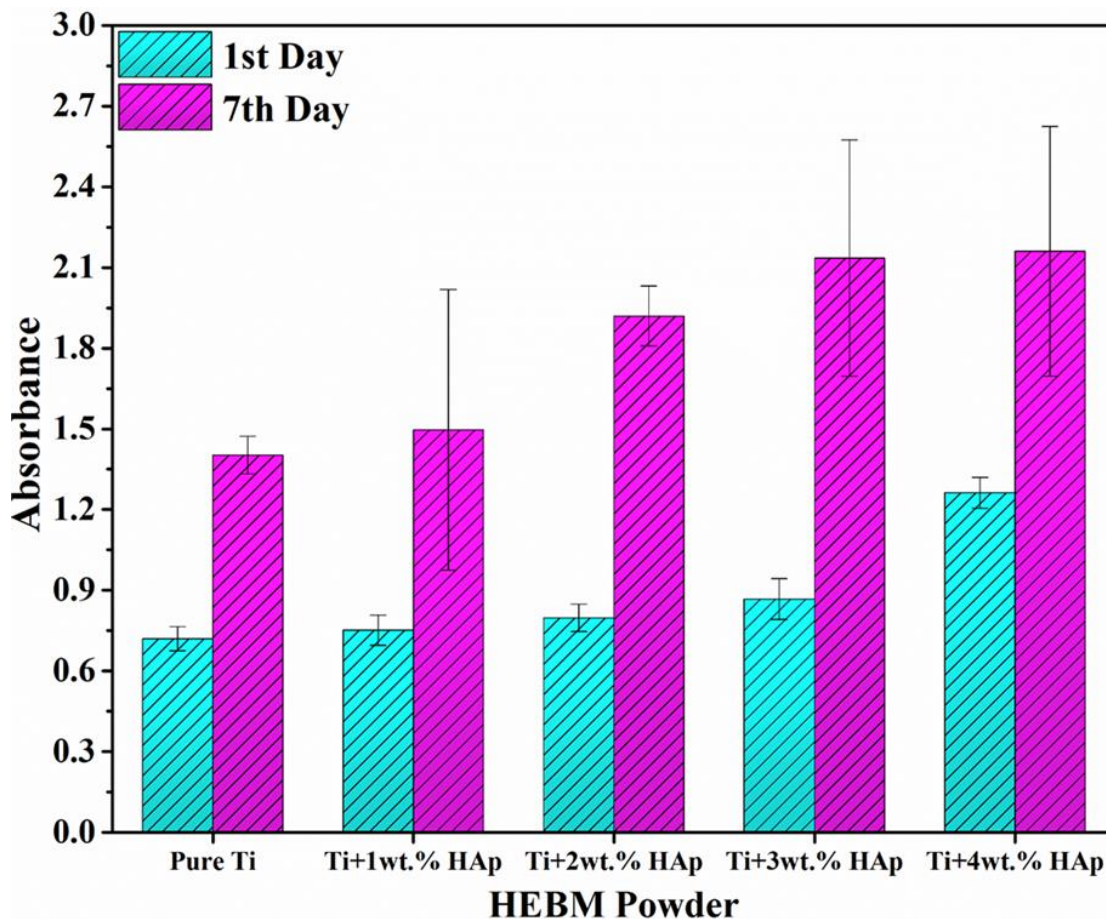


Fig. 3.9- MTT Assays result for cell absorbance with different duration of time

3.6 Discussion

The morphological and elemental distribution of the milled powders shows a reduction in particle size, and proper homogenized alloy has been obtained after a 4hrs. of high-energy milling. An appreciable reduction in particle size and compressibility of powder

particles has been obtained due to the long milling time. The distinct peaks of O with Ti in XPS results indicate that oxidation possibly occurred at such a high speed during the dry milling. The presence of Ca and P elements and their ratio is within the requisite range of 1.6, making it suitable for hard tissue applications and further tissue growth for self-healing damaged bones. The lattice-related information obtained from the XRD data and its calculations using various classical formulae has been extensively analyzed. The HEBM powders show mostly stable and crystalline behaviour, decreasing crystallinity with increasing HAp composition. It may be because of the amorphous nature of ceramic HAp, which reduces the overall crystallinity of the resulting homogenized powders. The Scherrer and W-H plots show a significant broadening of peaks, decreasing strain values, and increasing FWHM for the milled powders. The W-H characteristics represent the anisotropic behavior of milled powders with increasing HAp composition.

The lattice vibration with different functional groups and their stability is effectively analyzed using FTIR results. The dissolution of the hydroxyl group and the existence of strong phosphate (PO_4^{3-}) bonds are the contributing functional groups that allow an effective cell absorbance. The in-vitro cell culture study from the MTT assay exhibits the powder samples' good cell absorbance characteristics. The MTT assay study concluded that the HEBM Ti- μ -HAp powders are viable with mouse fibroblast cells and have good cytocompatibility properties. The mechanically alloyed material showed better elemental, structural, and biological characteristics than pure-Ti materials. Hence, it can be concluded that the Ti- μ -HAp alloys will be more effective for bone-tissue interactions and, thus, suitable for implant materials. The quantification of cell growth through MTT assay concluded that HAp concentration is vital for the processed powder samples' cell adhesion and cell culture.

3.7 Summary

The micron-sized Ti and HAp powders have been effectively processed using a dry HEBM process with varying compositions of HAp, resulting in homogenized composition for its possible application in the fabrication of bio-implants. All the alloyed samples exhibit perfect crystallinity even after 4hrs. of milling. The powder morphology represents a possible agglomeration of powder particles, and the XPS results show distinct and clear peaks of Ca and P elements with the presence of a significant peak of O-element, representing the possible oxidation of powders during HEBM. The average crystalline size reduced from 17.95 to 15.92 nm with the subsequent addition of HAp upto 4wt. % and thus peak broadening increases. The presence of a strong O-H group, along with PO_4^{3-} . FTIR responses exhibit dissolution of hydroxyl and phosphate groups in HEBM powders, making

this metal-ceramic material an appropriate substitute for existing pure metallic material for its application as bio-implant and tissue culture. Thus, it can be concluded from MTT assays after seven days that the cell absorbance values are increasing. Thus, the cell viability increases with increasing HAp content in the samples.


Chapter-4

Chapter 4

Synthesis and Characterization of Ti-HAp-based Bio-Composites

This chapter discusses the second objective of the present work, i.e., processing of Metal-Ceramic based alloyed material to fabricate composites through microwave sintering. The fabricated composites are characterized to study their morphological, chemical, mechanical, corrosion, tribological, and biological properties.


journal of the mechanical behavior of biomedical materials 142 (2023) 105852



Contents lists available at [ScienceDirect](#)

Journal of the Mechanical Behavior of Biomedical Materials

journal homepage: www.elsevier.com/locate/jmbbm



Micro-hydroxyapatite reinforced Ti-based composite with tailored characteristics to minimize stress-shielding impact in bio-implant applications

Rakesh Kumar, Anupam Agrawal^{*}

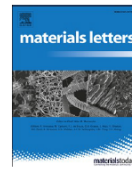
Advanced Manufacturing Technology Lab, Department of Mechanical Engineering, Indian Institute of Technology Ropar, Rupnagar, 140001, Punjab, India

ARTICLE INFO

Keywords:
Biomaterials
Titanium (Ti)
Hydroxyapatite
Sintering
Stress-shielding
Nano-indentation

ABSTRACT

Biomaterials having higher strength and increased bioactivity are widely researched topics in the area of scaffold and implant fabrication. Metal-based biomaterials are favorably suitable for load-bearing implants due to their outstanding mechanical and structural properties. The issue with pure metallic material used for bio-implant is the mismatch between the mechanical properties of the human body parts and the implant. The mismatch in modulus and hardness values causes damage to muscles and other body parts due to the phenomena of 'stress-shielding'. As per the rule of mixture, combining a biocompatible ceramic with metals will not only lower the overall mechanical strength, but will also enhance the composite's bioactivity. In the present work, a Metal-Ceramic composite of Ti and μ -HAp is processed through high-energy mechanical alloying. The μ -HAp powders (in a weight fraction of 1%, 2%, and 3%) were alloyed with Pure Ti powder sintered using microwave hybrid heating (MHH). The homogeneously alloyed materials were inspected for chemical and elemental characteristics using XRD, SEM-EDX, and FTIR analyses. Nano-mechanical and micro-hardness properties were inspected for the fabricated Ti- μ -HAp composites and it shows a decreasing trend. Elastic modulus declined from 130.8 GPa to 50.11 GPa for 3 wt% μ -HAp compared to pure-Ti sample. The mechanical behaviour of developed composites confirms that it can minimize the stress-shielding impact due to comparatively lesser strength and hardness than pure metallic samples.



Bio-corrosion susceptibility of surface voids and pores in microwave sintered Ti-HAp based bio-composites

Rakesh Kumar, Anupam Agrawal*

Advanced Manufacturing Technology Lab, Department of Mechanical Engineering, Indian Institute of Technology Ropar, Rupnagar, Punjab, 140001 India

ARTICLE INFO

Keywords:
Biomaterials
Pores and voids
Corrosion
Tafel Analysis
Microscopy
EDS

ABSTRACT

Deterioration of implants caused by human blood plasma and liquid influence is termed Bio-corrosion. It is detrimental for metal-based implants to function and affects their lifespan adversely. Hybrid-microwave sintered Titanium-Hydroxyapatite-based metal-ceramic composites were studied for corrosion behaviour in Hank's Balanced Salt solution using an electrochemical test in linear polarization potential mode. The sintering induces surface voids and pores, thus its influence on corrosion for Ti-HAp sintered composite was studied. Different corrosion characteristics were determined, and the corrosion sites were analyzed using SEM-EDS. The study could lead to the development of corrosion-resistant porous bio-implants under an actual physiological body-fluid environment.

4.1 Sintering of Metal-Ceramic based composite using Microwave Hybrid Heating

This study used the High Energy Ball Milling (HEBM) processed Pure-Ti and μ -HAp alloy materials to fabricate composites (**Fig. 4.1**). The μ -HAp mixed with a wt. fraction of 1%, 2%, and 3% with CP-Ti is used to prepare Metal-Matrix composites. The amount of μ -HAp is kept limited to 3%, as it was observed that alloying with 4–5 wt.% of HAp makes the sample **more susceptible to brittle failure (show surface cracks after sintering itself)** and mechanical properties degraded due to significantly enhanced surface cracks upon sintering because of high oxide formation.

The homogeneously alloyed powder particles were cold compacted using incremental uniaxial compaction pressure with a maximum pressure of 650 MPa and dwell time of 5 min to ensure the proper consolidation of the powder particles. A similar approach as of [Fang et al. \[121\]](#) was followed to sinter the HEBM-processed Ti- μ -HAp-based composites. **Fig. 4.2** represents the compaction and sintering parameters for compacting and sintering the green samples. The consolidated green samples were further sintered under an inert atmosphere using MHH for a sintering temperature of 1250 °C with a heating rate of ~83 °C/min. A holding time of 5 minutes is used; hence, the compacted sample was exposed to microwave radiation for 20 minutes during the sintering process. The furnace cooling is

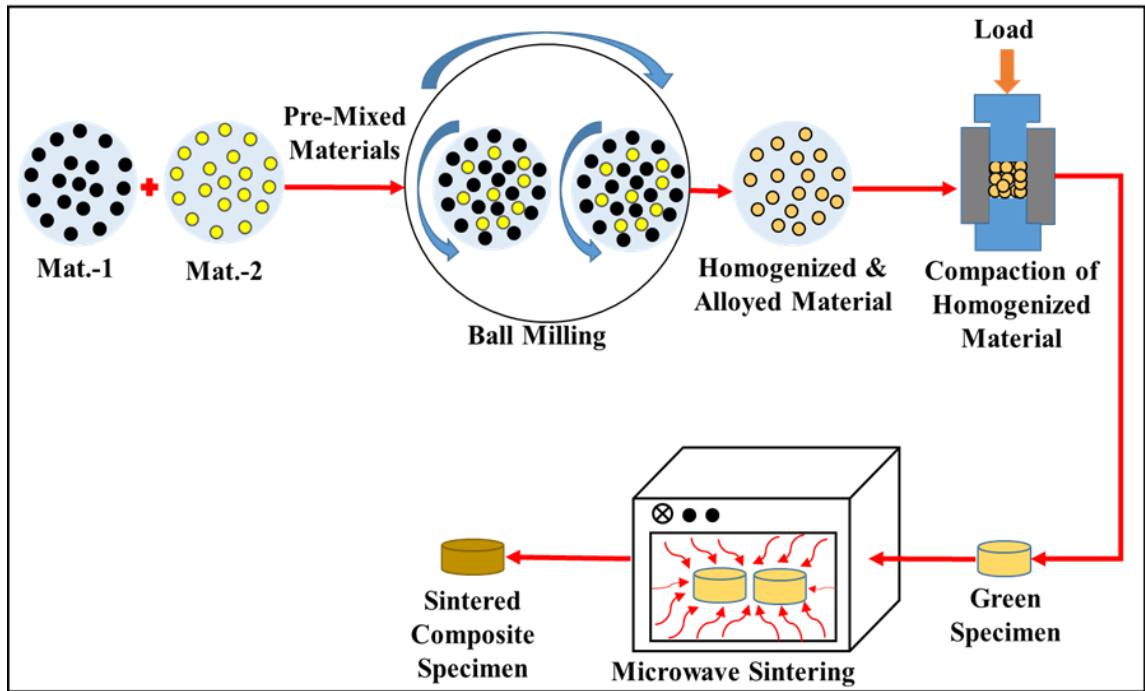


Fig. 4.1- Schematic representation of the synthesis of bio-composite using Powder metallurgy process

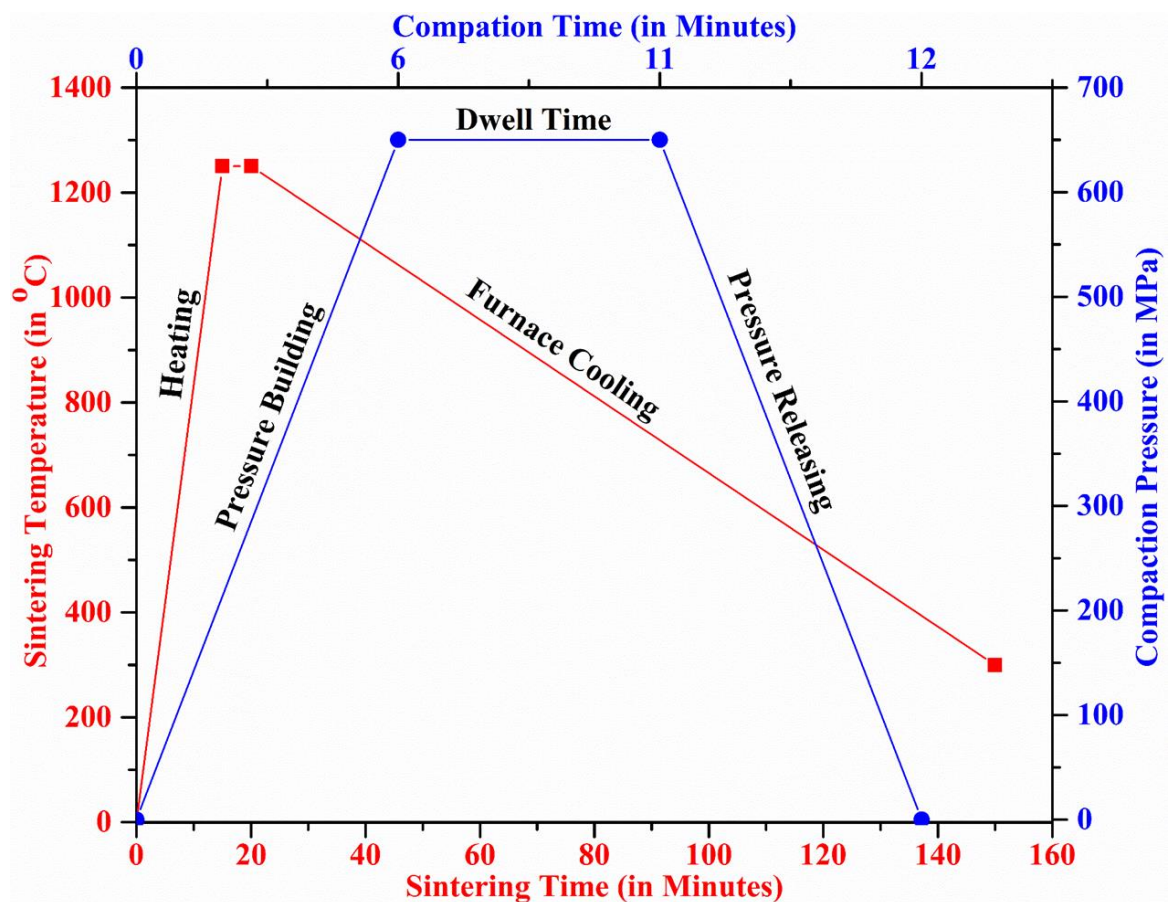


Fig. 4.2- Compaction and Sintering curve of alloyed Ti-μ-HAp powder for densification

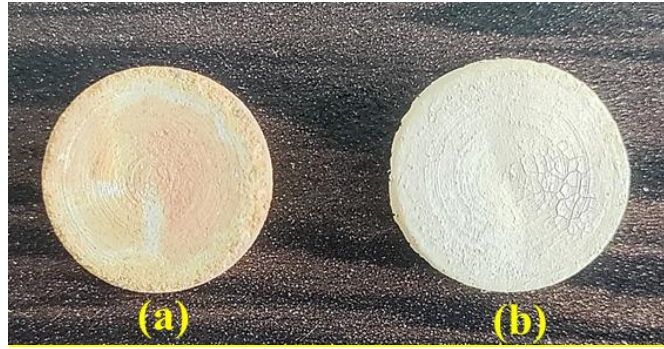


Fig. 4.3- Failed samples during processing **(a)** 4 wt.% HAp sample, & **(b)** 5 wt.% HAp sample

performed to eliminate contamination with atmospheric gasses at high-temperature and thus reduce the chances of further oxide formation. The sintered composites are tested for their morphological and tribological characteristics, which are studied using nano-mechanical, surface-wear, wettability, and corrosion tests. An In-vitro biocompatibility test with mouse fibroblast cells is performed to analyze cell-adhesion and growth.

The variation in density of the sintered composite is measured using Archimedes' principle and represented in **Fig. 4.4**. The obtained experimental density is equivalent to the density obtained using the rule of mixture. The dominant effect of hybrid microwave sintering for material development promotes improved densification and bonding between the matrix and reinforcement phase [122]. The maximum density in the current study is 3.89 g/cm³ in the case of Pure Ti, and it is reduced to 3.26 g/cm³ with a reinforcement of 3 wt.% μ -HAp. The addition of reinforcement of μ -HAp in the Ti slightly reduces the density of the composite. The composite's reduced density can be attributed to the forming of small clusters, ceramic phases, and increased pores.

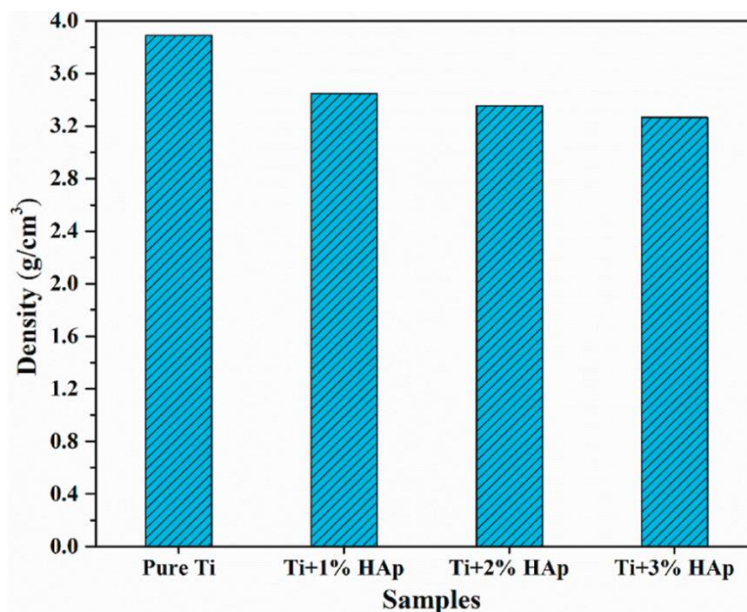


Fig. 4.4- Measured density of the sintered composites samples using Archimedes' principle

4.2 Morphological and Elemental Characterization of Sintered composite samples

Fig. 4.5 represents the surface morphology of MHH sintered samples without post-processing. **Fig. 4.5(a)** is for pure Ti sintered sample; it exhibits the formation of minor oxide residue over the surface due to high-temperature sintering. The other samples (Fig. 7(b)–(d)) are for composites with reinforcement of μ -Hap; they exhibit a flake-like structure over the surface. These flake-like structures represent the presence of crystalline HAp particles in the samples. With increasing μ -HAp, the flake-like structure also increases, which signifies the formation of hydroxycarbonate Appetite layers over the surface during the sintering process. The surface pores are also increasing with the increasing concentration of μ -HAp, which can be further confirmed with the surface microscopy of the polished samples.

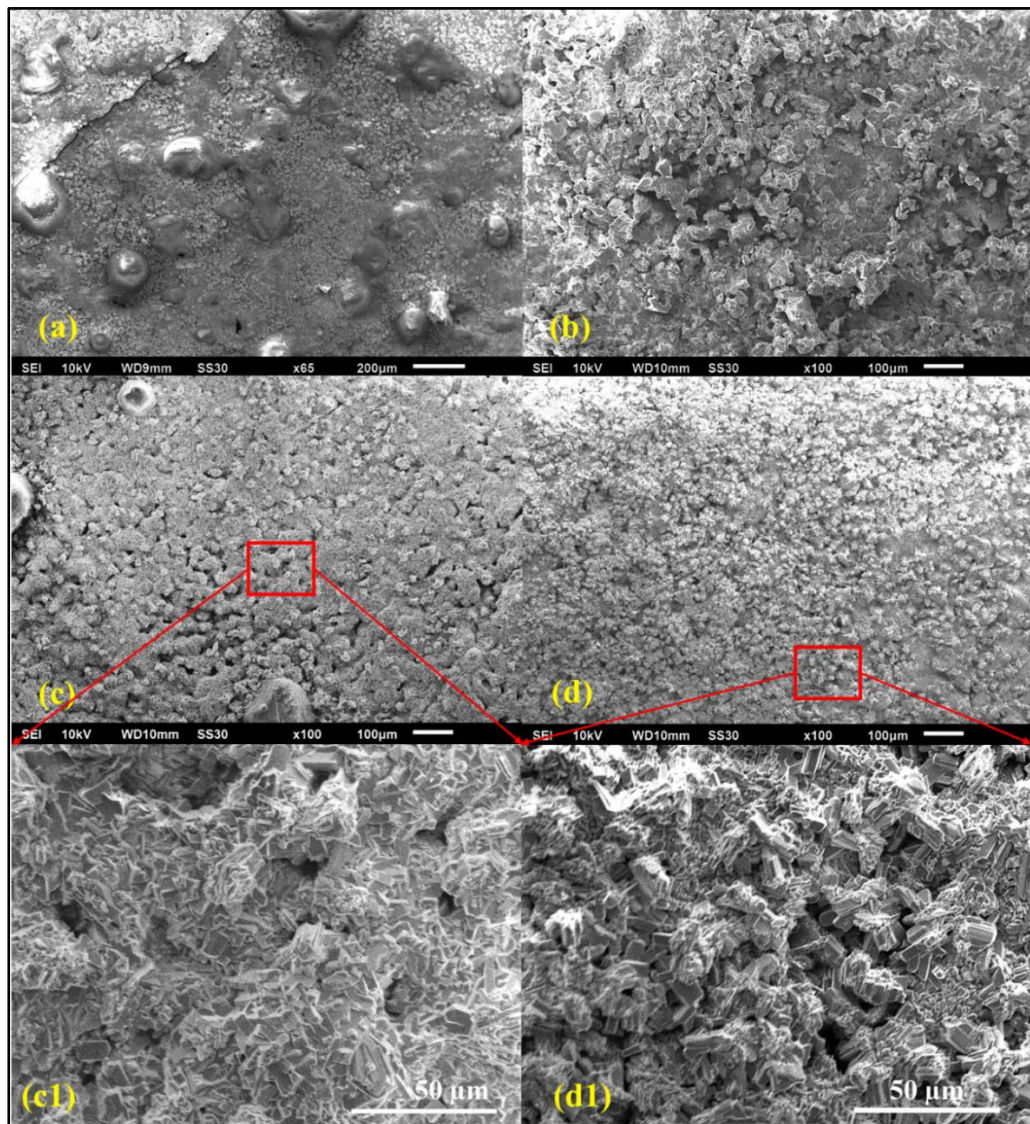


Fig. 4.5- SEM images of untreated sintered samples representing the diffusion of μ -HAp with Ti (a) Pure Ti, (b) Ti+1 wt% μ -HAp, (c) Ti+2 wt% μ -HAp, and (d) Ti+3 wt% μ -HAp

Fig. 4.6 shows the EDS-based elemental mapping of the MHH sintered samples to analyze the elemental distribution over the surface. The elemental mapping exhibits the uniform distribution of each element throughout the inspected area of each sample, which confirms that the proper homogenization of raw powder material has been done during the HEBM process. **Table 4.1** represents the percentage distribution of elements exhibited by mapping in each sample. The pure-Ti sample contains approximately 23.05% of Oxygen, which exhibits oxide formation over the top surface. As [Bovand et al. \[123\]](#) suggested, Ti and HAp powders undergo a chain of chemical reactions at high sintering temperatures, forming titanium dioxide (TiO₂) and free oxygen and phosphorus radicals. Further, in composite samples, the presence of Oxygen was recorded due to the availability of O-molecules in HAp composition. The existing Ca and P ratios are within the permissible range of 1.6 to exhibit the biological properties of the sintered composites for effective tissue growth. The presence of pores and overall porosity play important roles in bio-implant and tissue engineering. Pores are responsible for cell seeding and culture zones in scaffolds and implants. **Fig. 4.7** shows the SEM images of polished surfaces with pores and voids for each MHH sintered sample. High-resolution SEM images (inset) show the pores present in each sample. The density of pores increases with increased wt.% of μ -HAp in the sintered samples. The observed porosity distribution is random due to non-uniform particle size and shape. The inset **Fig. 4.7(a)** indicates the possibility of the existence of α (white lamellar structure) and β -phases in the pure-Ti sample simultaneously. This co-existence of both phases may be due to high-temperature sintering. **Fig. 4.8** shows the FTIR results, giving information about the transmittance, presence of different functional groups, and chemical bonds exhibited by the HEBM powder samples. The Phosphate (PO_4^{3-}) functional group groups exist for wave numbers between 400 and 1600 cm^{-1} . In this range of wave number, the existence of PO_4^{3-} evidenced the stable phase of HAp in the powder.

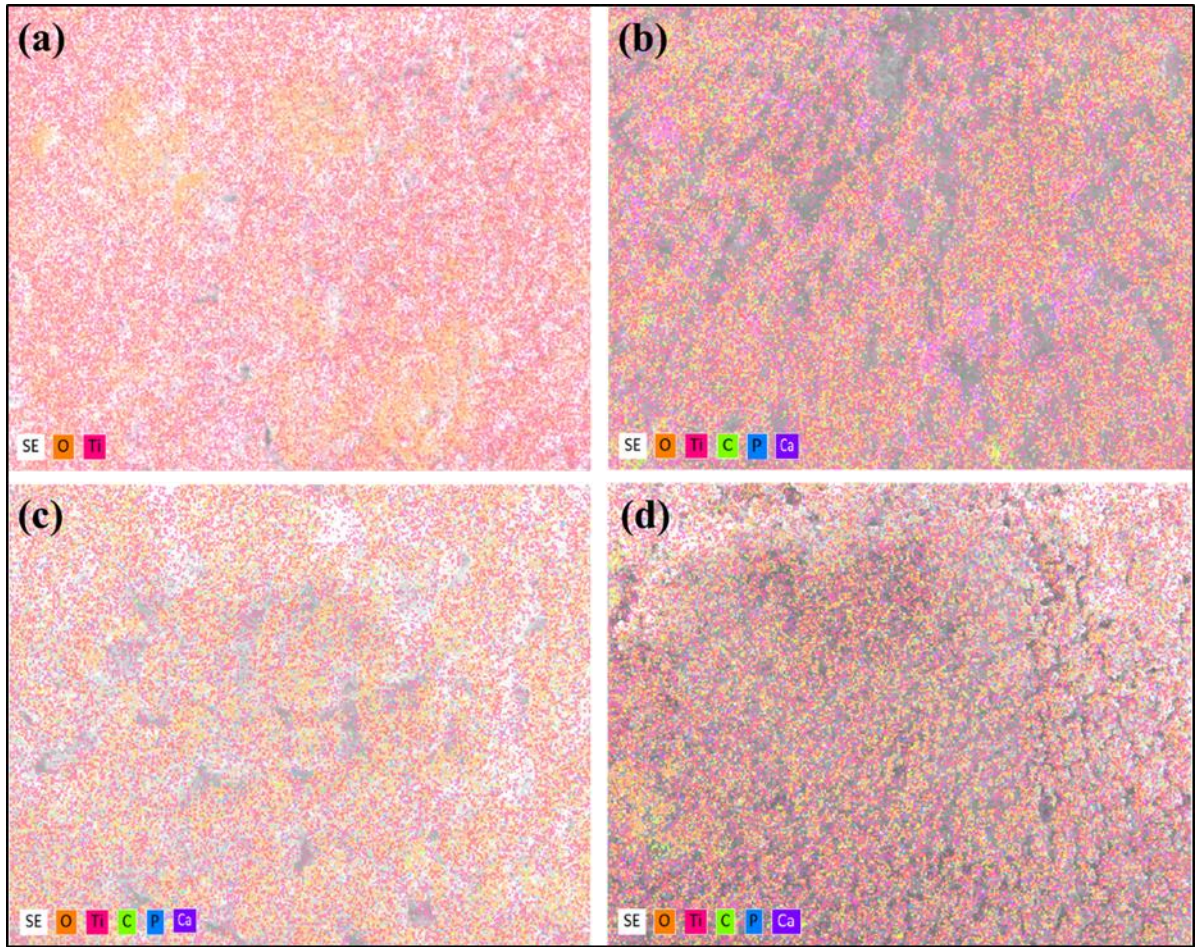


Fig. 4.6- EDX-Mapping of untreated sintered samples representing the diffusion of μ -HAp with Ti (a) Pure Ti, (b) Ti+1 wt% μ -HAp, (c) Ti+2 wt% μ -HAp, and (d) Ti+3 wt% μ -HAp

Table 4.1- Elemental composition (in %) of the sintered sample obtained through EDS

SI No.	Samples	Ti	O	C	Ca	P	Rest
01	Pure Ti	75.42	23.05	-	-	-	1.53
02	Ti+1 wt.% μ -HAp	68.93	24.17	7.81	0.55	0.36	-
03	Ti+2 wt.% μ -HAp	65.26	23.71	9.78	0.79	0.46	-
04	Ti+3 wt.% μ -HAp	48.09	36.18	14.08	1.00	0.65	-

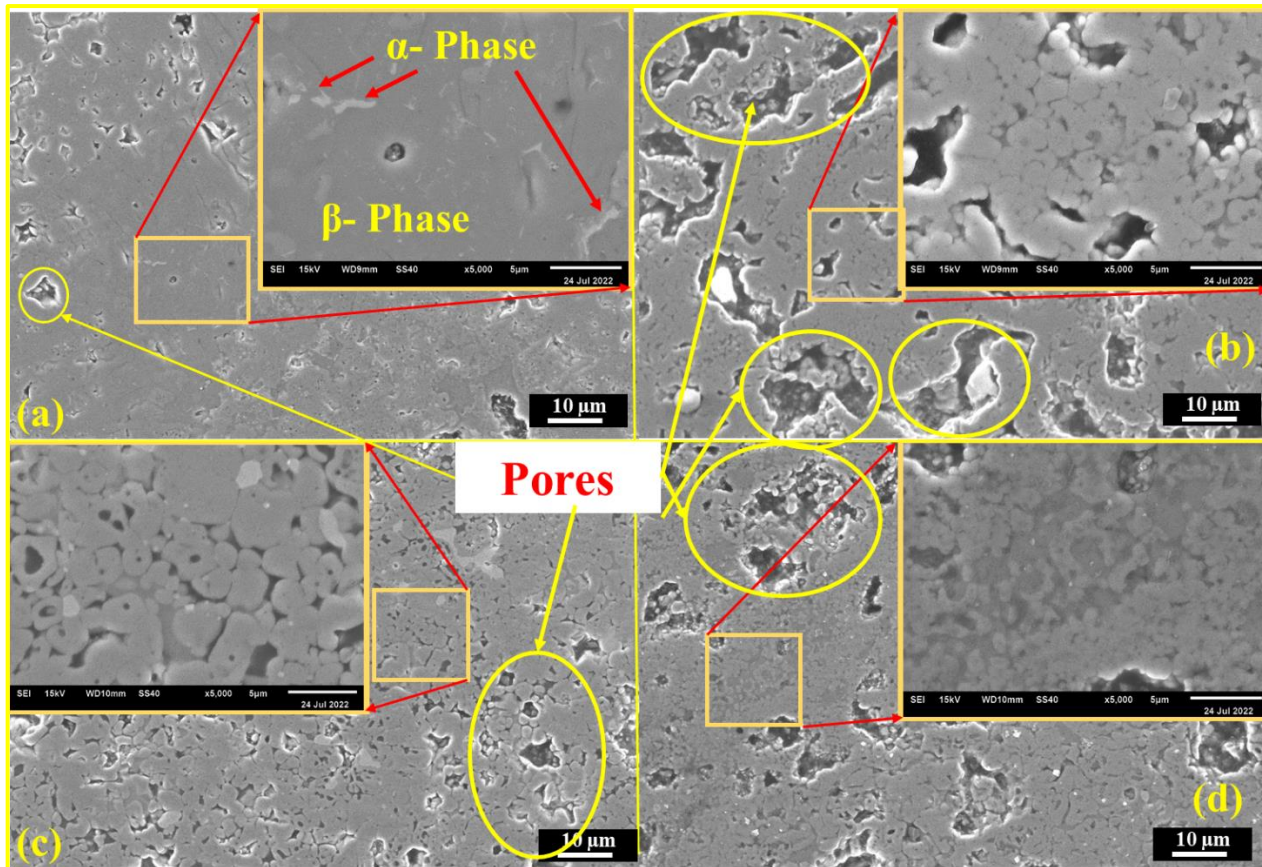


Fig. 4.7- SEM Images of polished sintered samples representing the diffusion of μ -HAp with Ti (a) Pure Ti, (b) Ti+1 wt.% μ -HAp, (c) Ti+2 wt.% μ -HAp, and (d) Ti+3 wt.% μ -HAp

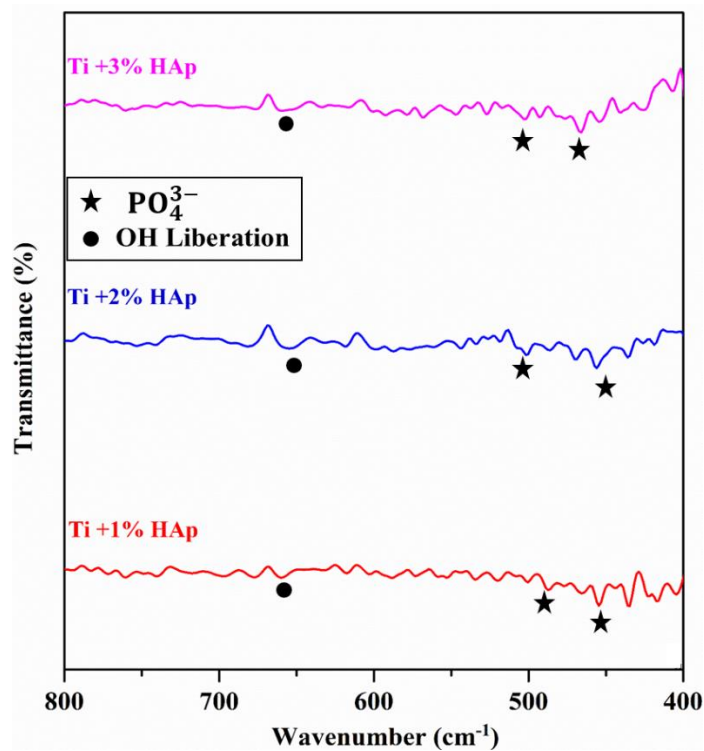


Fig. 4.8- Transmittance results of Ball-Milled powders using FTIR

4.3 Mechanical Characteristics of the Sintered composite samples

4.3.1 Nano-Mechanical Characteristics

The Nano-mechanical characterization of the sintered composites is performed using the nanoindentation (Hysitron-TI950) method. Berkovich indented with a 10 k- μ N (10 mN) maximum load, was used to perform the nanoindentation. The elastic modulus and nano-hardness of each sample are calculated according to the method developed by Oliver and Pharr [124,125], i.e., by analyzing the unloading curve obtained during the nanoindentation test (**Fig. 4.9**). Nano-hardness is a function of maximum applied load (P_{max}) and projected area (A) of indentation, and it is calculated by **Eq. (4.1)**.

$$H = \frac{P_{max}}{A} \quad (4.1)$$

$$A = 24.5 h_c^2 \quad (4.2)$$

$$h_c = h_{max} - \varepsilon \frac{P_{max}}{S} \quad (34.)$$

here, h_c and h_{max} are the contact depth and displacement at the ultimate load, respectively. The term ' ε ' is determined from the dimension of the indenter, and S is the stiffness of the unloading curve at the ultimate load (**Eq. (4.4)**).

$$S = \frac{dp}{dh} = \beta \frac{2}{\sqrt{\pi}} E_r \sqrt{A} \quad (4.4)$$

Here, p and h are determined from the load vs. depth curve of the nanoindentation test. β is the indenter constant, which depends upon its shape and dimension ($\beta = 1.034$ for Berkovich Indenter) and E_r is the reduced modulus obtained using **Eq. (4.5)**. Where ν_i and E_i having values 0.07 and 1140 GPa are Poisson's ratio and elastic modulus of Berkovich indenter material (i.e., Diamond in this study), respectively, whereas ν (≈ 0.33) and E are corresponding values of the test specimen.

$$\frac{1}{E_r} = \frac{1 - \nu^2}{E} + \frac{1 - \nu_i^2}{E_i} \quad (4.5)$$

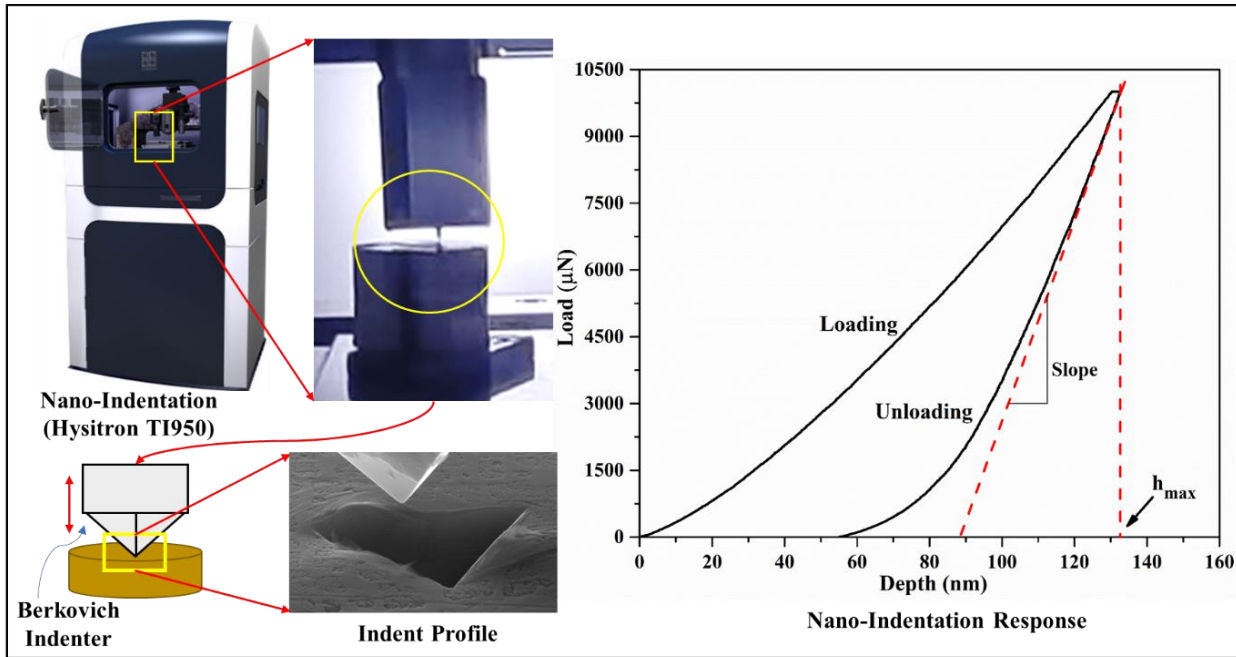


Fig. 4.9- A schematic representation of nano-mechanical testing through the nanoindentation technique

The sintered Ti- μ HAp composite samples are tested for surface mechanical characteristics. The finely polished samples are tested using a diamond Berkovich indenter at a maximum applied load of 10 mN with a holding time of 2 sec. The load vs. indentation depth responses is recorded and further processed to calculate the modulus and nano-hardness of the inspected samples. Each sample is indented at ten different locations to estimate the average and standard deviation. **Fig. 4.11** represents the sintered sample's modulus (E) and nano-hardness (nH). The modulus values decreased from 379.25 GPa to 232.36 GPa for the pure-Ti to Ti+ 3% HAp composite sample (**Fig. 4.11(a)**).

Similarly, the nano-hardness of the sintered samples decreases from 35.36 GPa to 22.44 GPa for pure-Ti and Ti+ 3% HAp, respectively (**Fig. 4.11(b)**). It can be seen that 'E' and 'nH' values exhibit the softening, i.e., less stiffening of sintered samples with the increasing composition of μ -HAp as reinforcement. The presence of α and β phases in sintered Pure-Ti samples contributes to its high hardness and modulus values, as combining both makes the Ti stronger. The corresponding reduced modulus (E_r) has been calculated using Eq. (3) and represented in Table 2, respectively. The hardness and elastic modulus collectively indicate the wear properties of the material [126]; as a result, these parameters can be used to assess the anti-wear capabilities. Wear caused by gradual material removal depends on the plastic deformation of inspected material during the nanoindentation test [127]. The ability to resist elastic strain to failure is defined as the wear resistance of a material. For nanoindentation test it is indicated by the ratio of hardness to

reduced modulus ($\frac{nH}{E_r}$) [88] value, and similarly, the ratio ($\frac{nH^3}{E_r^2}$) [102,126] represents the resistance to plastic deformation or yield pressure of the tested samples. Hence, from the **Table 4.2** the decreasing trend of plasticity index ($\frac{nH^3}{E_r^2}$) indicates decrease in the wear resistance, which is due to increase of μ -HAp in the composition. The reported results exhibit that with addition of HAp in Ti-matrix can reduce the stress-shielding effect having significantly lower wear resistance of the composite.

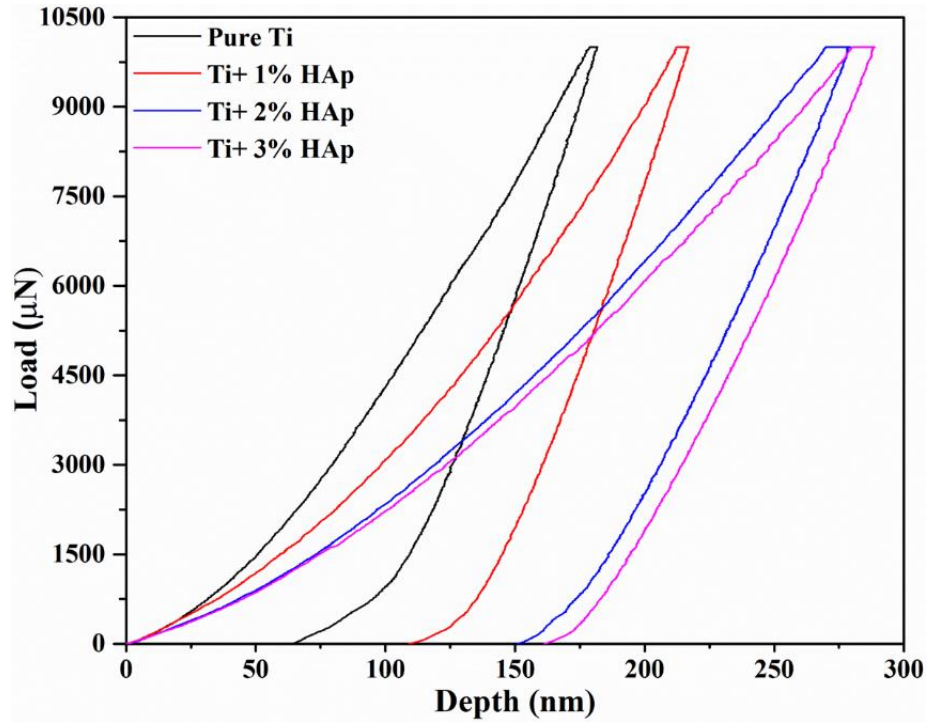


Fig. 4.10- Nano-mechanical Load vs. Indentation depth responses of the sintered samples

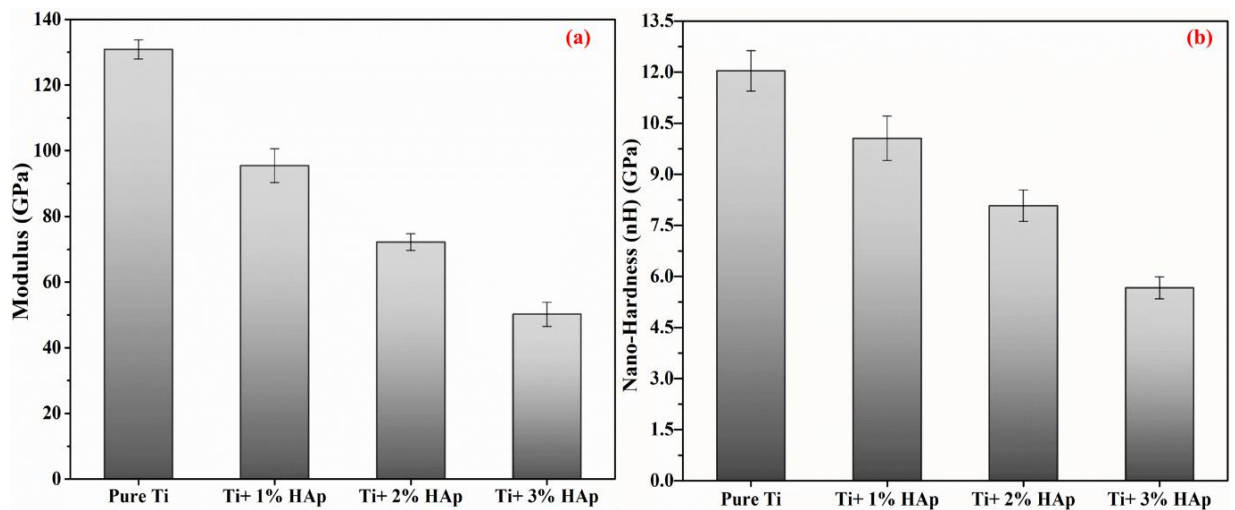


Fig. 4.11- Nano-indentation responses of the sintered samples (a) Elastic Modulus, (b) Nano-Hardness

Table 4.2– Calculated plasticity index values of sintered Ti-HAp composites based upon Nano-Mechanical responses

Sintered Samples	Maximum Depth (h_{max}) (in nm)	Avg. Reduced Elastic Modulus (E_r) (in GPa)	Avg. Nano-Hardness (nH) (in GPa)	Plasticity Index	
				$\frac{nH}{E_r}$	$\frac{nH^3}{E_r^2}$
Pure Ti	181.475	137.746	12.182	0.08843	0.0952
Ti+1% HAp	216.709	102.168	10.002	0.09789	0.0958
Ti+2% HAp	278.991	78.118	8.0719	0.10332	0.0861
Ti+3% HAp	286.669	54.857	5.658	0.10314	0.0601

4.4 Surface Tribological Characteristics of Sintered Composites

4.4.1 Surface Wettability

The implant undergoes various biological activities when placed inside a human body. The first and foremost activity is wetting of its surface in the presence of biological fluids and serums. The absorption of the proteins, nutrients, and adhesion of cells with the implant surface is mainly driven by the wetting characteristics of the biomaterial and its surface [128]. The wettability of a surface primarily depends upon its morphological characteristics and chemical composition. A contact angle measurement experiment uses a contact angle goniometer to measure the surface's wettability. A Sessile drop of 2 μ l distilled water has been deposited with the micro-syringe over the finely polished sintered samples. Based on the measured contact angle, it can be determined whether the respective surface is hydrophilic or hydrophobic [129]. The wettability of a bio-implant significantly impacts the cell growth/culture over it, i.e., its surface should have sufficient wettability characteristics or be hydrophilic (contact angle less than 90°). The wettability of the sintered composites was inspected using the contact angle made by a drop of distilled water over its surfaces. All the samples exhibit hydrophilic characteristics, as the contact angle is less than 90° (**Fig. 4.12**). The contact angle for 1-2 wt. % HAp samples are higher compared to pure-Ti samples but with 3 wt. % HAp, the angle decreases to 58.91°; this may be because of increased pores volume in the sintered composites. The results show a promising hydrophilic surface of the sintered Ti- μ -HAp composite, allowing possible absorbance of blood plasma and biological fluids for effective apatite layer formation.

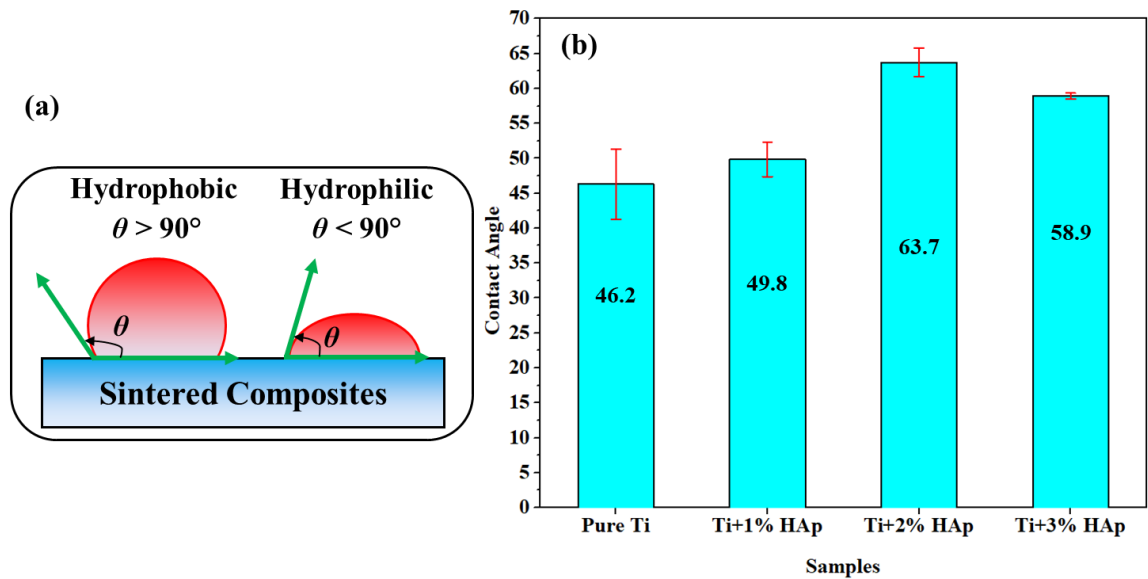


Fig. 4.12- Analysis of wettability of the sintered composites, (a) Schematic representation of wettability analysis, and (b) Comparative measured contact angle values of the sintered samples

4.4.2 Surface wear

A composite reinforcement particle influences the hardness properties due to the formation of the intermetallic bond between two constitutive particles, and thus it affects the surface wear characteristics and friction behaviour. The frictional behaviour of a surface can be calculated by applying a normal load over the surface. **Fig. 4.13(a)-(b)** and **4.13(c)-(d)** represent the frictional force along with the coefficient of friction variation throughout the scratched line, using Tribometer, for a uniformly applied load (20 N) and continuously increasing load (2-20 N) respectively for the sintered composite sample. The decrease in the coefficient of friction with increasing HAp content indicates the suitability of this biomaterial as an application to joint replacement, where relative movement between the two body parts is always present.

The wear mode is studied by inspecting the wear tracks using SEM imaging. Each scratched sintered composite sample is ultrasonically cleaned with ethanol solution for 5 mins. **Fig. 4.14** represents the morphology of each scratch-wear track. For the pure-Ti sample, a clean ductile failure was observed without any trace of adhered debris/particles over the wear track **Fig. 4.14(a)**. The traces of debris and particles fill the available pores; hence, densification along the scratch-wear track is visible. Morphology of the respective

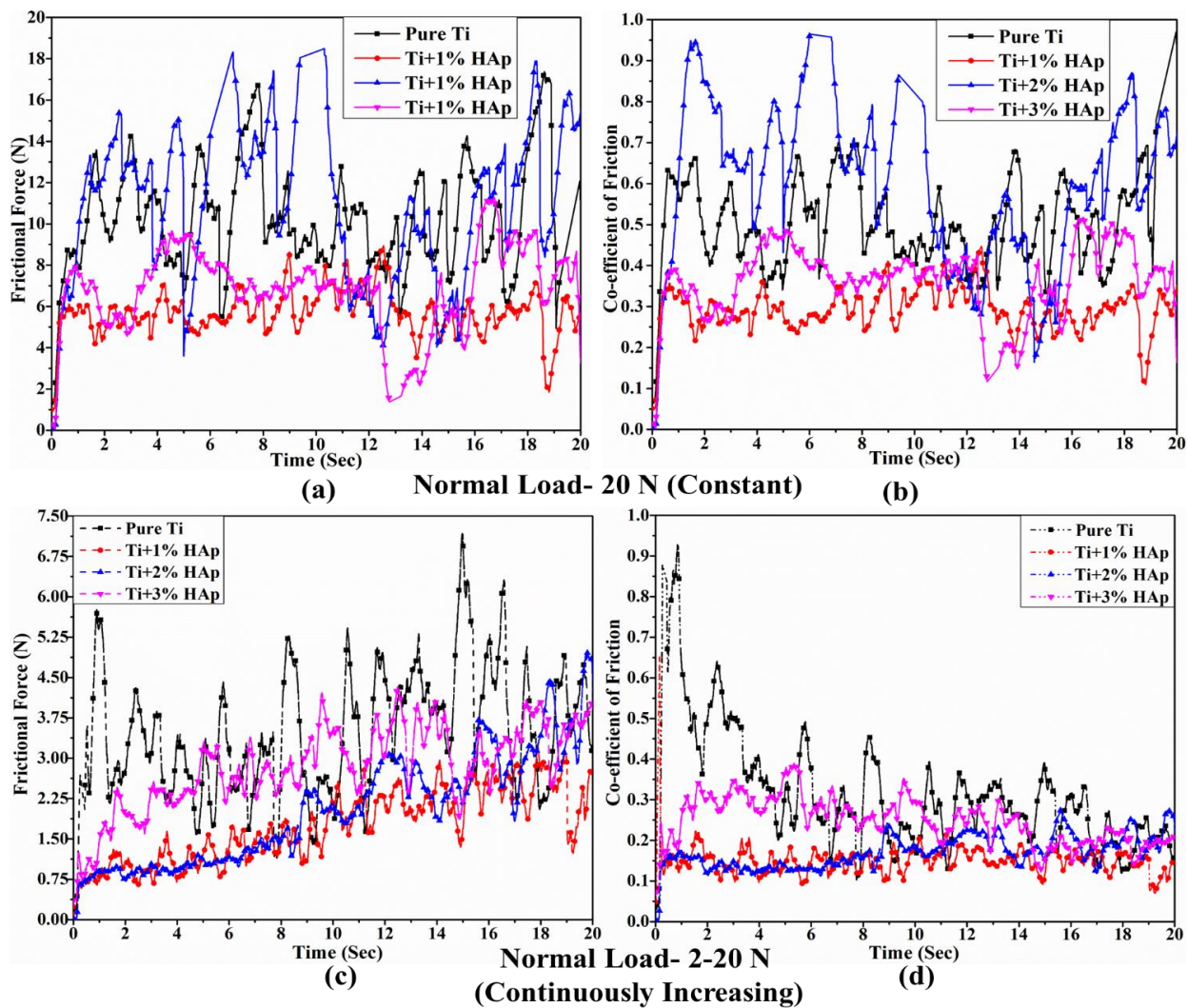


Fig. 4.13- Frictional force and Coefficient of Friction data, (a)-(b) for a constant normal load of 20 N, (c)-(d) for continuously increasing normal load of 2-20 N

wear track shows that the increasing HAp composition in the sintered composite exhibits more prominent micro-cracks due to shearing on the scratch track and abrasion near the scratch boundaries. The cracking visible in the samples are due single track scratch wear, the scratch wear usually shows a patterned cracking along the direction of sliding of indenter. The sliding diamond tip indenter deforms the surface both plastically and elastically. As the tip moves forward a groove with increasing depth forms. Under the tip there is both plastic and elastic deformation while in the surface behind the tip only the plastic part. Here, with increasing HAp composition a distinct increase in cracking is observed, reflecting brittleness of the composite. The addition of HAp increases brittleness of the sample and hence more prominent abrasive wear shown by the samples. Few randomly distributed debris and fragmented particles are also observed with increased HAp compositions because the pure-Ti sintered sample is comparatively denser and harder than Ti-HAp composites. The scratched boundaries are inspected using EDS to analyze the

elemental composition and presence of oxide over the surface. The fragmentation of wear particles and the exhibition of oxide particles indicate abrasion wear. Increasing HAp composition increases the wear rate because of less density and lower mechanical properties (modulus and hardness).

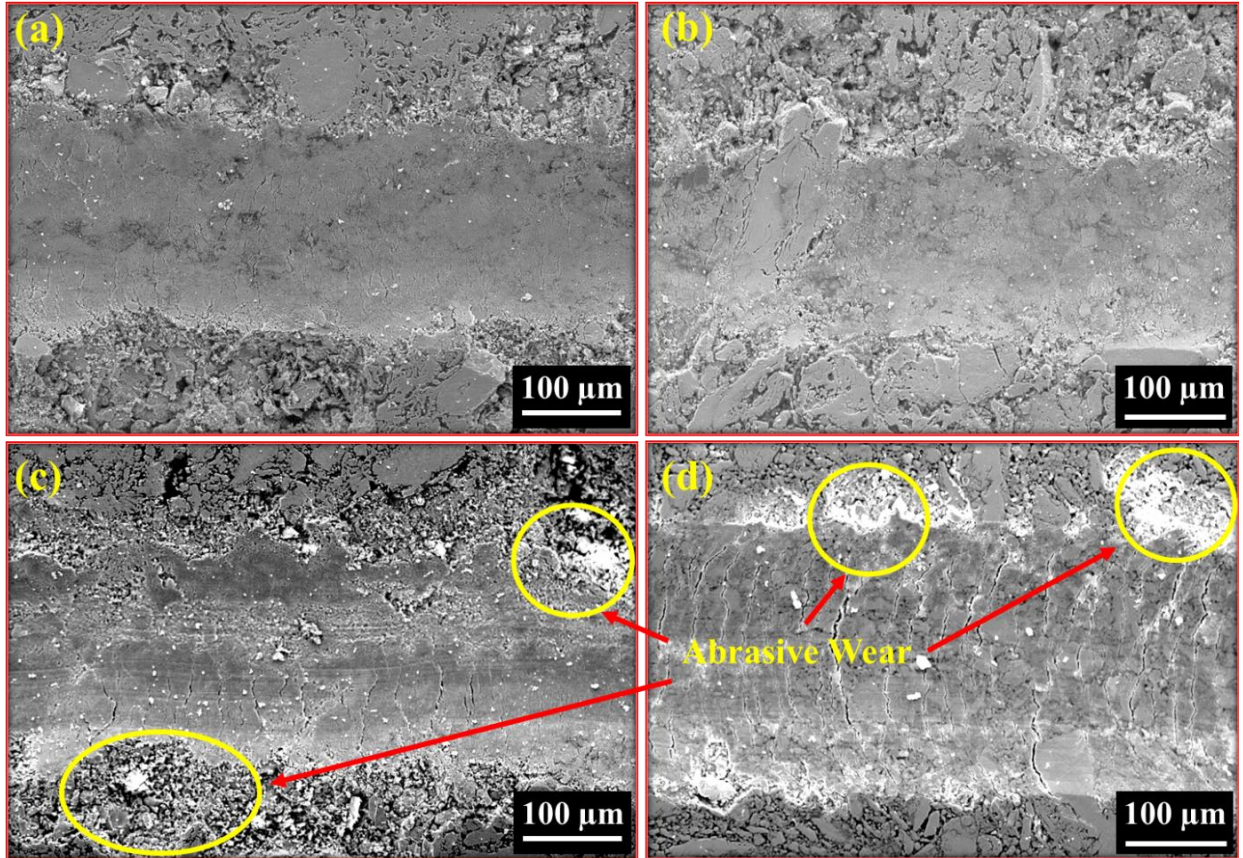


Fig. 4.14- Morphology of the scratch wear track for constant applied load (a) Pure-Ti, (b) Ti+ 1 wt.% HAp, (c) Ti+ 2 wt.% HAp, and (d) Ti+ 3 wt.% HAp

4.4.3 Corrosion Study

The finely polished sintered composite samples are examined for accelerated corrosion behaviour as per Standard ASTM G5-14 [14] electrochemical linear polarization potential measurement method using Autolab modular potentiostat (Make- Metrohm) with a 3-electrode cell set-up. For the experiment, the cell configuration consists of Platinum as the counter electrode, Ag-AgCl as the reference electrode, and the sintered Ti- μ -HAp composites having 50.265 mm² of exposure area as the working electrode (**Fig. 4.15(a)**). The physiological simulated body fluid (Hank's Balanced Salt solution (HBSS)) having a pH value similar to human blood plasma (i.e., pH 7.4) is used as an electrolytic medium and operated at a temperature of 37°C to perform the electrochemical corrosion experiments. The Tafel extrapolation technique [130,131] is used to analyze the test data to

determine the corrosion resistance (**Eq. 4.6**) and rate in detail using a standard procedure (**Fig. 4.15(b)**).

$$\text{Corrosion resistance } (R_p) = \frac{\beta_a * \beta_c}{2.3 * i_{corr} * (\beta_a + \beta_c)} \quad (4.6)$$

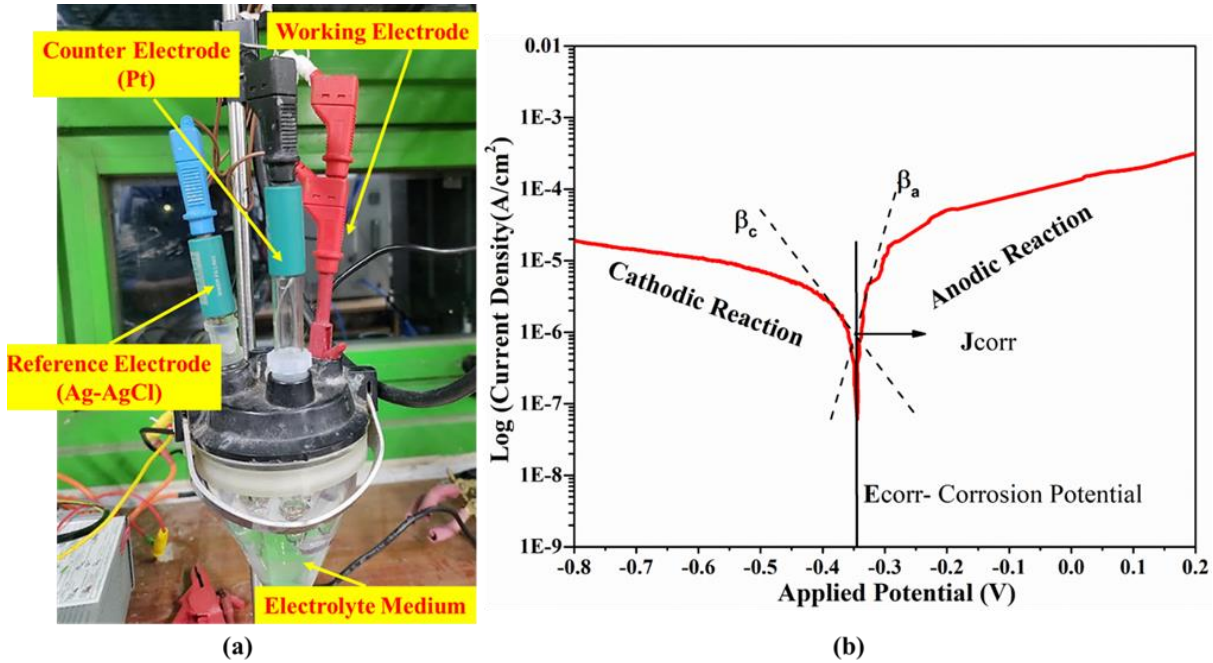


Fig. 4.15- (a) Relative density of sintered samples, (b) Three-electrode cell set-up for Electrochemical Corrosion test

The obtained morphology depicts increased pores and pore density with increasing HAP constituent. Thus, due to increasing pore density, with small cluster regions and ceramic phases in the pores, the bulk density of the sintered composite samples reduced slightly, from 3.45 g/cm³ for 1wt. % HAP to 3.26 g/cm³ for 3wt. % HAP, whereas the density of the sintered pure-Ti sample is 3.89 g/cm³. The calculated relative density of the sintered composite shows a decreasing trend with increasing HAP content, thus indicating the possibility of increased pores and surface voids along with increasing composition of HAP in the composite. **Fig. 4.16** shows the schematic depiction of the corrosion mechanism. Oxidation at the top layer has been predominantly because of the formation of Anatase (TiO₂), various oxides of calcium, and the reduction of HBSS solution into different ions [132].

Each polished sintered composite sample was consecutively used as a working electrode in an electrochemical corrosion test in a three-electrode cell set-up. The electrodes were immersed in the electrolyte solution and left for stabilization for 10 minutes to minimize the potential fluctuation and estimate a stabilized potential value for each

sample. The obtained stabilized potential value is considered open-circuit potential (OCP) for the respective samples. Once the OCP values for respective samples are obtained, the samples are further tested for a range of potential varied from -1V in anodic direction to the OCP values, at a scan rate of $1 \text{ mV}\cdot\text{s}^{-1}$, so that it can cover all the possible potential region in which corrosion may occur. The corresponding current and current density are measured for each sample for the input range of potential values. Subsequently, a tafel plot (**Fig. 4.17**) has been drawn and analyzed to calculate different corrosion characteristics using slopes of cathodic and anodic reactions. The obtained corrosion characteristics for each inspected sintered sample have been tabulated in **Table 4.3** to draw a comparative inference.

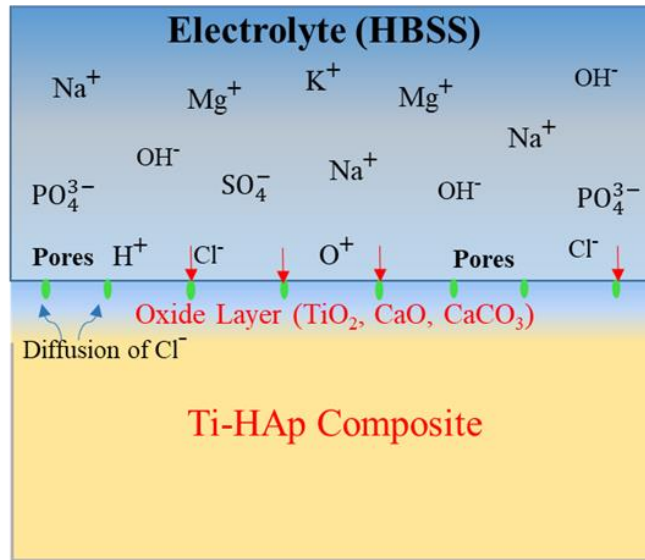


Fig. 4.16- Schematic representation of the corrosion mechanism in Ti-HAp composite

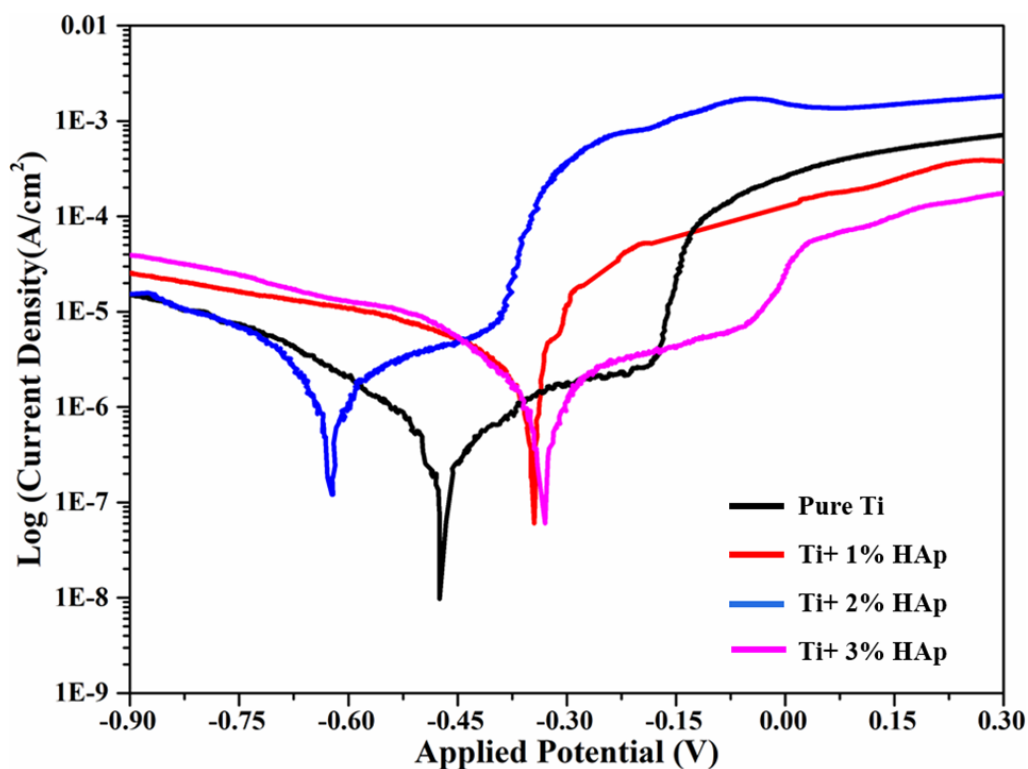


Fig. 4.17- Polarization curves (Tafel plot) obtained from Electrochemical corrosion test

Table 4.3– Electrochemical parameters acquired from Tafel analysis of sintered composite samples

Samples	OCP (V)	I _{corr} (A)	E _{corr} (V)	J _{corr} (A/cm ²)	Resistance (Ohm)	Corrosion Rate (mm/year)
Pure Ti	-0.084	2.45*e ⁻⁷	-0.47	4.84*e ⁻⁷	2.27e ⁵	0.00657
Ti+ 1% HAp	-0.231	1.55*e ⁻⁶	-0.345	3.105*e ⁻⁶	0.762e ⁵	0.0762
Ti+ 2% HAp	-0.373	7.79*e ⁻⁷	-0.626	1.553*e ⁻⁶	0.641e ⁵	0.0873
Ti+ 3% HAp	-0.103	9.81*e ⁻⁷	-0.335	1.953*e ⁻⁶	0.545e ⁵	0.0895

The surface morphology of polished sintered and corroded composite samples is inspected using SEM-EDS. **Fig. 4.18(A1-D1)** exhibits the presence of micro-pores and voids; as the HAp composition increases, the pore size and density increase, too. **Fig. 4.18(A2-D2)** shows the surface morphology of corroded samples. The pore boundaries get covered with a white corrosive layer as the present HAp forms a layer of ion in that region and restricts further corrosion of the bulk sample. The white layer is possibly CaO and CaCO₃ phases, as EDS results give predominant Ca, O, and C peaks. The EDS-Mapping reports the formation of an oxide layer over the corroded samples, along with adhered ions of Na, Mg, K, and Cl, which is the composition of HBSS used as electrolytes in the electrochemical corrosion test (**Table 4.4**). The content of Ca and P increased marginally

in the case of composite samples compared to the pure-Ti sample. This increase indicates possible apatite layer formation upon immersion into HBSS. The sintered composite exhibited good cell adhesion and growth characteristics under in-vitro conditions. The increased mineral content at the pores and voids area results in a suitable environment for the faster formation and growth of damaged bone parts [133].

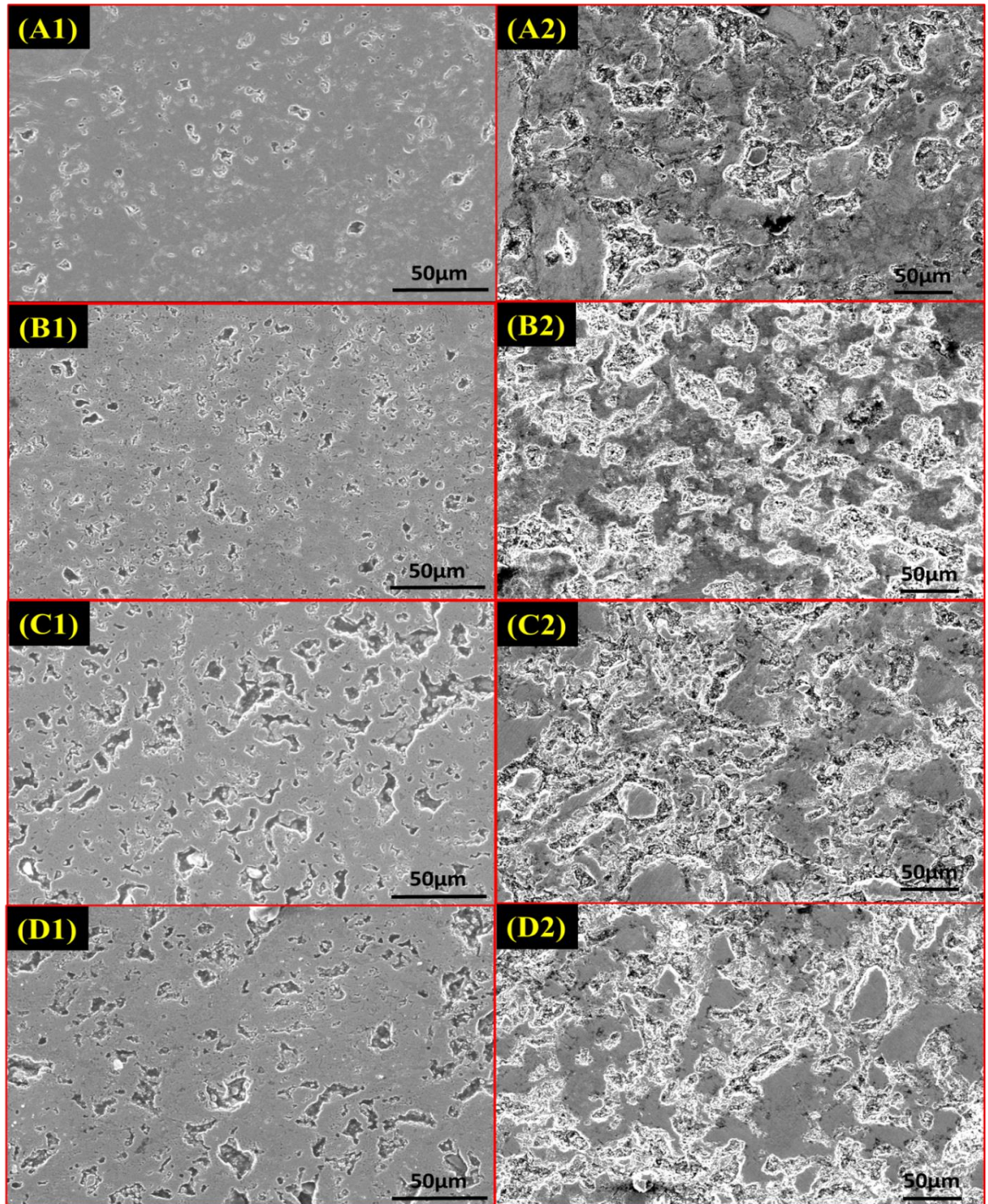


Fig. 4.18- Surface morphology of sintered samples, (A1-D1) polished as-sintered samples, (A2-D2) corroded surface after electrochemical corrosion

Table 4.4– Elemental distribution (in %) over the sintered composite surface before and after the Electrochemical corrosion test

Samples	Condition	Ti	O	C	Ca	P	Na	Mg	K	Cl	Rest
Pure Ti	As sintered	75.42	23.05	-	-	-	-	-	-	-	1.53
	After Corrosion	60.71	31.11	6.24	0.46	-	0.31	0.85	0.02	0.31	-
Ti+ 1% HAp	As sintered	68.93	24.17	5.99	0.55	0.36	-	-	-	-	-
	After Corrosion	61.36	25.88	8.17	0.45	0.09	1.61	0.63	0.12	1.68	-
Ti+ 2% HAp	As sintered	67.78	23.71	7.26	0.79	0.46	-	-	-	-	-
	After Corrosion	61.20	29.97	4.97	1.07	0.51	0.58	1.01	0.02	0.67	-
Ti+ 3% HAp	As sintered	58.03	34.77	5.55	1.00	0.65	-	-	-	-	-
	After Corrosion	47.97	33.51	15.45	1.04	0.53	0.75	0.19	0.03	0.54	-

These voids and pores are critical zones that increase the exposed area and allow electrolytes to diffuse in these zones, resulting in an increased corrosion rate. A similar observation has been observed through morphologies and elemental mapping of the corroded surfaces. The formed oxide layer further enhances The electrochemical and biological properties of Ti-based materials [134]. Oxidation of Ti formed the Anatase phase (TiO₂), resulting in bone-like apatite layer formation, contributing to enhanced bioactivity [135]. The corrosive region near the boundaries of voids and pore areas shows the formation of apatite layers with increased accumulation of ions of various minerals present as a constituent in HBSS. It exhibits the susceptibility of surface voids and pores towards corrosion and further increases the corrosion in bulk sintered composites.

4.5 In-vitro Cytocompatibility of Sintered Composite Samples

The MHH sintered Ti-μHAp composite pallets/samples are investigated for an In-vitro biocompatibility test by performing an MTT assay. It is a colorimetric assay method to

determine metabolically active cells on the surfaces of materials quantitatively. Mitochondrial enzymes of metabolically active cells react with Tetrazolium salt (3(4, 5-dimethylthiazol-2-yl)-2, 5-diphenyl tetrazolium bromide (MTT) and form purple color formazan crystals. Initially, fresh mouse fibroblast cells are cultured in the RPMI media for four hours, then centrifuged before seeding to the composite pallets after being washed

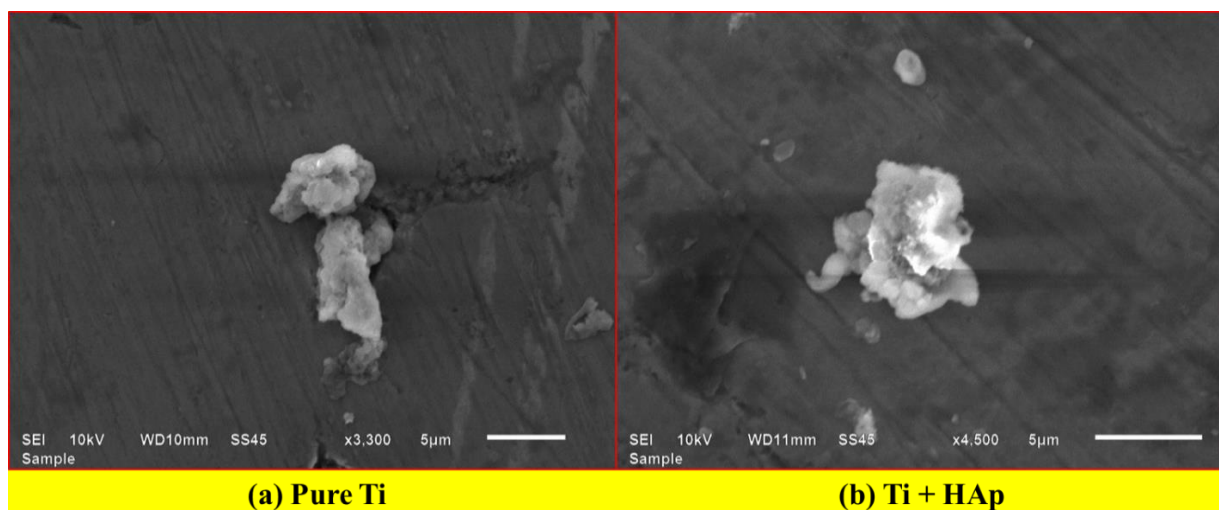


Fig. 4.19 - Adherence and growth of cells after first day of incubation

with media solution and incubated for four hours. Further, the seeded cells are cultured in a CO₂ incubator (with 5% CO₂ and 95% relative humidity) at 37.4°C for 1 (Fig. 4.19- to show the cell adhere and growth after 1 day) and 7 Days. After incubating for a designated period, the MTT solution is removed and treated with the DMSO solution. Then, the treated samples are inspected for cell absorbance. A Thermo Scientific™ Multiskan-GO Microplate Spectrophotometer is used to analyze the quantitative absorbance of cells at 570 nm wavelength for the mechanically alloyed powders. The adherence of the cells was inspected through the microscopy technique to represent the bioactivity of sintered composite samples.

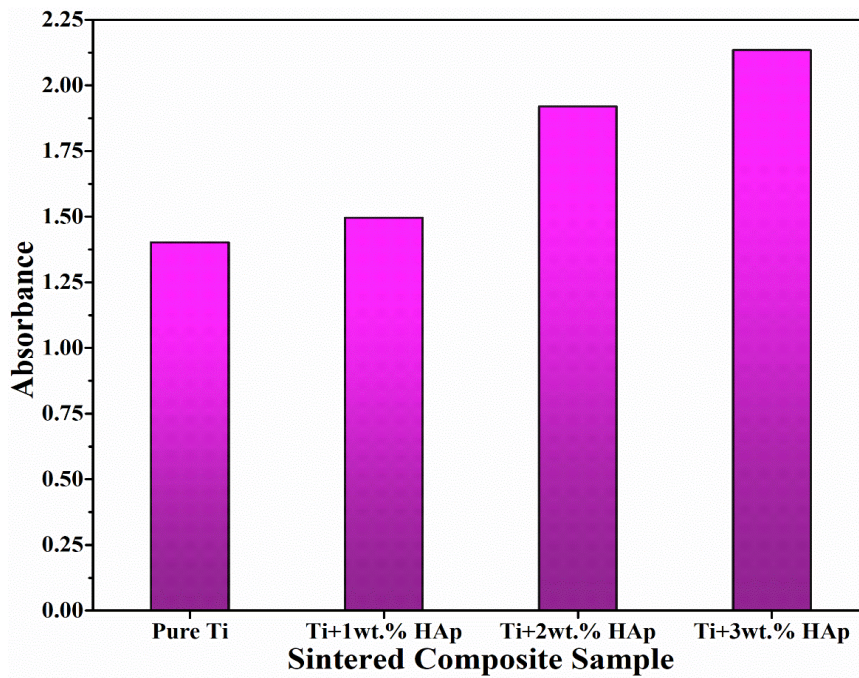


Fig. 4.20 - Cytocompatibility analysis of the sintered composite samples using MTT Assays

A biomaterial is cytocompatible if it does not harm the cells and allows cell growth. The sintered composites are tested for in-vitro cell culture with mouse fibroblast cells, and an MTT assay test is performed to quantify the cell absorbance by the samples. The cell-seeded sintered Ti-HAp samples are kept inside an RPMI media for seven days; during this period, the fresh media solution is supplied at regular intervals to keep the cells healthy by providing the required proteins and nutrients for cell growth. The MTT result (**Fig. 4.20**) and SEM images (**Fig. 4.21- to show the density of cell adherence**) indicate that with higher HAp composition, the cell absorbance has been considerably increased. As the HAp is favorable for tissue/cell growth, its addition to Ti makes it suitable for high-load-bearing implants with enhanced biocompatibility. The SEM images of cell-cultured composites show that a layer has been deposited near the cell area, which exhibits the formation of an apatite layer over a period of time. With more HAp composition and seeding time period, the cell becomes more flattened, and clearly visible proliferation over the surface is observed [119]. The formation of an apatite layer, which is essential for bone-cell attachment, shows that the composite surface has undergone a possible bio-dissolution, and it suggests that the in-vitro-tested material is suitable for bone-implant applications [136]. From **Fig. 4.21 (c) & (d)**, it appears that the surface voids of the composites are being filled with the grown cells, representing the formation of a chain of extra-cellular matrix, which helps the cell to attach and further grow for the functioning of the cell lines.

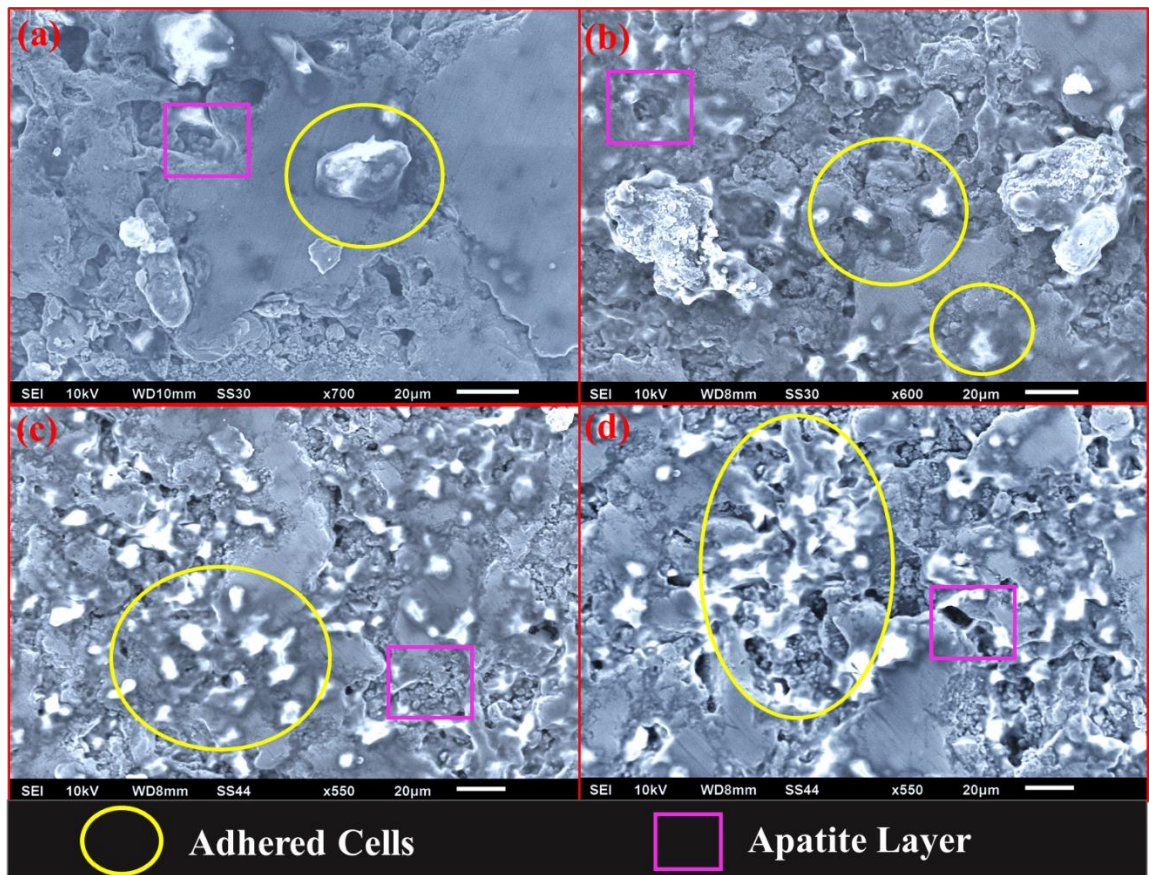


Fig. 4.21- SEM images of adhered cell and apatite layer over the sintered composites, (a) Pure-Ti, (b) Ti+ 1 wt.% HAp, (c) Ti+ 2 wt.% HAp, and (d) Ti+ 3 wt.% HAp

4.6 Discussion

The metal-ceramic composites sintered using the MHH process show uniformly distributed elements in the bulk. The sintered composites have been tested and analyzed for mechanical, tribological, electrochemical corrosion, and biological characteristics. All the sintered Ti-HAp composites retain the Ca: P ratio well within the permissible range of 1.6, suitable for metallic implants for effective tissue and cell growth [137]. The nano-mechanical characteristics show it decreased modulus and nano-hardness values with increasing HAp compositions, showing a potential composite for minimizing the stress-shielding behaviour. Similarly, the frictional forces and coefficient of friction values also follow the decreasing trend, exhibiting the softness or smoother surface with increasing HAp compositions, showing feasible interfacial properties of resulting bio-material and tissue interaction. The sample's relative density and surface morphologies show an increase in surface voids and pores in the sintered composites, with the increase in HAp composition acting as critical zones responsible for corrosion. It increases the exposure area and allows electrolytes to diffuse, resulting in an increased corrosion rate. The formed oxide layer further enhances The electrochemical and biological properties of Ti-based materials [134].

Oxidation of Ti forms the Anatase phase (TiO_2), resulting in bone-like apatite layer formation, contributing to enhanced bioactivity [138]. Further, it increases the corrosion in the bulk sintered composites, as pore and surface voids act as nucleation sites for corrosion by exposing internal surfaces to an open environment with increased surface area. The formation of an apatite-like layer with feasible wettability properties indicates enhanced bioactivity for the sintered composites with a higher composition of HAp. A similar result has been observed through MTT assays and micrographs of cell-adhered samples.

4.7 Summary

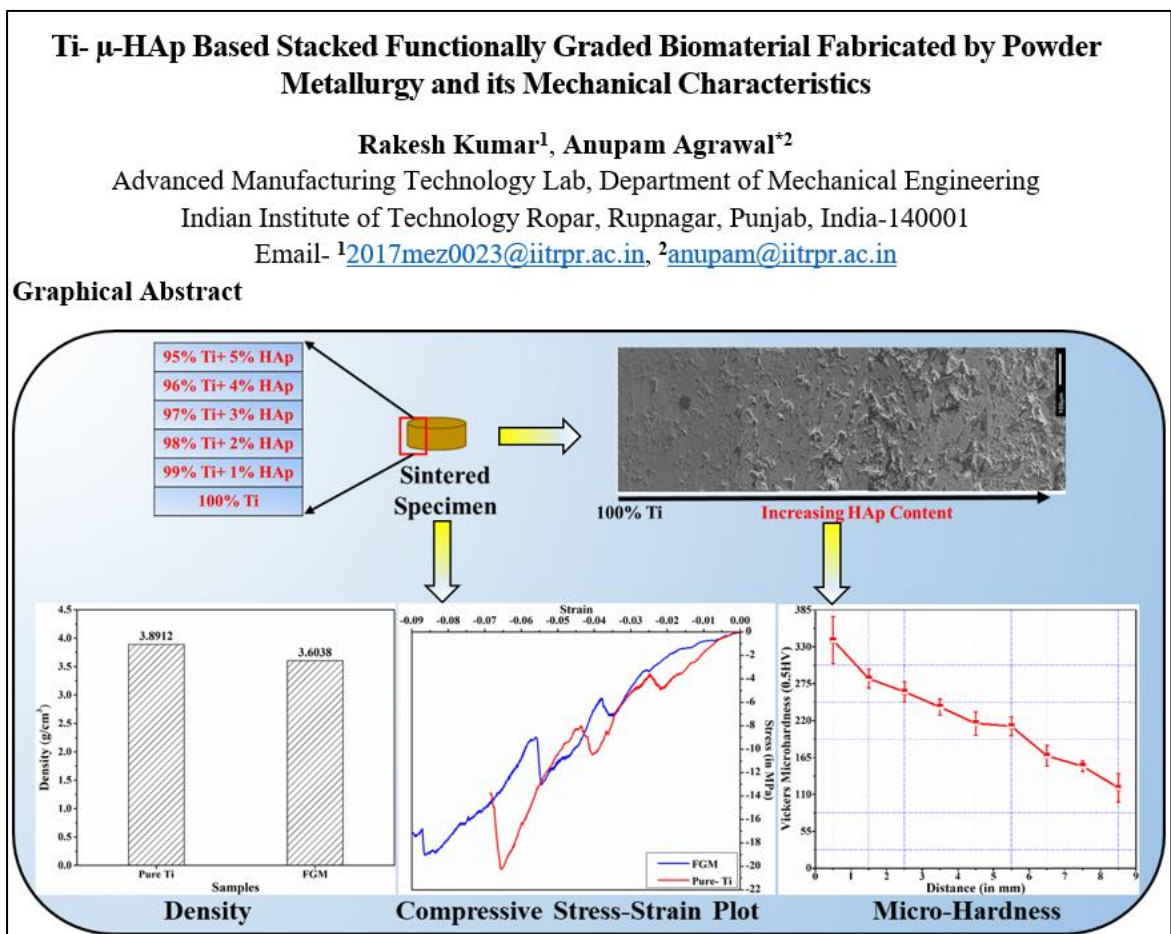
By reinforcing with HAp, Ti-based composites were effectively sintered through powder metallurgy and hybrid microwave sintering processes to address the stress-shielding effect. The primary outcomes of the present study are as follows:

- The composite HEBM powders contain Ca: P in the limiting range of 1.6:1, and it is uniformly distributed in the sintered bulk composite samples, which is acceptable for use as a chemically stable biocompatible material.
- Compared to the Pure-Ti sample, an appreciable reduction of 16.09% in density is observed for reinforcement of 3 wt.% μ -HAp.
- The microscopy confirms the presence of micro-pores over the sintered samples, which can be a possible nucleation site for tissue culture and cell growth, which is further effectively visualized by in-vitro cytocompatibility test.
- The increasing concentration of μ -HAp reduces the nano-hardness and surface elastic modulus values. The sintered composite with 3 wt.% of HAp exhibits approx. 46.5% and 61.69% lesser nano-hardness and elastic modulus, respectively, compared to sintered Pure-Ti sample.

Chapter-5

Fabrication of Functionally Graded Bio-Material and its Characterization

This chapter discusses the third objective of the present work, i.e., the fabrication of Functionally Graded Material (FGM) using HEBM processed metal-ceramic alloyed materials by microwave sintering process. The fabricated FGM is characterized by its mechanical and tribological properties to understand the effect of gradation of materials.



5.1 Synthesis of Ti-HAp-based FGM

Commercially pure Ti with 100-120 mesh size and μ -HAp with 270-300 mesh size powders having irregular shaped particles are used as raw material to fabricate the desired metal-ceramic FGM (schematic presented in **Fig. 5.1**). Pure-Ti pre-mixed with 1-5 wt.% of μ -HAp is homogenously alloyed individually using high energy ball milling (HEBM) process with tungsten ball media. The powder-to-ball ratio is maintained at 1:10 for each composition for easy dispersion of HAp particles over CP-Ti. It is noticed that there is an appreciable reduction in particle size after an effective milling of 4 hours. Properly homogenized and alloyed powders are stacked in a cylindrical die with an increasing

composition of HAp. To ensure each composition's uniform thickness, a fixed volume of milled powder is stacked and compacted at a maximum pressure of 650 MPa using a hydraulic press to provide effective cohesion and strength to the green specimen. The compacted green specimen is sintered using a microwave hybrid heating furnace at a maximum temperature of 1250°C, followed by furnace cooling. The heating rate is maintained at 80-85°C/min and holding it for 5 min at the maximum temperature to ensure proper densification and consolidation of the green specimen upon sintering [139].

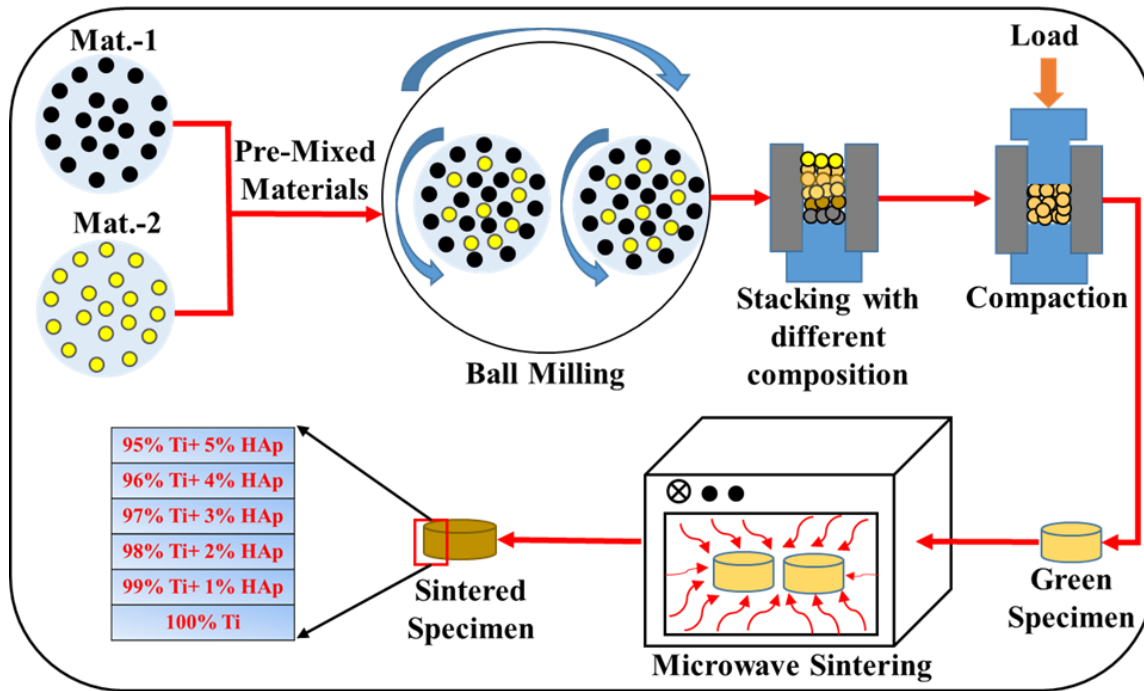


Fig. 5.1- Schematic of the steps followed to fabricate FGM using the PM route

5.2 Morphological and Elemental Characterization using SEM-EDS

The milled and homogenously alloyed powders were effectively cold compacted by stacking each composition to achieve a material gradient. The stacked green compact samples were further processed through MHH for sintering to attain proper densification and strength. The sintered FGM was grounded and polished using abrasive papers followed by diamond suspension to achieve a smooth and flat surface. After polishing, the sintered FGM was inspected through SEM to inspect its surface morphology. **Fig. 5.2** shows a magnified SEM image of the polished FGM along the direction of increasing HAp composition. With the increasing composition of HAp, the surface exhibits an increase in surface voids, pore density, and size. The metal-ceramic composites usually get bonded through diffusion at the interface of individual particles (**Fig. 5.3**). The magnified SEM image of the surface shows surface characteristics in a better way, consisting of coalescence of individual particles resulting in effective bond formation to provide strength. Few shiny

particles exist between two particles representing ceramic (HAp) dominant particulate. To check the grading of composition, elemental line-mapping of the sintered bulk sample along the gradation direction has been investigated and plotted in **Fig. 5.4**. The percentage distribution of Titanium decreases, and that of Calcium and Phosphorus increases along the increasing HAp composition direction. **As Ti is highly susceptible to oxygen, hence with increasing HAp compositions the Ti concentration is decreasing and concentration of “O” and “C” elements are increasing due to possible formation of oxide and dissolution of Carbon atom from HAp.**

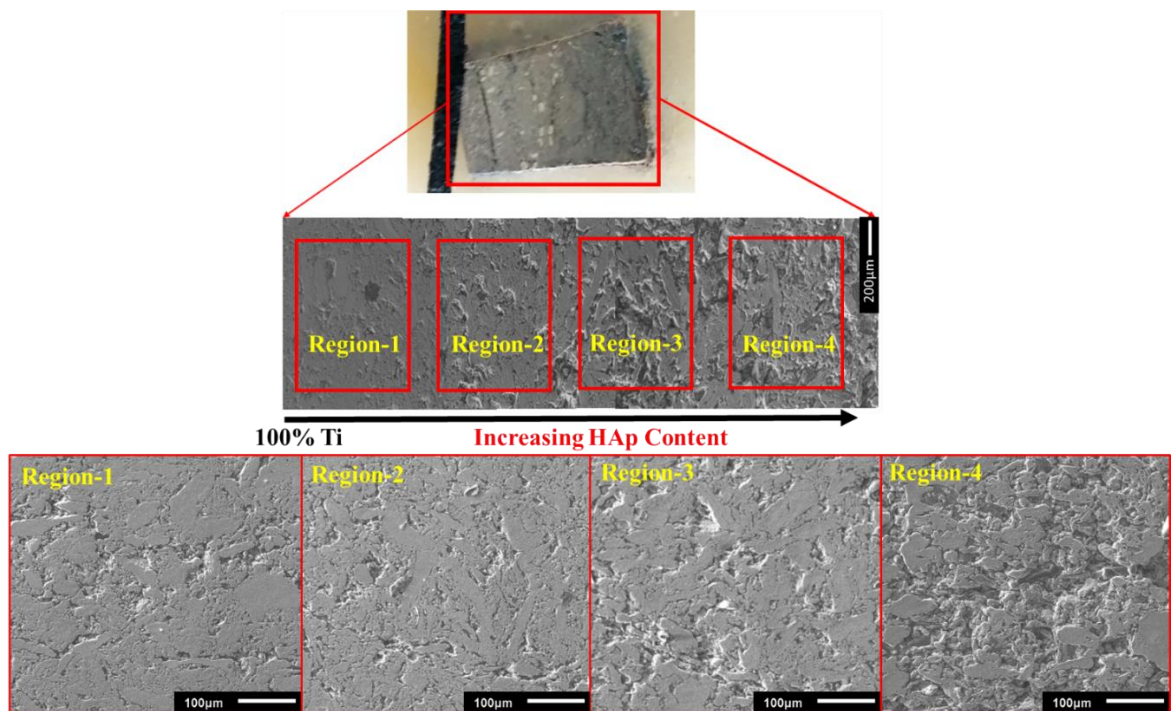


Fig. 5.2- SEM image of sintered FGM through powder metallurgy route exhibiting variation in pores density too with varying composition

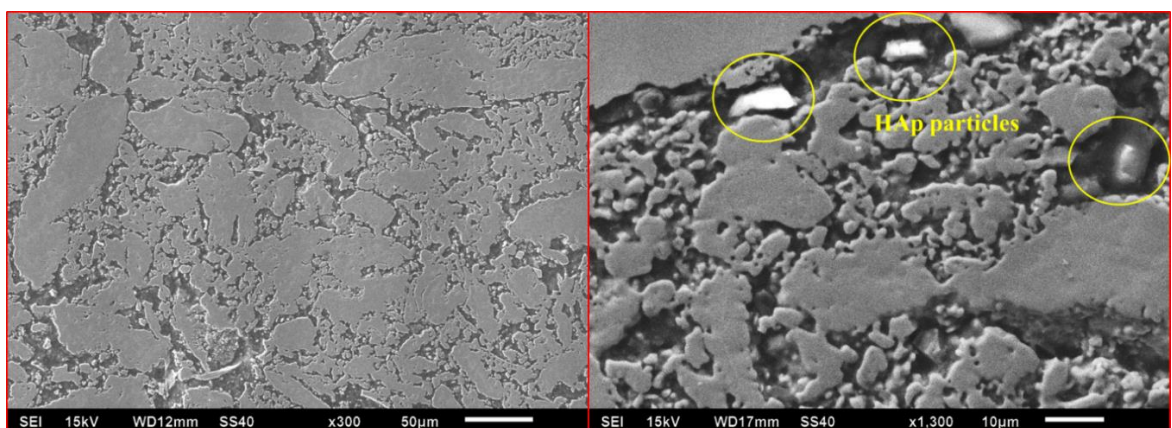


Fig. 5.3- Magnified image showing bonding of sintered particles

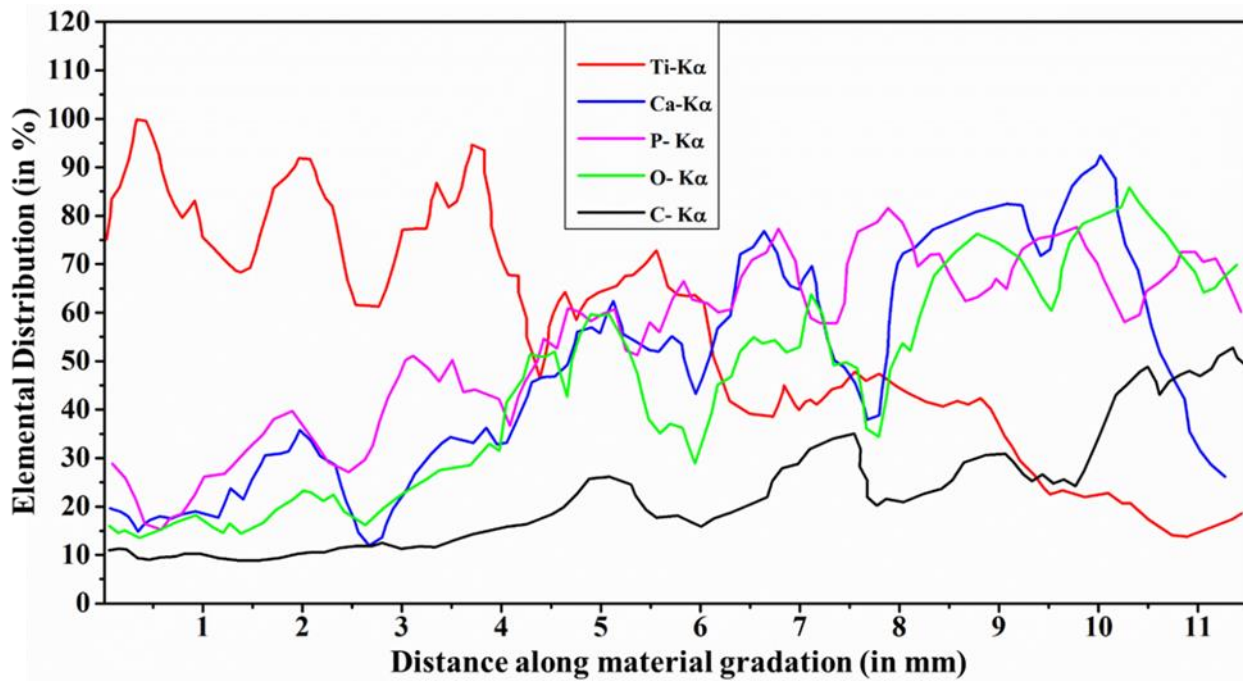


Fig. 5.4- EDS-Line mapping of sintered FGM

5.3 Mechanical Characteristics of Sintered FGM

The sintered homogenously distributed Ti- μ -HAp sample is inspected using a Scanning Electron Microscope equipped with Energy Dispersive Spectroscopy (SEM-EDS) to check the grading of material and elemental composition along the stacked direction. The line-scanning method was used to map the elemental distribution along the gradient direction. The density of the fabricated graded samples is measured using the water displacement method (Archimedes' principle) and compared with a sintered pure-Ti sample processed through a similar procedure. The sintered cylindrical FGM sample is cut across the rectangular plane along the height and cold-mounted using polymer resin. The mounted specimens are finely grounded and polished using SiC emery paper with a grit size of 400-2500, followed by cloth polishing in diamond suspension medium. The polished scratch-free surfaces were inspected using SEM-EDS to analyze the morphology and elemental distribution in the bulk. The microhardness is tested experimentally using Vickers' Microhardness testing set-up at 0.5 kgf (5N) load with diamond indenter. The polished sample's bulk mechanical properties (modulus and strength) are measured through compression tests at 0.5 mm/min deformation rate with a load cell of 10 kN using hydraulic Universal Testing Machines (Make- Shimadzu, Japan).

5.3.1 Density Measurement

The microscopic images and elemental distribution confirm the effective sintering of stacked HEBM powdered material to fabricate FGM. The density of the as-sintered FGM

sample (ρ_{sample}) were experimentally determined using Archimedes' principle by immersing in water and measuring the displaced weight ($\Delta Wt.$). Here Wt_{air} and Wt_{water} represents the sample weight when suspended in air and when fully immersed in water, respectively. The density of the FGM sample is obtained as 3.60 g/cm^3 , which is relatively less than the sintered pure-Ti sample (Fig. 5.5) because of the addition of HAp in a stacking manner, and the same can be mathematically validated using the principle of “rule of mixture.”

$$\rho_{sample} = \frac{\rho_{water} \times Wt_{air}}{\Delta Wt.} \quad (5.1)$$

$$\Delta Wt. = Wt_{air} - Wt_{water} \quad (5.2)$$

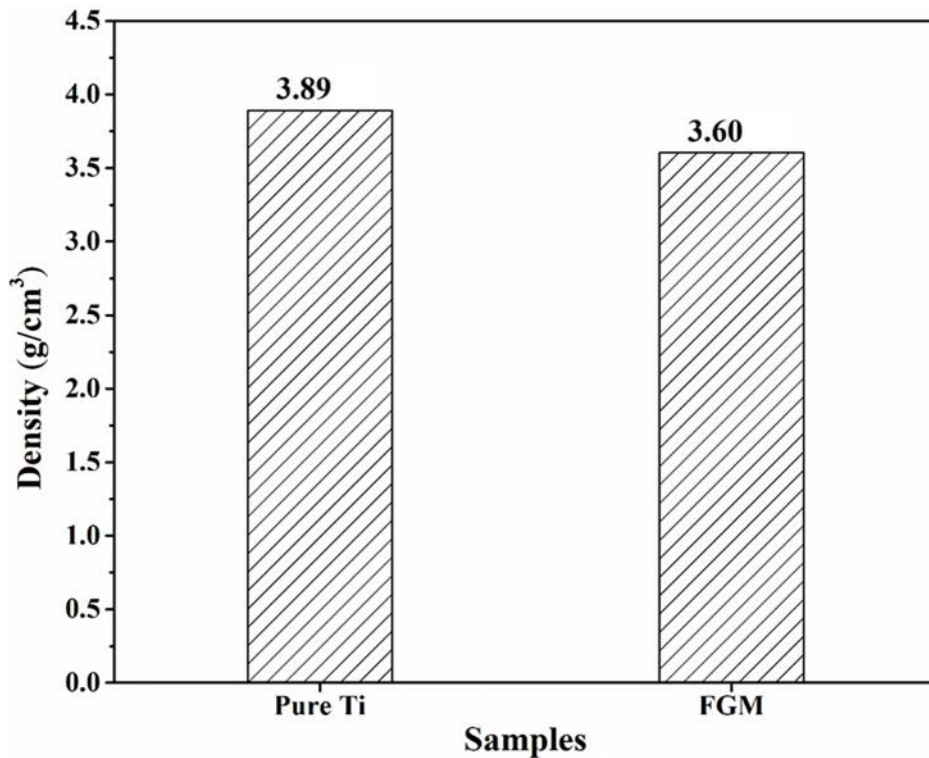


Fig. 5.5- Density of sintered samples measured using Archimedes' principle

5.3.2 Compression Behaviour

The stacked sintered FGM has been tested for compressive properties using a uniaxial compression test. The samples are tested by applying a compressive load along the stacking direction till it gets crushed. The obtained FGM's compression result is compared with the sintered Pure-Ti sample (Fig. 5.6). The crushed sintered sample shows a ductile failure with a crack having an inclination angle of around 40-45 degrees, which is followed by the

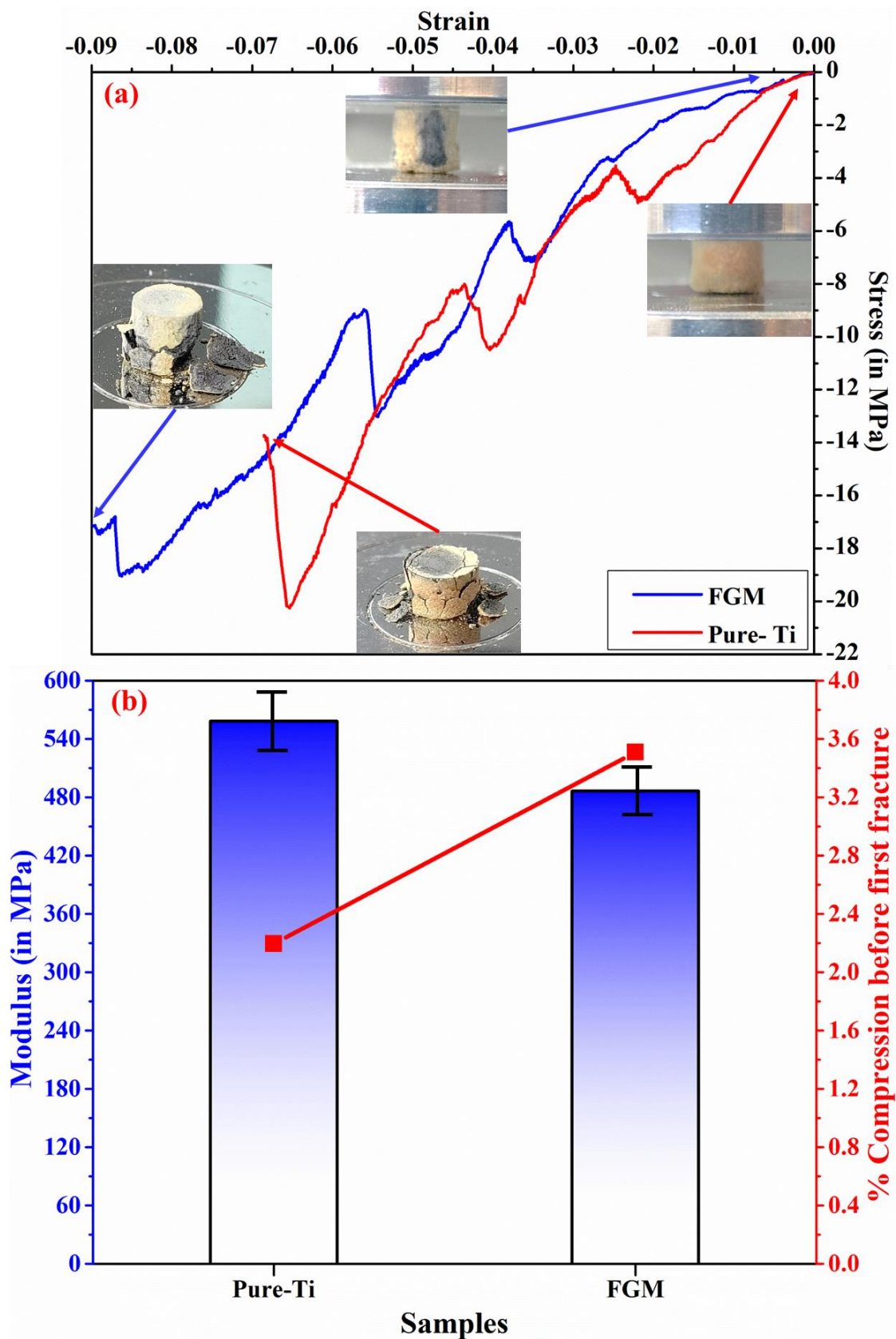


Fig. 5.6- Compression behaviour of sintered FGM (a) compressive stress vs strain plot, (b) comparative modulus and compression before first fracture point

accumulation of the damaged portion, resulting in increase in stress values (densification). **Table 5.1** shows the comparative mechanical properties obtained for both samples from compression tests. The Pure-Ti sample outperforms the FGM sample significantly with respect to all the mechanical characteristics. It deduces that fabricated FGM has lower modulus and compressive elongation, and thus, its application in making bio-implants can appreciably minimize the stress-shielding effect.

Table 5.1- Mechanical Properties calculated after compression test

Properties (Units)	Values	
	Pure-Ti	FGM
Modulus (MPa)	558.25± 24.2	486.23± 19.2
Deformation (in %)	2.20	3.51
Stiffness (kN-mm)	4.947	3.149

5.3.3 Microhardness

The finely polished sintered FGM sample is tested using a Vickers Micro-hardness test set-up with a diamond indenter along the direction of increasing HAp composition. The mounted sample was marked at an equal interval of 1 mm to define the position for indentations. An indentation load of 0.5 kgf for 10 sec was used and multiple indents were made along a defined line in each section to calculate average micro-hardness values. **Fig. 5.7** shows obtained micro-hardness values and linearly fitted trend line toward increasing HAp composition. With an increase in HAp composition in the FGM, the hardness values decreases. The regression coefficient (R^2) of the fitted trend line is 0.979, which represents the smooth transition/stacking of material in the bulk FGM. The decreasing micro-hardness trend exhibited the gradient-softening nature of the FGM in the direction of gradation of HAp. This may help to design and fabricate the actual bone structure with varying mechanical properties (cortical and cancellous bone together) with varying material composition.

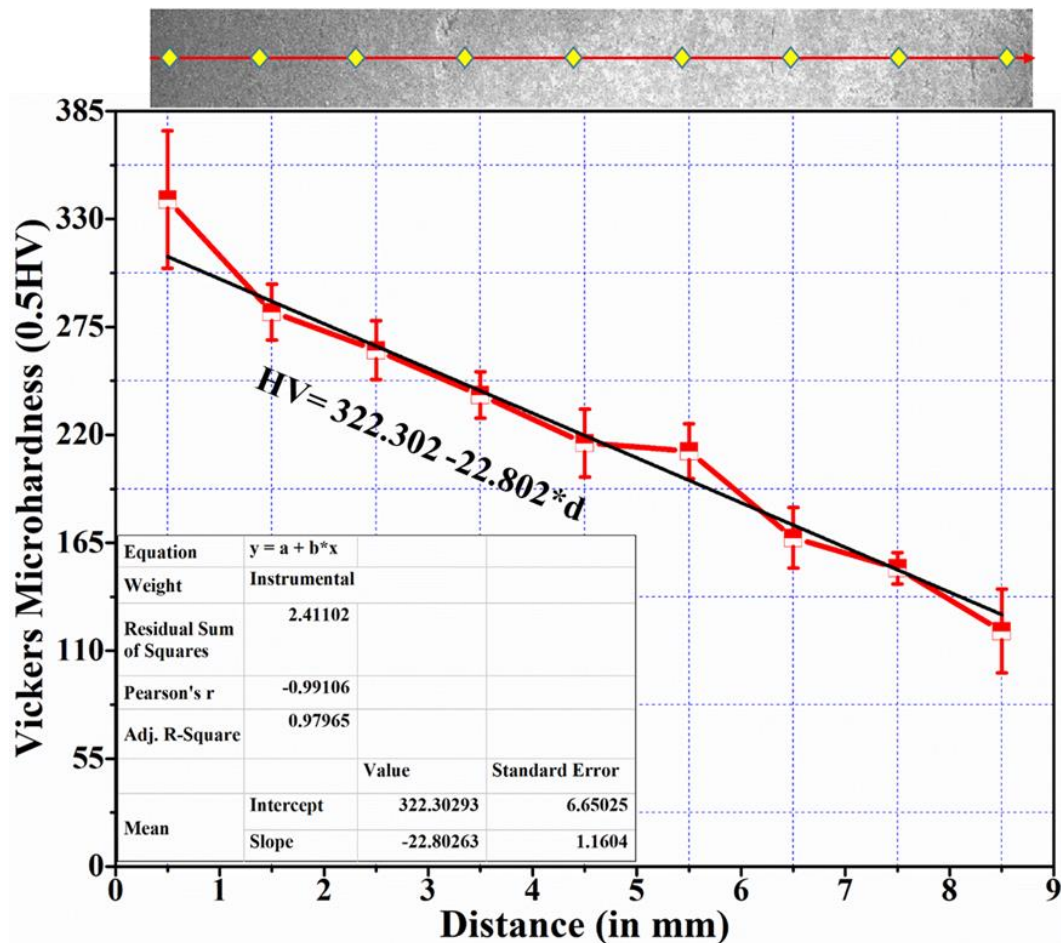


Fig. 5.7- Vickers micro-hardness values of sintered FGM

5.4 Surface and Wear Characteristics

The surface wear and frictional characteristics are tested and analyzed using a Universal Tribometer Set-up (CETR-UMT-2) employing a scratch testing method. The frictional forces and coefficient of friction are also calculated to study the tribological properties of fabricated FGM. With the help of a conical diamond indenter, a scratch is marked over the polished surface of sintered FGM. A linear scratch of 10 mm in length at a speed of 0.5 mm/sec with a constant load of 2kgf (20 N). The scratch profile is analyzed using SEM-EDS to study the wear mode and morphology. **Fig. 5.8** shows the variation of resulting frictional forces and coefficient of friction along the scratch track. At the start of the track for both samples, the frictional force remains equal and changes as the composition gradation starts. The frictional force values for the FGM are comparatively lower than the pure-Ti sample in the gradation direction. The coefficient of friction values show similar trends along the scratch track. The frictional forces and coefficient of friction results show that increasing the HAp composition along the track depicting the synthesized FGM, is getting softer and smoother resulting in lesser reaction forces and lower coefficient of friction values.

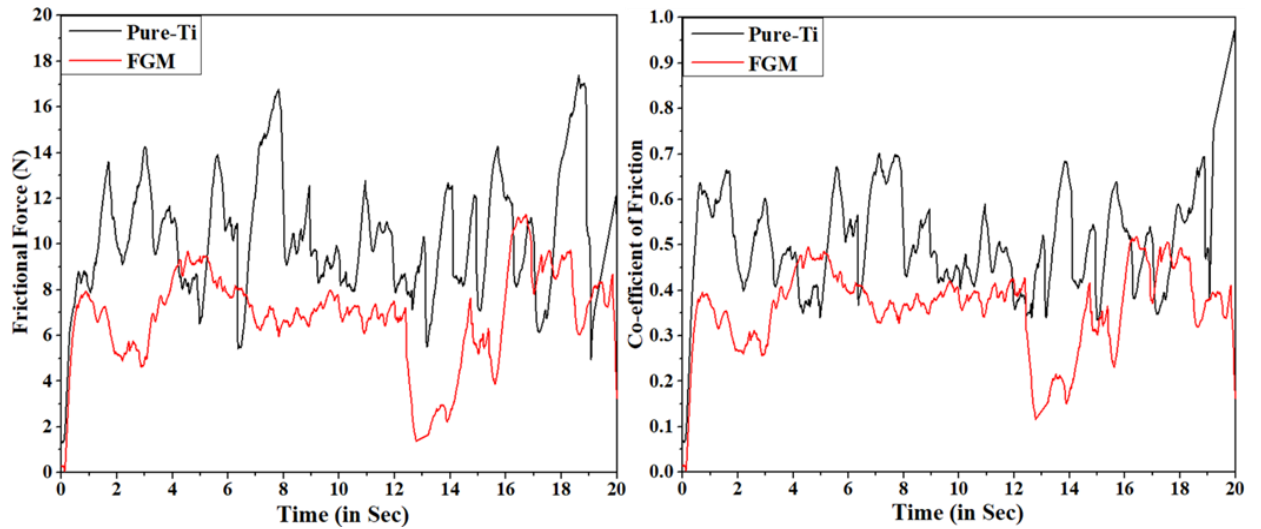


Fig. 5.8- Comparative frictional force and coefficient of friction

The scratch track marked to test the surface properties (frictional forces and coefficient of friction values) is inspected using SEM to study the surface morphology near the tracks to study the wear characteristics of the inspected samples. The SEM images have been captured at different locations along the increasing HAp direction (**Fig. 5.9**). Increasing HAp content in the FGM, increases wear track width, it indicates that more indenter penetration has taken place due to softening of bulk material in the direction of HAp gradation. As well as in the exposed white shiny surface and chipped-out debris particles towards higher HAp composition exhibit abrasion wear of the tested samples, as these shiny

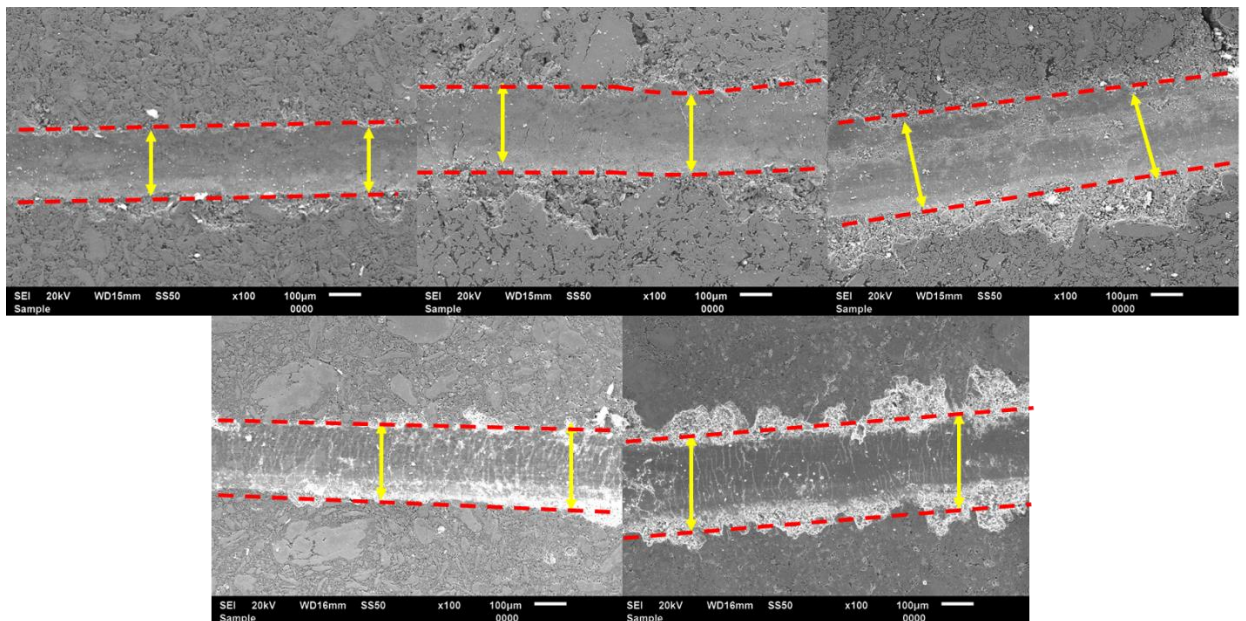


Fig. 5.9- Morphology of scratched wear tracks at different locations

layers are characterized as oxides of the constituent Ti element, causing abrasion during scratch testing. With increasing HAp composition, the worn-out region has clearly visible cracks in the scratched track region. The micro-cracks show shearing in the material as sheared marks observed over the scratched tracks. The aggressive wear of FGM towards the HAp dominant region confirms the softness of the material, which can carry lower load.

5.5 Discussion

The FGM is effectively sintered using HEBM-processed homogeneously alloyed powders, followed by an MHH sintering process with better relative density and uniform dispersion of elements in bulk. The morphological and elemental study of the sintered FGM exhibit proper gradation of HAp. However, like composites, the pore density increases along the gradation direction (with increasing HAp). Hence, effective density is lower for the FGM compared to the pure-Ti sintered sample. The Vickers micro-hardness tests performed with FGM exhibit a reduction of hardness value in the direction of gradation because adding HAp reduces the overall hardness of the composition, confirming that a proper sintering of FGM has been done. The modulus of the sintered FGM is relatively lower than that of the pure-Ti sample. Thus, it can be concluded that the FGM can be used in fabrication of bio-mimicked load-bearing implants having nearly the same architecture and mechanical properties as that of natural bone [140,141]. The comparative results of mechanical properties between fabricated FGM and natural bone (from reference) has been included in **Table 5.2**. In brief, as the fabricated FGM is aimed to be used as a replacement of high load bearing implant (i.e, femur, knee joint and hip cup, etc.). The obtained mechanical properties of FGM are comparable with the literature data with close agreement (**Fig. 5.10**).

Table 5.2- Mechanical properties for human cortical femur bone [142]

	Male	Female	P value
Tensile strength MPa	39.74±4.80	30.08±7.96	<0.001
Compressive strength MPa	141.6±15.91	118.91±18.99	<0.001
Young's modulus MPa	338.3±179.74	404.7±314	0.322

The decreasing frictional and wear properties with increasing HAp composition also reflect the behavior of fabricated FGM as a possible solution for minimizing stress-shielding and interfacial properties compared to mono-material (metal or ceramics) for implant design and fabrication. The modulus of implant materials is a core factor in adequate transfer of stress to the surrounding bone. The more rigid the stem, the less load

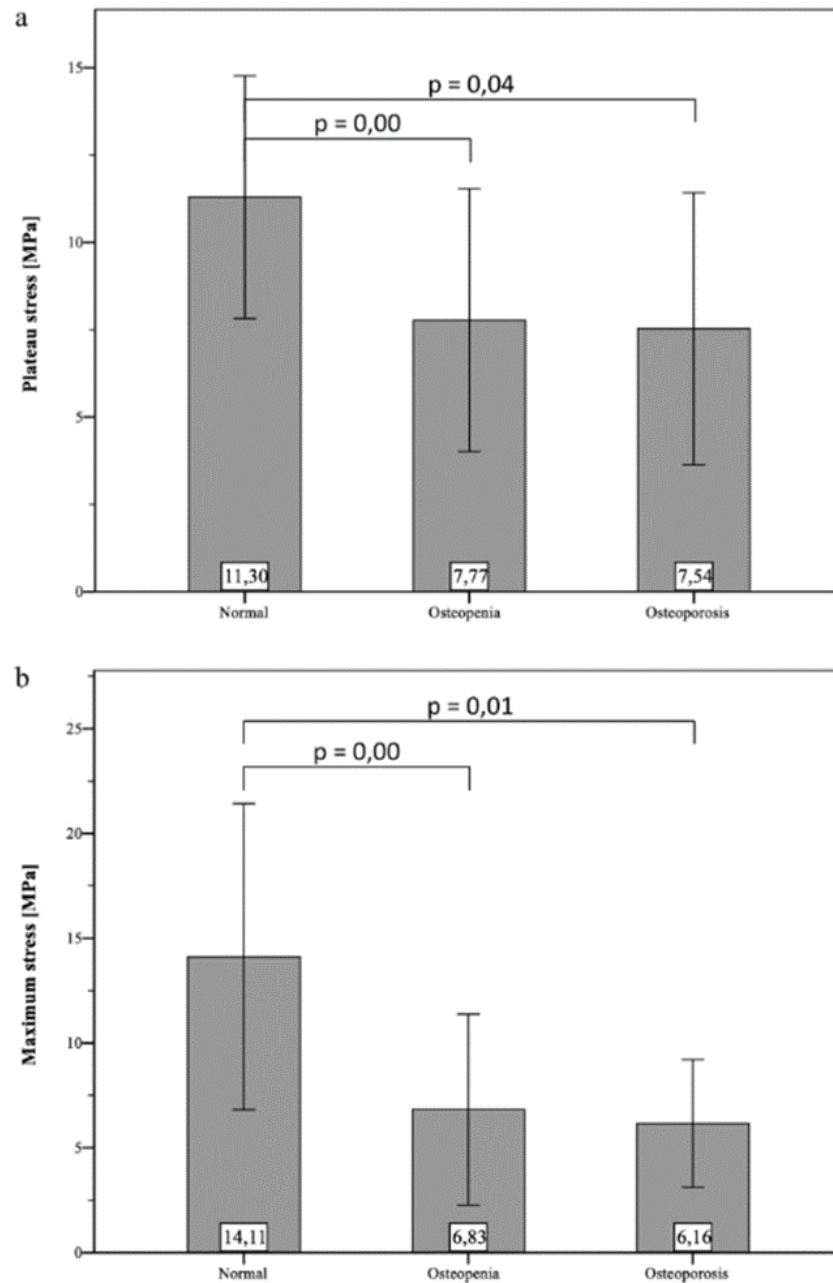


Fig. 5.10- Mean values (with standard deviation) of the determined mechanical properties [143]

it transfers proximally so the greater the stress shielding of the proximal femur. By decreasing the implant modulus of elasticity enhances implant-to-bone stress loading and can minimize bone atrophy due to stress shielding. As such no quantitative data for stress shielding of any bioimplant is available. However, as an assertion to signify the stress-shielding data a comparison has been conducted to show case the acceptability of fabricated FGM (Table 5.3),

Table 5.3- Ratio of modulus values to represent as a stress-shielding indicator

Compressive Modulus of Femur bone (M_{fb})	Compressive Modulus of Pure Ti (M_{Ti})	Compressive Modulus of FGM (M_{FGM})	Ratio	
			M_{Ti} / M_{fb}	M_{FGM} / M_{fb}
338.3 MPa	558 MPa	486 MPa	1.65	1.43

5.6 Summary

The HEBM-processed Ti-HAp powders were compacted and sintered with 1-5 wt.% of HAp composition in a graded manner to synthesize the FGM. The detailed characterization draws the following conclusions to prove it for suitable application as implants by mimicking the architecture of high load-bearing bone.

- The HEBM-processed materials with specific compositions were effectively sintered in a graded manner using the Microwave sintering process to achieve proper densification and strength.
- The SEM-EDS results through pore density, morphological, and elemental distribution confirm the materials' gradation from stacking during the synthesizing process compaction stage.
- The obtained micro-hardness results in the HAp gradation direction exhibits how the mechanical properties vary along the gradation direction, and thus it effectively mimics the actual architecture of natural bone structure.
- The compressive modulus and compression values for synthesized FGM are comparatively lower than the pure-Ti sample.
- The frictional and wear characteristics exhibit the softening and abrasion wear of FGM in the direction of HAp gradation in the bulk, depicting the feasibility of it being used as a potential implant material to minimize the stress-shielding behaviour in existing implant materials.

Chapter-6

6.1 Conclusions

Titanium is the most suitable and widely researched metallic biomaterial for biomedical applications. However, its higher mechanical properties (modulus and hardness) compared to natural bone architecture may cause damage to the existing bones and bone-tissue interface due to stress-shielding. The stress-shielding of implants leads to severe suffering due to the deterioration of surrounding natural bone and tissues, followed by inflammation and irritation in the affected area. Extensive literature suggests that multi-material (metal-ceramics or metal-metal) based implants can appreciably reduce the mechanical modulus and hardness and provide requisite mechanical characteristics, thus providing possible solutions to severe issues like interaction and stress-shielding of existing implant materials. In this work, raw materials, a metal- Pure-Ti and a ceramic-HAp, have been processed and synthesized to fabricate suitable materials for such applications.

In the first objective, an effective homogenization and alloying of raw materials has been performed using the HEBM process, resulting in uniform dispersion of ceramics over the Ti powder particle with stable crystalline phases having a requisite strong bond of the functional group responsible for cell culture and apatite layer formation. The in-vitro cytocompatibility test confirms an enhanced cell absorbance with higher HAp powders.

In the second objective, the HEBM-processed raw materials were sintered into composites using the MHH process. The morphological, chemical, mechanical, tribological, corrosion, and biological characteristics (MTT Assay) have been evaluated and analyzed to study various properties. The nano-indentation study of the inspected composites revealed decreasing modulus and hardness values for higher HAp compositions. With the increasing HAp composition, the coefficient of friction decreases, and cell viability increases, showcasing the potential of HAp addition to pure-Ti material.

Similar to composites, in the third objective of the study, the milled raw materials were compacted and sintered into FGM by stacking each composition of materials in the desired sequence of increasing HAp. The synthesized FGM exhibits an appreciable decrease in modulus and micro-hardness in the increasing HAp composition compared to the sintered pure-Ti sample, which can help minimize the stress-shielding behaviour of high-load bearing implant during its usage. The tribological and wear properties and in-vitro

cytocompatibility test show the superior behaviour of Ti-HAp composite than the pure metallic counterparts.

6.2 Future Scope

The need for healthcare facilities with improved lifestyles is never-ending in healthcare industries. With the advancement or development in science and technology, a lot of new and unique advanced devices and tools are coming. Hence, the future work can be undertaken in the following areas,

- a) Introducing more advanced synthetic material having much lower mechanical strength equivalent to the natural bone architecture.
- b) Introducing controlled porosity variation in the bulk and material composition variation for enhanced cell proliferation.
- c) Introducing a layered additive manufacturing process to fabricate compositionally gradient materials will ease the fabrication of porosity-controlled implants/scaffolds.
- d) A plethora of research is going on with lattice-based structural architecture with better mechanical properties, so the developed metal-ceramic-based composites can be used to fabricate such lattice-based femur or hip-cup implant fabrication.

Bibliography

- [1] C.F. van Eck, A.F. Chen, B.A. Klatt, J. D'Antonio, F. Fu, The Classification of Implants: Class I, II, III, J. Long. Term. Eff. Med. Implants 19 (2009) 185–193. <https://doi.org/10.1615/JLongTermEffMedImplants.v19.i3.30>.
- [2] Z. Caplan, M. Rabe, The Older Population: 2020, (2020). <https://www2.census.gov/> (accessed November 22, 2023).
- [3] Global Bio-implant Market Size, Share | Industry Report, 2019-2026, n.d. <https://www.grandviewresearch.com/industry-analysis/bio-implants-market> (accessed April 30, 2023).
- [4] Bio-implants Market Size, Share, Outlook & Trends - 2023 | FMI, n.d. <https://www.futuremarketinsights.com/reports/bio-Implants-market> (accessed April 30, 2023).
- [5] Elderly in India 2021, 2021.
- [6] M. Saini, Implant biomaterials: A comprehensive review, World J. Clin. Cases 3 (2015) 52. <https://doi.org/10.12998/wjcc.v3.i1.52>.
- [7] J.D.G. Stephen, G.L. Kumar, R. Vinesh, G. Vikram, Bio implant materials: Requirements, Types and Properties– A review, (2017) 18–26.
- [8] S. Desai, B. Bidanda, P. Bartolo, Metallic and Ceramic Biomaterials: Current and Future Developments, in: Bio-Materials Prototyp. Appl. Med., Springer US, Boston, MA, 2008: pp. 1–14. https://doi.org/10.1007/978-0-387-47683-4_1.
- [9] Q. Chen, G.A. Thouas, Metallic implant biomaterials, Mater. Sci. Eng. R Reports 87 (2015) 1–57. <https://doi.org/10.1016/j.mser.2014.10.001>.
- [10] R. Kumar, A. Agrawal, Emerging Functionally Graded Materials for Bio-implant Applications—Design and Manufacturing, in: Addit. Manuf. Bio-Implants - Des. Synth., Springer, Singapore, 2024: pp. 137–146. https://doi.org/10.1007/978-981-99-6972-2_9.
- [11] A.T. Sidambe, Biocompatibility of advanced manufactured titanium implants-A review, Materials (Basel). 7 (2014) 8168–8188. <https://doi.org/10.3390/ma7128168>.
- [12] V. Secchi, S. Franchi, M. Dettin, A. Zamuner, K. Beranová, A. Vladescu, C. Battocchio, V. Graziani, L. Tortora, G. Iucci, Hydroxyapatite surfaces functionalized with a self-assembling peptide: XPS, rairs and nexafs study, Nanomaterials 10 (2020) 1151. <https://doi.org/10.3390/nano10061151>.
- [13] V.S. Kattimani, S. Kondaka, K.P. Lingamaneni, Hydroxyapatite—Past, Present, and Future in Bone Regeneration, Bone Tissue Regen. Insights 7 (2016) BTRI.S36138. <https://doi.org/10.4137/btri.s36138>.
- [14] M. Geetha, A.K. Singh, R. Asokamani, A.K. Gogia, Ti based biomaterials, the ultimate

choice for orthopaedic implants – A review, *Prog. Mater. Sci.* 54 (2009) 397–425.
<https://doi.org/10.1016/j.pmatsci.2008.06.004>.

- [15] S. Limmahakhun, A. Oloyede, K. Sitthiseripratip, Y. Xiao, C. Yan, Stiffness and strength tailoring of cobalt chromium graded cellular structures for stress-shielding reduction, *Mater. Des.* 114 (2017) 633–641.
<https://doi.org/10.1016/j.matdes.2016.11.090>.
- [16] M. Naim, A. Alhussein, M. Chemkhi, Tribocorrosion of Additively Manufactured (AM-ed) Metallic Biomaterials in Hip Implants : Review on Methodology and Post Treatments, *J. Bio- Tribo-Corrosion* 2023 94 9 (2023) 1–29.
<https://doi.org/10.1007/S40735-023-00783-4>.
- [17] Y. Onuki, U. Bhardwaj, F. Papadimitrakopoulos, D.J. Burgess, A Review of the Biocompatibility of Implantable Devices: Current Challenges to Overcome Foreign Body Response, *J. Diabetes Sci. Technol.* 2 (2008) 1003–1015.
<https://doi.org/10.1177/193229680800200610>.
- [18] S. Limmahakhun, A. Oloyede, K. Sitthiseripratip, Y. Xiao, C. Yan, Stiffness and strength tailoring of cobalt chromium graded cellular structures for stress-shielding reduction, *Mater. Des.* 114 (2017) 633–641.
<https://doi.org/10.1016/j.matdes.2016.11.090>.
- [19] Z.Y. Qiu, Y. Cui, X.M. Wang, Natural Bone Tissue and Its Biomimetic, *Miner. Collagen Bone Graft Substitutes* (2019) 1–22. <https://doi.org/10.1016/B978-0-08-102717-2.00001-1>.
- [20] F. Butz, H. Aita, C.J. Wang, T. Ogawa, Harder and Stiffer Bone Osseointegrated to Roughened Titanium, [Http://Dx.Doi.Org/10.1177/154405910608500616](http://dx.doi.org/10.1177/154405910608500616) 85 (2006) 560–565. <https://doi.org/10.1177/154405910608500616>.
- [21] W. Winter, S.M. Heckmann, H.P. Weber, A time-dependent healing function for immediate loaded implants, *J. Biomech.* 37 (2004) 1861–1867.
<https://doi.org/10.1016/J.JBIOMECH.2004.02.033>.
- [22] P. Branemark, H. Bo, R. Adell, U. Breine, J. Lindström, O. Hallén, A. Öhman, Osseointegrated implants in the treatment of the edentulous jaw. Experience from a 10-year period., *Scand. J. Plast. Reconstr. Surg. Suppl.* (1977).
- [23] X. Gao, M. Fraulob, G. Häiat, Biomechanical behaviours of the bone-implant interface: A review, *J. R. Soc. Interface* 16 (2019) 20190259.
<https://doi.org/10.1098/rsif.2019.0259>.
- [24] S. Virtanen, Corrosion of biomedical implant materials, *Corros. Rev.* 26 (2008) 147–172. <https://doi.org/10.1515/corrrev.2008.147>.
- [25] A.A. Campbell, Bioceramics for implant coatings, *Mater. Today* 6 (2003) 26–30.
[https://doi.org/10.1016/S1369-7021\(03\)01128-3](https://doi.org/10.1016/S1369-7021(03)01128-3).

- [26] M. Gasik, A. Keski-Honkola, Y. Bilotsky, M. Friman, Development and optimisation of hydroxyapatite- β -TCP functionally graded biomaterial, *J. Mech. Behav. Biomed. Mater.* 30 (2014) 266–273. <https://doi.org/10.1016/j.jmbbm.2013.11.017>.
- [27] W. Pompe, H. Worch, M. Epple, W. Friess, M. Gelinsky, P. Greil, U. Hempel, D. Scharnweber, K. Schulte, Functionally graded materials for biomedical applications, *Mater. Sci. Eng. A* 362 (2003) 40–60. [https://doi.org/10.1016/S0921-5093\(03\)00580-X](https://doi.org/10.1016/S0921-5093(03)00580-X).
- [28] Y. Shinohara, *Functionally Graded Materials*, Second Edi, Elsevier, 2013. <https://doi.org/10.1016/B978-0-12-385469-8.00061-7>.
- [29] J.S. Bergström, D. Hayman, An Overview of Mechanical Properties and Material Modeling of Polylactide (PLA) for Medical Applications, *Ann. Biomed. Eng.* 44 (2016) 330–340. <https://doi.org/10.1007/s10439-015-1455-8>.
- [30] S. Oh, N. Oh, M. Appleford, J.L. Ong, Bioceramics for Tissue Engineering Applications - A Review, *Am. J. Biochem. Biotechnol.* 2 (2006) 49–56. <https://doi.org/10.3844/ajbbbsp.2006.49.56>.
- [31] H. Hermawan, Biodegradable Metals: State of the Art, in: *Biodegrad. Met.*, Springer, New York, 2012: pp. 13–22. https://doi.org/10.1007/978-3-642-31170-3_2.
- [32] D.F. Williams, Definitions in biomaterials : proceedings of a consensus conference of the European Society for Biomaterials, Chester, England, 4 (1987) 72.
- [33] C.M. Agrawal, J.L. Ong, M.R. Appleford, G. Mani, *Introduction to Biomaterials: Basic Theory with Engineering Applications*, Cambridge University Press, 2013. <https://doi.org/10.1017/cbo9781139035545>.
- [34] D.F. Williams, On the mechanisms of biocompatibility, *Biomaterials* 29 (2008) 2941–2953. <https://doi.org/10.1016/J.BIOMATERIALS.2008.04.023>.
- [35] S. Ghosh, S. Sanghavi, P. Sancheti, Metallic biomaterial for bone support and replacement, in: *Fundam. Biomater. Met.*, Elsevier, 2018: pp. 139–165. <https://doi.org/10.1016/B978-0-08-102205-4.00006-4>.
- [36] S.R. Paital, N.B. Dahotre, Calcium phosphate coatings for bio-implant applications: Materials, performance factors, and methodologies, *Mater. Sci. Eng. R Reports* 66 (2009) 1–70. <https://doi.org/10.1016/j.mser.2009.05.001>.
- [37] Y. Watanabe, Y. Inaguma, H. Sato, E. Miura-Fujiwara, A Novel Fabrication Method for Functionally Graded Materials under Centrifugal Force: The Centrifugal Mixed-Powder Method, *Materials (Basel)*. 2 (2009) 2510–2525. <https://doi.org/10.3390/ma2042510>.
- [38] Y. Watanabe, H. Sato, Review Fabrication of Functionally Graded Materials under a Centrifugal Force, in: *Nanocomposites with Unique Prop. Appl. Med. Ind.*, InTech, 2011. <https://doi.org/10.5772/20988>.

- [39] R.A. Brand, M.A. Mont, M.M. Manring, Biographical sketch: Themistocles Gluck (1853-1942), in: Clin. Orthop. Relat. Res., Association of Bone and Joint Surgeons, 2011: pp. 1525–1527. <https://doi.org/10.1007/s11999-011-1836-8>.
- [40] M. Navarro, A. Michiardi, O. Castaño, J.. Planell, Biomaterials in orthopaedics, J. R. Soc. Interface 5 (2008) 1137–1158. <https://doi.org/10.1098/rsif.2008.0151>.
- [41] R. Davis, A. Singh, M.J. Jackson, R.T. Coelho, D. Prakash, C.P. Charalambous, W. Ahmed, L.R.R. da Silva, A.A. Lawrence, A comprehensive review on metallic implant biomaterials and their subtractive manufacturing, Int. J. Adv. Manuf. Technol. 120 (2022) 1473–1530. <https://doi.org/10.1007/s00170-022-08770-8>.
- [42] S.J. Gobbi, Requirements for Selection/Development of a Biomaterial, Biomed. J. Sci. Tech. Res. 14 (2019) 001–006. <https://doi.org/10.26717/bjstr.2019.14.002554>.
- [43] F.J. O'Brien, Biomaterials & scaffolds for tissue engineering, Mater. Today 14 (2011) 88–95. [https://doi.org/10.1016/S1369-7021\(11\)70058-X](https://doi.org/10.1016/S1369-7021(11)70058-X).
- [44] H. Huang, P. Zhang, M. Tang, L. Shen, Z. Yu, H. Shi, Y. Tian, Biocompatibility of micro/nano structures on the surface of Ti6Al4V and Ti-based bulk metallic glasses induced by femtosecond laser, Biomater. Adv. 139 (2022) 212998. <https://doi.org/10.1016/j.bioadv.2022.212998>.
- [45] M. Singh, A.S. Gill, P.K. Deol, A. Agrawal, S.S. Sidhu, Drug eluting titanium implants for localised drug delivery, J. Mater. Res. (2022) 1–21. <https://doi.org/10.1557/s43578-022-00609-y>.
- [46] C. Zhou, C. Deng, X. Chen, X. Zhao, Y. Chen, Y. Fan, X. Zhang, Mechanical and biological properties of the micro-/nano-grain functionally graded hydroxyapatite bioceramics for bone tissue engineering, J. Mech. Behav. Biomed. Mater. 48 (2015) 1–11. <https://doi.org/10.1016/j.jmbbm.2015.04.002>.
- [47] S. Singh, P. Vashisth, A. Shrivastav, N. Bhatnagar, Synthesis and characterization of a novel open cellular Mg-based scaffold for tissue engineering application, J. Mech. Behav. Biomed. Mater. 94 (2019) 54–62. <https://doi.org/10.1016/j.jmbbm.2019.02.010>.
- [48] M. Kaur, K. Singh, Review on titanium and titanium based alloys as biomaterials for orthopaedic applications, Mater. Sci. Eng. C 102 (2019) 844–862. <https://doi.org/10.1016/j.msec.2019.04.064>.
- [49] Kaur, Ghadirinejad, Oskouei, An Overview on the Tribological Performance of Titanium Alloys with Surface Modifications for Biomedical Applications, Lubricants 7 (2019) 65. <https://doi.org/10.3390/lubricants7080065>.
- [50] D.T. Waghmare, C. Kumar Padhee, R. Prasad, M. Masanta, NiTi coating on Ti-6Al-4V alloy by TIG cladding process for improvement of wear resistance: Microstructure evolution and mechanical performances, J. Mater. Process. Technol. 262 (2018) 551–

561. <https://doi.org/10.1016/j.jmatprotec.2018.07.033>.
- [51] Ş. Danişman, D. Odabas, M. Teber, The Effect of Coatings on the Wear Behavior of Ti6Al4V Alloy Used in Biomedical Applications, IOP Conf. Ser. Mater. Sci. Eng. 295 (2018) 012044. <https://doi.org/10.1088/1757-899X/295/1/012044>.
- [52] S. Datta, M. Das, V.K. Balla, S. Bodhak, V.K. Murugesan, Mechanical, wear, corrosion and biological properties of arc deposited titanium nitride coatings, Surf. Coatings Technol. 344 (2018) 214–222. <https://doi.org/10.1016/j.surfcoat.2018.03.019>.
- [53] J. Ureña, S. Tsipas, A.M. Pinto, F. Toptan, E. Gordo, A. Jiménez-Morales, Corrosion and tribocorrosion behaviour of β -type Ti-Nb and Ti-Mo surfaces designed by diffusion treatments for biomedical applications, Corros. Sci. 140 (2018) 51–60. <https://doi.org/10.1016/j.corsci.2018.06.024>.
- [54] B. Rahmati, A.A.D. Sarhan, W.J. Basirun, W.A.B.W. Abas, Ceramic tantalum oxide thin film coating to enhance the corrosion and wear characteristics of Ti 6Al 4V alloy, J. Alloys Compd. 676 (2016) 369–376. <https://doi.org/10.1016/j.jallcom.2016.03.188>.
- [55] I. Simsek, D. Ozyurek, Investigation of the electrochemical corrosion properties of high-energy milled Ti6Al4V alloy in simulated body fluid environment, Powder Metall. 62 (2019) 169–175. <https://doi.org/10.1080/00325899.2019.1607029>.
- [56] M.P. Staiger, A.M. Pietak, J. Huadmai, G. Dias, Magnesium and its alloys as orthopedic biomaterials: A review, Biomaterials 27 (2006) 1728–1734. <https://doi.org/10.1016/j.biomaterials.2005.10.003>.
- [57] B.A. Shaw, Corrosion Resistance of Magnesium Alloys, Corros. Fundam. Testing, Prot. (2003) 692–696. <https://doi.org/10.31399/ASM.HB.V13A.A0003675>.
- [58] S. Jaiswal, S. Agrawal, A. Dubey, D. Lahiri, Effect of multi-axial hot forging process on mechanical, and corrosion resistance behavior of Mg-3Zn alloy for temporary orthopedic implants, Eng. Reports 3 (2021). <https://doi.org/10.1002/eng2.12286>.
- [59] H.R. Tiyyagura, T. Mohan, S. Pal, M.K. Mohan, Surface modification of Magnesium and its alloy as orthopedic biomaterials with biopolymers, in: Fundam. Biomater. Met., Elsevier, 2018: pp. 197–210. <https://doi.org/10.1016/B978-0-08-102205-4.00009-X>.
- [60] I. Putrantyo, N. Anilbhai, R. Vanjani, B. De Vega, Tantalum as a Novel Biomaterial for Bone Implant: A Literature Review, J. Biomimetics, Biomater. Biomed. Eng. 52 (2021) 55–65. <https://doi.org/10.4028/www.scientific.net/JBBBE.52.55>.
- [61] C.G. Paganias, G.A. Tsakotos, S.D. Koutsostathis, G.A. MacHeras, Osseous integration in porous tantalum implants, Indian J. Orthop. 46 (2012) 505–513. <https://doi.org/10.4103/0019-5413.101032>.
- [62] M.S. Patel, J.R. McCormick, A. Ghasem, S.R. Huntley, J.P. Gjolaj, Tantalum: the next

biomaterial in spine surgery?, *J. Spine Surg.* 6 (2020) 72.
<https://doi.org/10.21037/JSS.2020.01.01>.

- [63] G. Thandapani, E. Radha, J. Annie Kamala Florence, P.N. Sudha, Bioactive metallic surfaces for bone tissue engineering, *Fundam. Biomater. Met.* (2018) 79–110.
<https://doi.org/10.1016/B978-0-08-102205-4.00004-0>.
- [64] C. Chua, S.L. Sing, C.K. Chua, Characterisation of in-situ alloyed titanium-tantalum lattice structures by laser powder bed fusion using finite element analysis, *Virtual Phys. Prototyp.* 18 (2023). <https://doi.org/10.1080/17452759.2022.2138463>.
- [65] J. Feng, Preparation and properties of poly(lactic acid) fiber melt blown non-woven disordered mats, *Mater. Lett.* 189 (2017) 180–183.
<https://doi.org/10.1016/J.MATLET.2016.12.013>.
- [66] G.M. Raghoobar, R.S.B. Liem, R.R.M. Bos, J.E. Van Der Wal, A. Vissink, Resorbable screws for fixation of autologous bone grafts, *Clin. Oral Implants Res.* 17 (2006) 288–293. <https://doi.org/10.1111/J.1600-0501.2005.01200.X>.
- [67] A. Salerno, M. Fernández-Gutiérrez, J. San Román Del Barrio, C. Domingo, Bio-safe fabrication of PLA scaffolds for bone tissue engineering by combining phase separation, porogen leaching and scCO₂ drying, *J. Supercrit. Fluids* 97 (2015) 238–246. <https://doi.org/10.1016/J.SUPFLU.2014.10.029>.
- [68] K.K. Kim, D.W. Pack, Microspheres for Drug Delivery, *BioMEMS Biomed. Nanotechnol.* (2006) 19. https://doi.org/10.1007/978-0-387-25842-3_2.
- [69] B. Gong, S. Cui, Y. Zhao, Y. Sun, Q. Ding, Strain-controlled fatigue behaviors of porous PLA-based scaffolds by 3D-printing technology, *J. Biomater. Sci. Polym. Ed.* 28 (2017) 2196–2204. <https://doi.org/10.1080/09205063.2017.1388993>.
- [70] M. Santoro, S.R. Shah, J.L. Walker, A.G. Mikos, Poly(lactic acid) nanofibrous scaffolds for tissue engineering, *Adv. Drug Deliv. Rev.* 107 (2016) 206–212. <https://doi.org/10.1016/j.addr.2016.04.019>.
- [71] F.S. Senatov, K. V. Niaza, M.Y. Zadorozhnyy, A. V. Maksimkin, S.D. Kaloshkin, Y.Z. Estrin, Mechanical properties and shape memory effect of 3D-printed PLA-based porous scaffolds, *J. Mech. Behav. Biomed. Mater.* 57 (2016) 139–148. <https://doi.org/10.1016/j.jmbbm.2015.11.036>.
- [72] A.A. Poinescu, R.-M. Ion, 316L Stainless Steel/Hydroxyapatite Composite Materials for Biomedical Applications, in: *Hydroxyapatite - Adv. Compos. Nanomater. Biomed. Appl. Its Technol. Facet., InTech*, 2018. <https://doi.org/10.5772/intechopen.71490>.
- [73] D.F. Zambrano, R. Hernández-Bravo, A. Ruden, D.G. Espinosa-Arbelaez, J.M. González-Carmona, V. Mujica, Mechanical, tribological and electrochemical behavior of Zr-based ceramic thin films for dental implants, *Ceram. Int.* 49 (2023) 2102–2114. <https://doi.org/10.1016/J.CERAMINT.2022.09.176>.

- [74] A.M. Ribeiro, A.C. Alves, F.S. Silva, F. Toptan, Electrochemical characterization of hot pressed CoCrMo-HAP biocomposite in a physiological solution, *Mater. Corros.* 66 (2015) 790–795. <https://doi.org/10.1002/maco.201407885>.
- [75] Z. Doni, A.C. Alves, F. Toptan, L.A. Rocha, M. Buciumeanu, L. Palaghian, F.S. Silva, Tribocorrosion behaviour of hot pressed CoCrMo–HAP biocomposites, *Tribol. Int.* 91 (2015) 221–227. <https://doi.org/10.1016/j.triboint.2015.04.009>.
- [76] X. Wang, Y. Chen, L.J. Xu, S. Xiao, F. Kong, K. Do Woo, Ti-Nb-Sn-hydroxyapatite composites synthesized by mechanical alloying and high frequency induction heated sintering, *J. Mech. Behav. Biomed. Mater.* 4 (2011) 2074–2080. <https://doi.org/10.1016/j.jmbbm.2011.07.006>.
- [77] N.-R. Park, C.-G. Song, I.-J. Shon, Fast low-temperature consolidation of a nanostructured 2Ti–ZrO₂ composite for biomedical applications, *Ceram. Int.* 40 (2014) 6311–6317. <https://doi.org/10.1016/j.ceramint.2013.10.034>.
- [78] K. Morsi, V. V. Patel, Processing and properties of titanium-titanium boride (TiBw) matrix composites - A review, *J. Mater. Sci.* 42 (2007) 2037–2047. <https://doi.org/10.1007/S10853-006-0776-2/FIGURES/6>.
- [79] N.K. Bhoi, H. Singh, S. Pratap, P.K. Jain, Microwave material processing: A clean, green, and sustainable approach, in: *Sustain. Eng. Prod. Manuf. Technol.*, Elsevier, 2019; pp. 3–23. <https://doi.org/10.1016/B978-0-12-816564-5.00001-3>.
- [80] N.K. Bhoi, H. Singh, S. Pratap, P.K. Jain, Aluminum Yttrium Oxide Metal Matrix Composite Synthesized by Microwave Hybrid Sintering: Processing, Microstructure and Mechanical Response, *J. Inorg. Organomet. Polym. Mater.* 32 (2022) 1319–1333. <https://doi.org/10.1007/s10904-021-02195-8>.
- [81] M.A. Janney, H.D. Kimrey, Diffusion-Controlled Processes in Microwave-Fired Oxide Ceramics, *MRS Proc.* 189 (1990) 215. <https://doi.org/10.1557/PROC-189-215>.
- [82] R. R. Menezes, P. M. Souto, R. H.G.A. Kiminami, Microwave Fast Sintering of Ceramic Materials, in: *Sinter. Ceram. - New Emerg. Tech.*, InTech, 2012. <https://doi.org/10.5772/34181>.
- [83] M.J. Oza, K.G. Schell, E.C. Bucharsky, T. Laha, S. Roy, Developing a hybrid Al–SiC-graphite functionally graded composite material for optimum composition and mechanical properties, *Mater. Sci. Eng. A* 805 (2021) 140625. <https://doi.org/10.1016/J.MSEA.2020.140625>.
- [84] S.W. Maseko, A.P.I. Popoola, O.S.I. Fayomi, Characterization of ceramic reinforced titanium matrix composites fabricated by spark plasma sintering for anti-ballistic applications, *Def. Technol.* 14 (2018) 408–411. <https://doi.org/10.1016/j.dt.2018.04.013>.
- [85] W. Xu, J. Tian, Z. Liu, X. Lu, M.D. Hayat, Y. Yan, Z. Li, X. Qu, C. Wen, Novel porous

Ti₃₅Zr₂₈Nb scaffolds fabricated by powder metallurgy with excellent osteointegration ability for bone-tissue engineering applications, *Mater. Sci. Eng. C* 105 (2019) 110015. <https://doi.org/10.1016/j.msec.2019.110015>.

- [86] M. Kaya, F. Yakuphanoglu, A study on microstructure of porous TiNbZr alloy produced as biomaterial, *Materwiss. Werksttech.* 50 (2019) 742–746. <https://doi.org/10.1002/mawe.201800235>.
- [87] C. Prakash, S. Singh, S. Ramakrishna, G. Królczyk, C.H. Le, Microwave sintering of porous Ti–Nb–HA composite with high strength and enhanced bioactivity for implant applications, *J. Alloys Compd.* 824 (2020) 153774. <https://doi.org/10.1016/j.jallcom.2020.153774>.
- [88] J. Xu, G.D. Wang, X. Lu, L. Liu, P. Munroe, Z.H. Xie, Mechanical and corrosion-resistant properties of Ti–Nb–Si–N nanocomposite films prepared by a double glow discharge plasma technique, *Ceram. Int.* 40 (2014) 8621–8630. <https://doi.org/10.1016/j.ceramint.2014.01.079>.
- [89] N. Singh, R. Ummethala, K.B. Surreddi, J. Jayaraj, R. Sokkalingam, M. Rajput, K. Chatterjee, K.G. Prashanth, Effect of TiB₂ addition on the mechanical and biological response of spark plasma sintered Ti₆Al₇Nb matrix composites, *J. Alloys Compd.* 924 (2022) 166502. <https://doi.org/10.1016/j.jallcom.2022.166502>.
- [90] M.M. Nemat-Alla, M.H. Ata, M.R. Bayoumi, W. Khair-Eldeen, Powder Metallurgical Fabrication and Microstructural Investigations of Aluminum/Steel Functionally Graded Material, *Mater. Sci. Appl.* 02 (2011) 1708–1718. <https://doi.org/10.4236/msa.2011.212228>.
- [91] R. Jojith, N. Radhika, Reciprocal dry sliding wear of SiCp/Al–7Si–0.3 Mg functionally graded composites: Influence of T6 treatment and process parameters, *Ceram. Int.* (2021). <https://doi.org/10.1016/j.ceramint.2021.07.225>.
- [92] T.C. Dzogbewu, W.B. du Preez, In situ alloying of Ti₁₀Mo fused tracks and layers via laser powder bed fusion, *Manuf. Rev.* 9 (2022) 23. <https://doi.org/10.1051/mfreview/2022022>.
- [93] J.Y. Lee, J. An, C.K. Chua, Fundamentals and applications of 3D printing for novel materials, *Appl. Mater. Today* 7 (2017) 120–133. <https://doi.org/10.1016/j.apmt.2017.02.004>.
- [94] N.E. Putra, M.J. Mirzaali, I. Apachitei, J. Zhou, A.A. Zadpoor, Multi-material additive manufacturing technologies for Ti-, Mg-, and Fe-based biomaterials for bone substitution, *Acta Biomater.* 109 (2020) 1–20. <https://doi.org/10.1016/j.ACTBIO.2020.03.037>.
- [95] W. Xu, A. Yu, Y. Jiang, Y. Li, C. Zhang, H. Singh, B. Liu, C. Hou, Y. Zhang, S. Tian, J. Zhang, X. Lu, Gyroid-based functionally graded porous titanium scaffolds for dental

- application: Design, simulation and characterizations, *Mater. Des.* 224 (2022) 111300. <https://doi.org/10.1016/j.matdes.2022.111300>.
- [96] A. Kumar, P.M. Pandey, Development of Mg based biomaterial with improved mechanical and degradation properties using powder metallurgy, *J. Magnes. Alloy.* 8 (2020) 883–898. <https://doi.org/10.1016/J.JMA.2020.02.011>.
- [97] J. Xu, M. Ji, L. Li, Y. Wu, Q. Yu, M. Chen, Improving wettability, antibacterial and tribological behaviors of zirconia ceramics through surface texturing, *Ceram. Int.* 48 (2022) 3702–3710. <https://doi.org/10.1016/j.ceramint.2021.10.152>.
- [98] L. Blunt, P. Bills, X. Jiang, C. Hardaker, G. Chakrabarty, The role of tribology and metrology in the latest development of bio-materials, *Wear* 266 (2009) 424–431. <https://doi.org/10.1016/J.WEAR.2008.04.015>.
- [99] O. Gingu, G. Benga, A. Olei, N. Lupu, P. Rotaru, S. Tanasescu, M. Mangra, I. Ciupitu, I. Pascu, G. Sima, Wear behaviour of ceramic biocomposites based on hydroxiapatite nanopowders, *Proc. Inst. Mech. Eng. Part E J. Process Mech. Eng.* 225 (2011) 62–71. <https://doi.org/10.1243/09544089JPME307>.
- [100] S. Bose, M. Roy, A. Bandyopadhyay, Recent advances in bone tissue engineering scaffolds, *Trends Biotechnol.* 30 (2012) 546–554. <https://doi.org/10.1016/j.tibtech.2012.07.005>.
- [101] K. Rahmouni, A. Besnard, K. Oulmi, C. Nouveau, A. Hidoussi, L. Aissani, M. Zaabat, In vitro corrosion response of CoCrMo and Ti-6Al-4V orthopedic implants with Zr columnar thin films, *Surf. Coatings Technol.* 436 (2022) 128310. <https://doi.org/10.1016/j.surfcoat.2022.128310>.
- [102] J. Fornell, N. Van Steenberge, A. Varea, E. Rossinyol, E. Pellicer, S. Suriñach, M.D. Baró, J. Sort, Enhanced mechanical properties and in vitro corrosion behavior of amorphous and devitrified Ti₄₀Zr₁₀Cu₃₈Pd₁₂ metallic glass, *J. Mech. Behav. Biomed. Mater.* 4 (2011) 1709–1717. <https://doi.org/10.1016/j.jmbbm.2011.05.028>.
- [103] S. Inayat-Hussain, N.F. Rajab, E.L. Siew, In vitro testing of biomaterials toxicity and biocompatibility, Woodhead Publishing Limited, 2008. <https://doi.org/10.1533/9781845695477.3.508>.
- [104] M. Roy, A. Bandyopadhyay, S. Bose, In vitro antimicrobial and biological properties of laser assisted tricalcium phosphate coating on titanium for load bearing implant, *Mater. Sci. Eng. C* 29 (2009) 1965–1968. <https://doi.org/10.1016/J.MSEC.2009.03.009>.
- [105] M.L. Raffa, V. Nguyen, P. Hernigou, C. Flouzat-Lachaniette, G. Haiat, Stress shielding at the bone-implant interface: Influence of surface roughness and of the bone-implant contact ratio, *J. Orthop. Res.* 39 (2021) 1174–1183. <https://doi.org/10.1002/jor.24840>.

- [106] R.M. Mahamood, E.T.A. Member, M. Shukla, S. Pityana, Functionally Graded Material : An Overview, *Proc. World Congr. Eng. III* (2012) 2–6.
- [107] E. Bouyer, F. Gitzhofer, M.I. Boulos, Morphological study of hydroxyapatite nanocrystal suspension, *J. Mater. Sci. Mater. Med.* 11 (2000) 523–531. <https://doi.org/10.1023/A:1008918110156>.
- [108] M.P. Ferraz, F.J. Monteiro, C.M. Manuel, Hydroxyapatite nanoparticles: A review of preparation methodologies, *J. Appl. Biomater. Funct. Mater.* 2 (2004) 74–80. <https://doi.org/https://doi.org/10.1177/228080000400200202>.
- [109] K. Niespodziana, Synthesis and Properties of Porous Ti-20 wt.% HA Nanocomposites, *J. Mater. Eng. Perform.* 28 (2019) 2245–2255. <https://doi.org/10.1007/s11665-019-03966-8>.
- [110] G.K. Williamson, W.H. Hall, X-ray line broadening from filed aluminium and wolfram, *Acta Metall.* 1 (1953) 22–31. [https://doi.org/10.1016/0001-6160\(53\)90006-6](https://doi.org/10.1016/0001-6160(53)90006-6).
- [111] C. Suryanarayana, Mechanical alloying and milling, *Prog. Mater. Sci.* 46 (2001) 1–184. [https://doi.org/10.1016/S0079-6425\(99\)00010-9](https://doi.org/10.1016/S0079-6425(99)00010-9).
- [112] A. Bhattacharjee, A. Gupta, M. Verma, M.P. Anand, P. Sengupta, M. Saravanan, I. Manna, K. Balani, Antibacterial and magnetic response of site-specific cobalt incorporated hydroxyapatite, *Ceram. Int.* 46 (2020) 513–522. <https://doi.org/10.1016/j.ceramint.2019.08.291>.
- [113] R.A. Nyquist, R.O. Kagel, *Handbook of Infrared and Raman Spectra of Inorganic Compounds and Organic Salts. Vol.4: Infrared Spectra of Inorganic Compounds (3800–45 cm⁻¹)*, Academic, San Diego, 1997.
- [114] G. Penel, G. Leroy, C. Rey, B. Sombret, J.P. Huvenne, E. Bres, Infrared and Raman microspectrometry study of fluor-fluor-hydroxy and hydroxy-apatite powders, *J. Mater. Sci. Mater. Med.* 8 (1997) 271–276. <https://doi.org/10.1023/A:1018504126866>.
- [115] I. Rehman, W. Bonfield, Characterization of hydroxyapatite and carbonated apatite by photo acoustic FTIR spectroscopy, *J. Mater. Sci. Mater. Med.* 8 (1997) 1–4. <https://doi.org/10.1023/A:1018570213546>.
- [116] M. Kukura, L.C. Bell, A.M. Posner, J.P. Quirk, Radioisotope determination of the surface concentrations of calcium and phosphorus on hydroxyapatite in aqueous solution, *J. Phys. Chem.* 76 (1972) 900–904. <https://doi.org/10.1021/j100650a019>.
- [117] T. Mandal, B.K. Mishra, A. Garg, D. Chaira, Optimization of milling parameters for the mechanosynthesis of nanocrystalline hydroxyapatite, *Powder Technol.* 253 (2014) 650–656. <https://doi.org/10.1016/j.powtec.2013.12.026>.
- [118] C. Wang, J. Ma, W. Cheng, R. Zhang, Thick hydroxyapatite coatings by

- electrophoretic deposition, *Mater. Lett.* 57 (2002) 99–105. [https://doi.org/10.1016/S0167-577X\(02\)00706-1](https://doi.org/10.1016/S0167-577X(02)00706-1).
- [119] D. Mondal, L. Nguyen, I.-H. Oh, B.-T. Lee, Microstructure and biocompatibility of composite biomaterials fabricated from titanium and tricalcium phosphate by spark plasma sintering, *J. Biomed. Mater. Res. Part A* 101A (2013) 1489–1501. <https://doi.org/10.1002/jbm.a.34455>.
- [120] S.C. Cox, P. Jamshidi, R.L. Williams, L.M. Grover, K.K. Mallick, The importance of processing conditions on the biological response to apatites, *Powder Technol.* 284 (2015) 195–203. <https://doi.org/10.1016/j.powtec.2015.06.061>.
- [121] Y. Fang, D.K. Agrawal, D.M. Roy, R. Roy, Fabrication of transparent hydroxyapatite ceramics by ambient-pressure sintering, *Mater. Lett.* 23 (1995) 147–151. [https://doi.org/10.1016/0167-577X\(95\)00016-X](https://doi.org/10.1016/0167-577X(95)00016-X).
- [122] S. Takayama, Y. Saito, M. Sato, T. Nagasaka, T. Muroga, Y. Ninomiya, Sintering behavior of metal powders involving microwave-enhanced chemical reaction, *Japanese J. Appl. Physics, Part 1 Regul. Pap. Short Notes Rev. Pap.* 45 (2006) 1816–1822. <https://doi.org/10.1143/JJAP.45.1816/XML>.
- [123] D. Bovand, M. Yousefpour, S. Rasouli, S. Bagherifard, N. Bovand, A. Tamayol, Characterization of Ti-HA composite fabricated by mechanical alloying, *Mater. Des.* 65 (2015) 447–453. <https://doi.org/10.1016/J.MATDES.2014.09.021>.
- [124] W.C. Oliver, G.M. Pharr, An improved technique for determining hardness and elastic modulus using load and displacement sensing indentation experiments, *J. Mater. Res.* 7 (1992) 1564–1583. <https://doi.org/10.1557/JMR.1992.1564>.
- [125] W.C. Oliver, G.M. Pharr, Measurement of hardness and elastic modulus by instrumented indentation: Advances in understanding and refinements to methodology, *J. Mater. Res.* 19 (2004) 3–20. <https://doi.org/10.1557/jmr.2004.19.1.3>.
- [126] A. Hynowska, E. Pellicer, J. Fornell, S. González, N. van Steenberge, S. Suriñach, A. Gebert, M. Calin, J. Eckert, M.D. Baró, J. Sort, Nanostructured β -phase Ti–31.0Fe–9.0Sn and sub- μ m structured Ti–39.3Nb–13.3Zr–10.7Ta alloys for biomedical applications: Microstructure benefits on the mechanical and corrosion performances, *Mater. Sci. Eng. C* 32 (2012) 2418–2425. <https://doi.org/10.1016/j.msec.2012.07.016>.
- [127] H. Attar, S. Ehtemam-Haghighi, D. Kent, I.V. Okulov, H. Wendrock, M. Bönisch, A.S. Volegov, M. Calin, J. Eckert, M.S. Dargusch, Nanoindentation and wear properties of Ti and Ti-TiB composite materials produced by selective laser melting, *Mater. Sci. Eng. A* 688 (2017) 20–26. <https://doi.org/10.1016/j.msea.2017.01.096>.
- [128] J.A. Nychka, M.M. Gentleman, Implications of wettability in biological materials

science, JOM 62 (2010) 39–48. <https://doi.org/10.1007/s11837-010-0107-6>.

- [129] D. Ahmad, I. van den Boogaert, J. Miller, R. Presswell, H. Jouhara, Hydrophilic and hydrophobic materials and their applications, *Energy Sources, Part A Recover. Util. Environ. Eff.* 40 (2018) 2686–2725. <https://doi.org/10.1080/15567036.2018.1511642>.
- [130] F. Mansfeld, Tafel slopes and corrosion rates obtained in the pre-Tafel region of polarization curves, *Corros. Sci.* 47 (2005) 3178–3186. <https://doi.org/10.1016/J.CORSCI.2005.04.012>.
- [131] E. McCafferty, Validation of corrosion rates measured by the Tafel extrapolation method, *Corros. Sci.* 47 (2005) 3202–3215. <https://doi.org/10.1016/j.corsci.2005.05.046>.
- [132] R. Kumar, A. Agrawal, Bio-corrosion susceptibility of surface voids and pores in microwave sintered Ti-HAp based bio-composites, *Mater. Lett.* 361 (2024) 136168. <https://doi.org/10.1016/j.matlet.2024.136168>.
- [133] V. Frauchiger, F. Schlottig, B. Gasser, M. Textor, Anodic plasma-chemical treatment of CP titanium surfaces for biomedical applications, *Biomaterials* 25 (2004) 593–606. [https://doi.org/10.1016/S0142-9612\(03\)00560-X](https://doi.org/10.1016/S0142-9612(03)00560-X).
- [134] S.A. Alves, R. Bayón, V.S. de Viteri, M.P. Garcia, A. Igartua, M.H. Fernandes, L.A. Rocha, Tribocorrosion Behavior of Calcium- and Phosphorous-Enriched Titanium Oxide Films and Study of Osteoblast Interactions for Dental Implants, *J. Bio- Tribo-Corrosion* 1 (2015) 1–21. <https://doi.org/10.1007/s40735-015-0023-y>.
- [135] A.M. Salantiu, C. Fekete, L. Muresan, P. Pascuta, F. Popa, C. Popa, Anodic oxidation of PM porous titanium for increasing the corrosion resistance of endosseous implants, *Mater. Chem. Phys.* 149 (2015) 453–459. <https://doi.org/10.1016/j.matchemphys.2014.10.044>.
- [136] M.-T.T. Choy, C.-Y.Y. Tang, L. Chen, W.-C.C. Law, C.-P.P. Tsui, W.W. Lu, Microwave assisted-in situ synthesis of porous titanium/calcium phosphate composites and their in vitro apatite-forming capability, *Compos. Part B Eng.* 83 (2015) 50–57. <https://doi.org/10.1016/j.compositesb.2015.08.046>.
- [137] H. Liu, H. Yazici, C. Ergun, T.J. Webster, H. Bermek, An in vitro evaluation of the Ca/P ratio for the cytocompatibility of nano-to-micron particulate calcium phosphates for bone regeneration, *Acta Biomater.* 4 (2008) 1472–1479. <https://doi.org/10.1016/J.ACTBIO.2008.02.025>.
- [138] H. Shahali, A. Jaggesar, P.K. Yarlagadda, Recent Advances in Manufacturing and Surface Modification of Titanium Orthopaedic Applications, in: *Procedia Eng.*, Elsevier, 2017: pp. 1067–1076. <https://doi.org/10.1016/j.proeng.2017.01.259>.
- [139] R. Kumar, A. Agrawal, Micro-hydroxyapatite reinforced Ti-based composite with

- tailored characteristics to minimize stress-shielding impact in bio-implant applications, *J. Mech. Behav. Biomed. Mater.* 142 (2023) 105852. <https://doi.org/10.1016/j.jmbbm.2023.105852>.
- [140] C. Petit, L. Montanaro, P. Palmero, Functionally graded ceramics for biomedical application: Concept, manufacturing, and properties, *Int. J. Appl. Ceram. Technol.* 15 (2018) 820–840. <https://doi.org/10.1111/ijac.12878>.
- [141] A. Jarrahi, H.A. Shirazi, A. Asnafi, M.R. Ayatollahi, Biomechanical analysis of a radial functionally graded dental implant–bone system under multi-directional dynamic loads, *J. Brazilian Soc. Mech. Sci. Eng.* 40 (2018). <https://doi.org/10.1007/s40430-018-1166-9>.
- [142] R. Havaladar, S. Pilli, B. Putti, Insights into the effects of tensile and compressive loadings on human femur bone, *Adv. Biomed. Res.* 3 (2014) 101. <https://doi.org/10.4103/2277-9175.129375>.
- [143] F. Metzner, C. Neupetsch, J.P. Fischer, W.G. Drossel, C.E. Heyde, S. Schleifenbaum, Influence of osteoporosis on the compressive properties of femoral cancellous bone and its dependence on various density parameters, *Sci. Rep.* 11 (2021) 13284. <https://doi.org/10.1038/s41598-021-92685-z>.

Brief Bio-Data



Rakesh Kumar is a Ph.D. Scholar in the Department of Mechanical Engineering at the Indian Institute of Technology Ropar, India. He joined the Ph.D. program at IIT Ropar in 2018. Before that, he received a Bachelor of Technology degree in Mechanical Engineering from BPUT Rourkela, Odisha, India, in 2013 and a Master of Technology degree in Mechanical Engineering with a Specialization in Production Engineering from VSSUT Burla, Odisha, India, in 2017. His current research interests include simulation and experimental studies of materials and manufacturing processes, specifically Metal and Metal-based multi-material Additive Manufacturing and Powder Metallurgy processing for potential biomedical, aerospace, and automobile industrial applications.